Singularities in fluid dynamics: from the classical approach to Monge-Ampere geometry

Roberto D'Onofrio

Thesis submitted to the University of Milano-Bicocca and the University of Surrey for the degree of Doctor of Philosophy

Department of Mathematics
University of Milano-Bicocca, 20125 Milano, Italy

School of Mathematics and Physics
University of Surrey, Guildford GU2 7XH, United Kingdom

E-mail address: donofrio.roberto@outlook.com

Scientific abstract

This thesis presents some recently published results ([10, 30]) regarding two classical models of fluid dynamics: the 1D shallow water equations (SWE) and the 3D incompressible semigeostrophic equations. In the context of SWEs, we examine the behavior of pre-existing C^1-class singular points in the solution, and point out the distinction between the hyperbolic regime and the parabolic regime. We provide a local description of the solution near the singular points by means of the so-called wavefront expansion and derive shock times where possible.

Concerning semigeostrophic equations, we study the relationship between hyperbolic-elliptic transitions and singularities. To this end, we adopt a geometric framework, coming from Lychagin's theory of Monge–Ampère equations, which provides a clear and useful representation of generalized solutions and singularities. Specifically, we study a pull-back metric on generalized solutions, seen as Lagrangian submanifolds of a suitable phase space, and its relations with the symbol type of the equations and their singularities. Finally, we study the Eady problem, a classical benchmark initial setting for the semigeostrophic equations, as an example of application of the ideas presented.

Lay summary

The singularities of a mathematical model are often its most intriguing features. They can reveal its limits of validity and suggest worthwhile new questions to ask on the underlying physical phenomenon. Singularities are especially relevant to fluid models. The Navier-Stokes existence and smoothness problem is one of the oldest on the Clay Institute's list, and has survived attacks by mathematicians for centuries. Since direct approaches have had limited success so far, researchers have turned to mathematical models in order to gain insights into the behavior of the parent equations. Models that derive from the Navier-Stokes equations through simplifying assumptions can isolate specific features such as nonlinear, dissipative, and dispersive effects, to be investigated separately. Also, studying models often leads to discovering mathematical structures and methods which motivates new research questions on the parent system, where one expects to be able to find similar structures. This is the spirit of the present thesis.

We will investigate these ideas with particular reference to two models. The first of them, called the "shallow water equations", comes from oceanography, and describes the motion of long waves on the surface of the water. The second, called the "semigeostrophic equations", comes from meteorology and is used in weather prediction on a subcontinental scale.

The partial differential equations that cosntitute a model can generally assume elliptic or hyperbolic behavior depending on their structure. For example, under "normal" conditions, shallow water equations are hyperbolic while semigeostrophic equations are elliptic. However, it is possible that the model is capable of assuming both elliptic and hyperbolic behavior depending on the choice of parameters and the solution at hand. For example, shallow water equations are hyperbolic where the surface of the water is strictly above the bottom and become elliptical where the surface lies below the bottom. Obviously, this last case has no physical meaning, a fact which is reflected in the instability that occurs in the solution as soon as it becomes elliptic. The transition point between the two regimes, where the free surface intersects the seabed, plays a special role. In fact, the solution still makes perfect sense there (just think of a dry point), but the system of equations becomes parabolic. Since the properties of a parabolic system differ substantially from those of a hyperbolic (or elliptic) system, it is commonly believed that the appearance of parabolic points in the solution must necessarily be accompanied by a singularity. Furthermore, singularities already present in the solution are expected to interact in some way with the parabolic points. The main objective of this thesis is to investigate these ideas in the two aforementioned models of shallow water equations and semigeostrophic equations.

Acknowledgements

This thesis is part of the author's dual doctoral project in agreement between the University of Milan-Bicocca and the University of Surrey. This work has received funding from the European Union's Horizon 2020 research and innovation program under the Marie Skłodowska-Curie grant no 778010 IPaDEGAN and the Istituto Nazionale di Fisica Nucleare (INFN), and was carried out under the auspices of the GNFM Section of INdAM.

The author would like to thank his supervisory team (Prof. Giovanni Ortenzi, Prof. Ian Roulstone and Prof Tom Bridges) for their commendable work, as well as Prof. Volodya Rubtsov, for his efforts to provide the author with visibility in the scientific community. The author would also like to thank Prof. Roberto Camassa, Prof. Gregorio Falqui, and Prof. Marco Pedroni for their collaboration in part of the author's doctoral work, as well as Prof. Mike Cullen, Lewis Napper, and Prof. Martin Wolf for helpful discussions.

Special thanks go to Prof. Ian Roulstone who carefully followed the author's career in all its stages and provided invaluable help with administrative issues related to the dual doctorate programme. The author is indebted to Prof. Giovanni Ortenzi, whose support has often gone beyond the limits of scientific research to concern bureaucratic and personal aspects of the author's doctoral path.

Contents

Introduction

The singularities of a mathematical model are often its most intriguing features. They can reveal its limits of validity and suggest worthwhile new questions to ask on the underlying physical phenomenon. Singularities are especially relevant to fluid models. The Navier-Stokes existence and smoothness problem is one of the oldest on the Clay Institute's list, and has survived attacks by mathematicians for centuries. Since direct approaches have had limited success so far, researchers have turned to mathematical models in order to gain insights into the behavior of the parent equations. Models that derive from the Navier-Stokes equations through simplifying assumptions can isolate specific features such as nonlinear, dissipative, and dispersive effects, and allow one to investigate them separately. Also, studying models often leads to discovering mathematical structures and methods useful for their analysis. This, in turn, motivates new research questions on the parent system, where one expects to be able to find similar structures. This is the spirit of the present thesis.

Once a specific model is selected, there are at least two approaches to the study of its singularities: (*i*) one can either fix time and study the spatial structure of a singularity already present in the solution, or (*ii*) try to understand how a singularity develops as the solution evolves in time. We use the terminology *kinematic* and *dynamic* singularities to distinguish between the two approaches. In this thesis, we are interested in a specific feature of fluid dynamics equations, i.e., their variable symbol type. The Navier-Stokes equations are mixed type PDE system, being able to assume elliptical, parabolic or hyperbolic behaviour across the domain depending on the solution at hand. The a priori knowledge of the flow regime (elliptic or hyperbolic) expected in the solution is crucial to correctly specify a mathematical problem (i.e., boundary conditions) based on the Navier–Stokes or Euler (inviscid Navier–Stokes) equations. If the flow regime happens to change at some point, the mathematical problem breaks down, and the solution usually becomes unstable. Because of this, it is generally believed that parabolic transitions cannot occur as long as the solution remains smooth.

The parabolic regions thus acquire a special importance, because it is where singularities are expected to occur.

We investigate these ideas within two mathematical models. The first of them consists of the so-called *shallow water equations* on a variable bottom topography. This is one of the simplest models for gravity waves on the surface of water, and neglects both dissipative and dispersive effects. Parabolic regions are found where the water surface intersects the bottom, that is, at "dry points". The second model we consider is the so called semigeostrophic equations, a three-dimensional model for numerical weather prediction on a subcontinental scale. Parabolic regions here correspond to the early formation stages of a weather front. Two fairly different mathematical frameworks are employed for each model: asymptotic power expansions are at the core of investigations on dry points, while Monge–Ampère geometry will be the main tool for studying weather fronts.

The thesis is organized as follows. We shall discuss the shallow water equations and dry points in Chapter 1, drawing material from the recent work [10]. This chapter contains almost exclusively original material, except made for §1.1 that serves as an introduction on the wavefront expansion technique. The semigeostrophic equations will take the rest of the thesis. They are introduced in Chapter 2, along with a review of the set of hypothesis underlying their derivation [91]. The second part of the chapter deals with the duality structure of the semigeostrophic equations [16], and is closed by a revisitation of the Chynoweth and Sewell fronts in three spatial dimensions. This chapter contains no original results, and the only element of novelty is the style of presentation. Chapter 3) deals with Monge–Ampère geometry and its applications to the semigeostrophic equations. Novel material is contained in the sections 3.3 and 3.4, where Monge–Ampère geometry is employed in the reconstruction of the velocity field for a given generalized solution, and the comparison of Chynoweth–Sewell fronts to gas dynamical shocks. This material is part of an article in preparation. Chapter 4 presents recently published material on pseudo-Riemannian geometry of generalized solutions in the semigeostrophic context [30]. Apart from the introductory paragraph, everything in this chapter is original material. Chapter 5 contains unpublished material on the Eady problem, a classical example of a dynamic singularity, analysed in light of the geometry introduced in Chapters 3 and 4. The presentation style is the only original element in Sections 5.1 and 5.2, devoted to a review of the mathematical problem and its solution. Original results are concentrated in Sections 5.3, 5.4, and 5.5, where the Eady problem is analysed from the point of view of Monge–Ampère geometry, and the velocity field is retrieved from the knowledge of the generalized solution using a numerical algorithm.

Chapter 1

The shallow water equations

Shallow water equations (SWE) are a classic oceanographic model used in studies of long gravitational waves on the water surface. Plane waves are governed by

$$\frac{\partial \eta}{\partial t} + \frac{\partial u\eta}{\partial x} = 0, \qquad \frac{\partial u}{\partial t} + u\frac{\partial u}{\partial x} + \frac{\partial(\eta + b)}{\partial x} = 0, \tag{1.1}$$

where $\eta(x,t)$ represents the thickness of the water layer, $b(x)$ is the bottom elevation over a reference level, and $u(x,t)$ represents the depth-averaged horizontal component of the velocity field [15, 87]. All the variables involved in (1.1) are considered dimensionless. An alternative form of SWE is obtained by using the absolute elevation ζ of the water surface as the dependent variable instead of the depth η,

$$\zeta(x,t) = b(x) + \eta(x,t), \tag{1.2}$$

whereby,

$$\frac{\partial \zeta}{\partial t} + \frac{\partial}{\partial x}(u(\zeta - b)) = 0, \qquad \frac{\partial u}{\partial t} + u\frac{\partial u}{\partial x} + \frac{\partial \zeta}{\partial x} = 0. \tag{1.3}$$

SWE represent one of the simplest fluid models that contemplates the interaction between the free surface and the seabed: the system, normally hyperbolic, becomes parabolic locally at the points where the water surface touches the seabed. The type transition that occurs at the dry points and its relation to the singularities of the solution is the main topic of this chapter, in which we will review some of the results published in [10]. Specifically, we consider a class of initial conditions for (1.1) in which the globally continuous water surface has discontinuous slope. We will show that the evolution of these initial conditions is substantially different depending on whether the

singular point is located within the fluid-filled domain or on its boundary (i.e., on a dry point).

The chapter is organized as follows. We start by reviewing the dynamics of first order singularities in the hyperbolic regime and the wavefront expansion technique in Section 1.1. We apply these ideas in Section 1.2 to study the dynamics of first-order hyperbolic singularities which which arise from a specific class of initial conditions. We conclude this chapter with a discussion on first order singularities occurring at the boundary of the fluid-filled domain, i.e., at dry points, in Section 1.3. All the material in this chapter is drawn and adapted from the recent publication [10].

1.1 Overview of near-front local analysis

When a disturbance propagates in still water, information about the solution can be extracted by the wavefront expansion technique [92]. This method essentially consists of an asymptotic expansion of the solution near the "wavefront", i.e., the disturbance front, which delimits the disturbed region of the solution from the quiescent one (see Figure 1.1). In hyperbolic conditions, the wavefront expansion can provide information on the motion of the front and the slope of the upstream surface. The wavefront expansion consists of three steps: (i) a translating reference frame moving with the disturbance front is adopted; (ii) an asymptotic expansion of the solution is carried out upstream of the wave front; (iii) the asymptotic expansion is inserted in the SWE to obtain a system of ODEs governing the evolution of its time-dependent coefficients.

We consider a globally continuous piecewise smooth solution to the SWE, with a jump discontinuity of the k-th order derivatives across a curve $x = X(t)$ in the spacetime plane (Figure 1.1), and we make two key assumptions: (i) the curve $x = X(t)$ is a characteristic curve of the system; (ii) a constant state is established downstream of $x = X(t)$. In this setting, it is convenient to use the form (1.3) of the SWE, so the constant equilibrium state downstream of the wavefront is simply represented by $\zeta = 0$ and $u = 0$. We adopt the translating coordinate system

$$\xi = x - X(t), \tag{1.4}$$

which brings the SWE (1.3) to the form

$$\frac{\partial \zeta}{\partial t} - \dot{X}\frac{\partial \zeta}{\partial \xi} + \frac{\partial}{\partial \xi}(u(\zeta - b)) = 0, \qquad \frac{\partial u}{\partial t} + (u - \dot{X})\frac{\partial u}{\partial \xi} + \frac{\partial \zeta}{\partial \xi} = 0. \tag{1.5}$$

Then, we make the following ansatz on the form of the solution upstream of the wavefront, that is, for $\xi < 0$,

$$\begin{aligned} \zeta\big|_{\xi<0} &= \zeta_0(t) + \zeta_1(t)\xi + \zeta_2(t)\xi^2 + \dots, \\ u\big|_{\xi<0} &= u_0(t) + u_1(t)\xi + u_2(t)\xi^2 + \dots. \end{aligned} \tag{1.6}$$

This ansatz essentially assumes that the solution is one-sided analytic in a neighbourhood of the wave front; henceforth, we will refer to it as the *wavefront expansion* of the solution. Its coefficients are to be determined by substituting expansion (1.6) back into (1.5). Although ζ_0 and u_0 are formally included in these expansions, both their values are fixed to zero to ensure that the series (1.6) continuously connect to the constant state at $\xi = 0$. Here $u_k(t)$ and $\zeta_k(t)$ can be viewed as limits of the relevant derivatives of u and ζ for $\xi \to 0^-$, that is

$$u_k(t) = \lim_{\xi\to 0^-} \frac{1}{k!}\frac{\partial^k u}{\partial \xi^k}(\xi, t), \qquad \zeta_k(t) = \lim_{\xi\to 0^-} \frac{1}{k!}\frac{\partial^k \zeta}{\partial \xi^k}(\xi, t). \tag{1.7}$$

Similarly, the bottom topography is expanded in powers of ξ,

$$b(X(t)+\xi)\big|_{\xi<0} = b_0(t) + b_1(t)\xi + b_2(t)\xi^2 + \dots, \tag{1.8}$$

where the time dependent coefficients b_k are evaluated as

$$b_k(t) = \frac{1}{k!}\frac{\partial^k b}{\partial \xi^k}(0, t) = \frac{1}{k!}\frac{d^k b}{dx^k}(X(t)). \tag{1.9}$$

Plugging the expansions (1.6) and (1.8) into equations (1.5) and collecting the various powers of ξ yields two infinite hierarchies of ODEs,

$$\begin{aligned} \dot\zeta_n + (n+1)\Big[(u_0 - \dot X)\zeta_{n+1} - b_0 u_{n+1}\Big] - (n+1)b_{n+1}u_0 + \\ + (n+1)\sum_{k=1}^{n}(\zeta_k - b_k)u_{n+1-k} = 0, \end{aligned} \tag{1.10}$$

$$\dot u_n + (n+1)\Big[\zeta_{n+1} + (u_0 - \dot X)u_{n+1}\Big] + \sum_{k=1}^{n} k\, u_k u_{n+1-k} = 0 \tag{1.11}$$

for $n \geq 1$, while, using $u_0 = \zeta_0 = 0$, $n = 0$ yields

$$-\dot X\zeta_1 - b_0 u_1 = 0, \qquad \zeta_1 - \dot X u_1 = 0. \tag{1.12}$$

Equations (1.12) can be used to determine the wavefront speed $\dot{X}$: if the solution has discontinuous first derivatives across the wavefront, at least one among u_1 and ζ_1 is different from zero; this in turn implies that the coefficient matrix of the linear system (1.12) is singular, that is

$$\dot{X}^2 + b_0 = 0, \tag{1.13}$$

where $b_0(\xi, t) \equiv b(X(t))$. This first order nonlinear equation can in principle be solved to get the wavefront motion, which will depend solely on the bottom topography (with the choice of sign of $\dot{X}$ set by the initial data). The same result is obtained if the solution has a k-th order jump, with $k < \infty$, across the wavefront.

The structure of equations (1.10)–(1.11) is such that, for any fixed n, variables of order up to $n+1$ are involved. However, higher order variables enter the system in such a way that both can be canceled by taking a single linear combination of the two equations. This becomes more transparent by writing system (1.10)–(1.11) in matrix form

$$\dot{\mathbf{U}}_n + (n+1)A\mathbf{U}_{n+1} + \mathbf{F}_n = 0, \qquad A = \begin{pmatrix} -\dot{X} & -b_0 \\ 1 & -\dot{X} \end{pmatrix}, \tag{1.14}$$

where $\mathbf{U}_n = (\zeta_n, u_n)^T$, and $\mathbf{F}_n$ comprises variables of order up to n. The matrix A is singular due to relation (1.13); thus, multiplying the above equation on the left by the eigenvector $(1, \dot{X})$ corresponding to the eigenvalue 0 of A, we get

$$\dot{\zeta}_n + \dot{X}\dot{u}_n + (1, \dot{X})\mathbf{F}_n = 0, \tag{1.15}$$

which is free of higher order variables. One of the two equations of order $(n-1)$ can now be used to replace ζ_n with u_n, or vice versa. For example, from (1.11) we get

$$\zeta_n = \dot{X}u_n - \frac{1}{n}\left(\dot{u}_{n-1} + \sum_{k=1}^{n-1} k u_k u_{n-k}\right). \tag{1.16}$$

Once (1.16) is substituted into (1.15), a first order differential equation is eventually obtained, where neither ζ_n nor any higher order variable appear, and the only unknown is u_n. By iterating this procedure, one can in principle solve the hierarchy (1.10)–(1.11) up to any desired order.

The case $n = 1$ is of crucial importance for the prediction of gradient catastrophes at the wavefront. Setting $n = 1$, equations (1.15) and (1.16) give

$$\dot{\zeta}_1 + \dot{X}\dot{u}_1 + 2(\zeta_1 - b_1)u_1 + \dot{X}u_1^2 = 0, \qquad \zeta_1 = \dot{X}u_1\,, \tag{1.17}$$

The bottom term b_1 in (1.17) can be expressed in terms of $X(t)$ from

$$2\ddot{X} + b_1 = 0, \tag{1.18}$$

which is obtained by taking the time derivative of (1.13). Using (1.18), equations (1.17) may be combined so as to obtain two independent ODEs for u_1 and ζ_1,

$$\dot{u}_1 + \frac{3}{2}u_1^2 + \frac{5\ddot{X}}{2\dot{X}}u_1 = 0, \qquad \dot{\zeta}_1 + \frac{3}{2\dot{X}}\zeta_1^2 + \frac{3\ddot{X}}{2\dot{X}}\zeta_1 = 0. \tag{1.19}$$

The Riccati-like mapping

$$\zeta_1 = \frac{2}{3}\dot{X}(t)\frac{\dot{\phi}(t)}{\phi(t)}$$

linearizes the second equation in (1.19),

$$5\dot{\phi}(t)\ddot{X}(t) + 2\ddot{\phi}(t)\dot{X}(t) = 0\,,$$

which yields the quadrature solution

$$\zeta_1(t) = \frac{(\dot{X}(0)/\dot{X}(t))^{3/2}}{\zeta_1(0)^{-1} + \frac{3}{2}\dot{X}(0)^{3/2}I(t)}, \quad \text{where} \quad I(t) = \int_0^t \dot{X}(s)^{-5/2}\,\mathrm{d}s. \tag{1.20}$$

It is often more convenient to focus on the dependence of the surface slope ζ_1 on the wavefront position rather than on time. By making use of (1.13) and the change of variable $t = X^{-1}(x)$, the integral above can be expressed as

$$I(x) = \int_{X^{-1}(x_0)}^{X^{-1}(x)} \dot{X}^{-\frac{5}{2}}(t')\,\mathrm{d}t' = \int_{x_0}^{x} \dot{X}^{-\frac{7}{2}}(X^{-1}(x'))\,\mathrm{d}x' = \int_{x_0}^{x} (-b(x'))^{-\frac{7}{4}}\,\mathrm{d}x', \tag{1.21}$$

where x_0 is the initial condition $X(0) = x_0$. Thus, equation (1.20) takes the form

$$\zeta_1(t) = \frac{(b(x_0)/b(x))^{3/4}}{\zeta_1(0)^{-1} + \frac{3}{2}(-b(x_0))^{3/4}I(X)}\Big|_{x=X(t)}. \tag{1.22}$$

Of course, this construction relies on the existence of the inverse function $X^{-1}(x)$, and is well defined only for as long as the wavefront advances in the same direction.

The last equation allows one to predict the development of a gradient catastrophe at the wavefront location based on the given initial conditions and the bottom shape. It was used by Greenspan [40] to investigate the

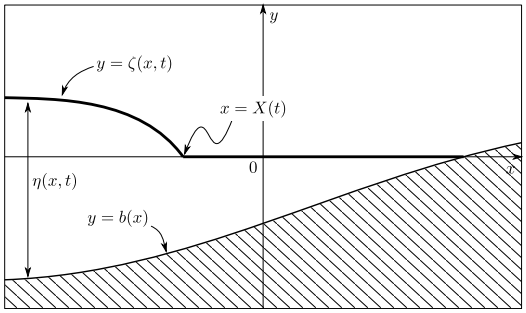

Figure 1.1: A wavefront $x = X(t)$ advancing towards the shore, i.e., $\dot{X} > 0$. It bounds a constant region on its right, where the fluid is quiescent, and a perturbed region on its left.

breaking of a wavefront approaching a sloping beach with a straight bottom, and by Gurtin [41], who extended Greenspan's analysis to general bottom shapes. In addition to the initial value $\zeta_1(0)$, the breaking conditions depend on the bottom topography, and in particular on its slope immediately close to the shoreline, which turns out to play a crucial role [41] (see also [42]).

1.2 Non-frontlike initial conditions

In the previous section we reviewed the wavefront expansion technique with application on a generic wavefront propagating in still medium. In this section we consider wavefronts generated by a class of initial data containing a singularity in the slope of the water surface.

In many physical interesting situations, the initial conditions for the SWE are piecewise smooth and globally continuous. The wavefront expansion technique provides a valuable tool for their analysis, especially in the presence of nontrivial bottom topographies. When $\frac{\partial b}{\partial x} = 0$, the shallow water system admits Riemann invariants and simple waves. This allows to look for singularities from a global perspective, and compute the least shock time associated with given initial conditions (see [12]). On the other hand, when $\frac{\partial b}{\partial x} \neq 0$, the SWE are inhomogeneous, and Riemann variables are no longer invariant along characteristic curves. Simple waves are unavailable as well, hence for general bottom shapes only the local viewpoint of the wavefront expansion for the study of singularities is in general available for analytical advances. We describe here how the machinery of the wavefront expansion applies to a prototypical example, and discuss the special case of a flat bottom in the next section.

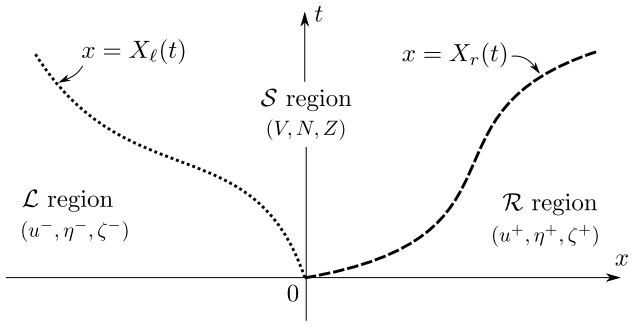

Figure 1.2: Sketch of trajectories of the two wavefronts $x = X_r(t)$ and $x = X_\ell(t)$ arising from piecewise differentiable initial conditions (1.23)–(1.24). This data class identifies three distinct regions, $\mathcal{L}$, $\mathcal{S}$ and $\mathcal{R}$, in the spacetime plane. The field variables of the SWE are denoted differently in each of the three regions so defined.

1.2.1 Piecewise smooth initial conditions

We assign initial conditions as follows: the fluid is initially at rest, and the water surface is composed by a constant part on the right, glued at the origin to a general smooth part on the left,

$$u(x, 0) = 0 \qquad \text{for any } x \in \mathbb{R} \tag{1.23}$$

and

$$\zeta(x, 0) = \begin{cases} \zeta_{\text{in}}(x) & \text{for } x \leq 0, \\ 0 & \text{for } x > 0. \end{cases} \tag{1.24}$$

Here, $\zeta_{\text{in}}(x)$ is a smooth function in $(-\infty, 0]$, subject to the condition $\zeta_{\text{in}}(0) = 0$, which ensures the global continuity of the initial data. We further require that $\zeta'_{\text{in}}(0) \neq 0$ (and bounded), so that the water surface has a discontinuous first derivative, a corner, at $x = 0$ for $t = 0$. Finally, we assume that $\zeta_{\text{in}}(x) > b(x)$ in some neighbourhood of $x = 0$. This assumption ensures that the SWE are locally hyperbolic so that a couple of distinct characteristics pass through the origin in the spacetime plane (see Figures 1.2 and 1.4). These characteristics satisfy

$$\begin{cases} \dot{X}_r = u + \sqrt{\eta} \\ X_r(0) = 0 \end{cases}, \qquad \begin{cases} \dot{X}_\ell = u - \sqrt{\eta} \\ X_\ell(0) = 0 \end{cases}. \tag{1.25}$$

As remarked in [92], higher order singularities in the solution to a hyperbolic system propagate along its characteristic curves. Because of this, the singular point initially located at $x = 0$ splits into a pair of singular points transported

along the two characteristic curves $x = X_r(t)$ and $x = X_\ell(t)$ after the initial time. Thus, for $t > 0$, and as long as shocks (gradient catastrophes) do not arise, the solution is composed by three distinct smooth parts defined by the above pair of characteristics (see Figure 1.2). We append the superscript "+" to variables in the region $\mathcal{R}$, that is for $x > X_r(t)$, characterized by the constant state $u^+(x,t) = 0$, $\zeta^+(x,t) = 0$. Similarly we denote with a "−" the variables in the region $\mathcal{L}$ ($x < X_\ell(t)$) which we regard as known functions of (x,t), i.e., $(u^-(x,t), \zeta^-(x,t))$ solve the SWE with initial condition $\zeta(x,0) = \zeta_{\text{in}}(x)$ on $x < 0$. Finally, we denote with capital letters V, N, Z the solution in the middle region $\mathcal{S}$, that is for $X_\ell(t) < x < X_r(t)$. We call this portion of the spacetime plane, enclosed by the two singular points, the *shoulder* [13, 12].

Even if no singularity were to occur in the $\mathcal{L}$ region, loss of regularity could certainly happen in the shoulder region $\mathcal{S}$. Although we cannot generally rule out the onset of singularities in the interior of $\mathcal{S}$, we focus here on its boundaries, i.e. the characteristic curves $x = X_\ell(t)$ and $x = X_r(t)$. The machinery described in the previous paragraph is immediately applicable to the right wavefront $x = X_r(t)$, whereas it requires some further adaptation to be used for $x = X_\ell(t)$ because it propagates across a nonconstant state. Thus, we focus on the solution near the right boundary of the shoulder region, $x = X_r(t)$.

Piecewise initial conditions (1.24) and (1.23) introduce an element of novelty with respect to the analysis of Gurtin [41] mentioned in the previous section. The setting considered by Gurtin consists of a travelling wavefront stemming from some unspecified initial conditions. The wavefront analysis is then applied to this dynamical setting, starting from some generic time, arbitrarily picked as the initial one. On the other hand, if the fluid is initially at rest, the wavefronts arise as a consequence of the fluid relaxation.

The shoulder region is empty at the initial time, so special attention is needed to identify initial conditions for the wavefront equations (1.19), which we rewrite here for convenience,

$$\dot{u}_1 + \frac{3}{2}u_1^2 + \frac{5\ddot{X}}{2\dot{X}}u_1 = 0, \qquad \dot{\zeta}_1 + \frac{3}{2\dot{X}}\zeta_1^2 + \frac{3\ddot{X}}{2\dot{X}}\zeta_1 = 0. \tag{1.26}$$

Note that neither u_1 or η_1 are defined at $t = 0$, as they represent the limits of the relevant quantities for $x \to X_r(t)^-$ with $X_\ell(t) < x < X_r(t)$. However, a consistent definition for $u_1(0)$ and $\zeta_1(0)$ can still be given in terms of appropriate limits as $(x,t) \to (0,0)$ from the interior of $\mathcal{S}$, provided the gradients

∇Z and ∇V are continuous up to the boundary $\partial\mathcal{S}$. Namely we define

$$\begin{cases} u_1(0) \equiv \lim_{(x,t)\to(0,0)} \frac{\partial V}{\partial x} \\ \zeta_1(0) \equiv \lim_{(x,t)\to(0,0)} \frac{\partial Z}{\partial x} \end{cases} \qquad \text{with } (x,t) \in \mathcal{S}. \tag{1.27}$$

These values are computed from the given initial conditions as follows. From the continuity hypothesis on the solution, the fields Z, V, as well as their gradients, can be extended to the boundary $\partial\mathcal{S}$ along the two characteristics X_r, X_ℓ by taking the appropriate limits (the same applies to $\zeta^-, u^-, \zeta^+, u^+$ on their respective domains), and we have

$$\zeta^-(X_\ell(t), t) = Z(X_\ell(t), t), \qquad 0 = Z(X_r(t), t). \tag{1.28}$$

Taking a time derivative, these two relations give

$$\frac{\partial \zeta^-}{\partial x}(X_\ell(t), t)\dot{X}_\ell(t) + \frac{\partial \zeta^-}{\partial t}(X_\ell(t), t) = \frac{\partial Z}{\partial x}(X_\ell(t), t)\dot{X}_\ell + \frac{\partial Z}{\partial t}(X_\ell(t), t), \tag{1.29}$$

and

$$0 = \frac{\partial Z}{\partial x}(X_r(t), t)\dot{X}_r + \frac{\partial Z}{\partial t}(X_r(t), t). \tag{1.30}$$

The continuity of $Z, \nabla Z$ on the closure of $\mathcal{S}$ implies

$$\lim_{t\to 0^+} \frac{\partial Z}{\partial x}(X_\ell(t), t) = \lim_{t\to 0^+} \frac{\partial Z}{\partial x}(X_r(t), t) \equiv \zeta_1(0), \tag{1.31}$$

and

$$\lim_{t\to 0^+} \frac{\partial Z}{\partial t}(X_\ell(t), t) = \lim_{t\to 0^+} \frac{\partial Z}{\partial t}(X_r(t), t). \tag{1.32}$$

Therefore, taking the difference of equations (1.29) and (1.30), and passing to the limit $t \to 0^+$ yields an expression for the initial value $\zeta_1(0)$,

$$\zeta_1(0) = \frac{\frac{\partial \zeta^-}{\partial x}(0,0)\dot{X}_\ell(0) + \frac{\partial \zeta^-}{\partial t}(0,0)}{\dot{X}_\ell(0) - \dot{X}_r(0)}. \tag{1.33}$$

This expression may be simplified by observing that, since the velocity field u is identically 0 at $t = 0$, equation (1.25) implies $\dot{X}_r(0) = -\dot{X}_\ell(0)$. Furthermore, the continuity equation (i.e., the first equation in (1.3)) implies $\frac{\partial \zeta}{\partial t}(x, 0) = 0$ for $x \neq 0$, so (1.33) simplifies to

$$\zeta_1(0) = \frac{1}{2}\frac{\partial \zeta^-}{\partial x}(0,0) \equiv \frac{\zeta'_{\text{in}}(0^-)}{2}, \tag{1.34}$$

where we have used the notation $\zeta'_{\text{in}}(0^-)$ to denote a one-sided derivative. Interestingly, immediately after the initial time, the slope of the water surface

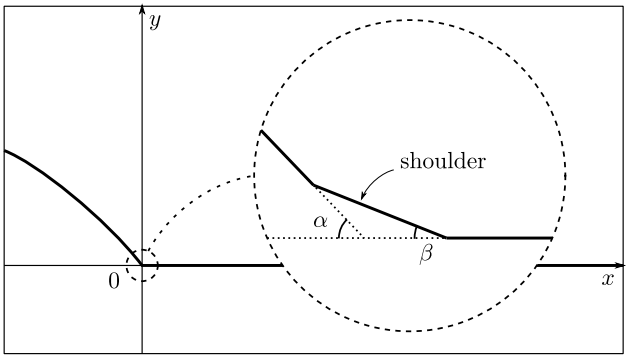

Figure 1.3: Sketch of the solution at a very early stage $t \ll 1$. The shoulder part is approximately a segment with slope $\tan(\beta) \simeq -\zeta_1(0)$, half of the surface slope in the region $\mathcal{L}$, $\tan(\alpha) \simeq -\zeta_0'(0^-)$.

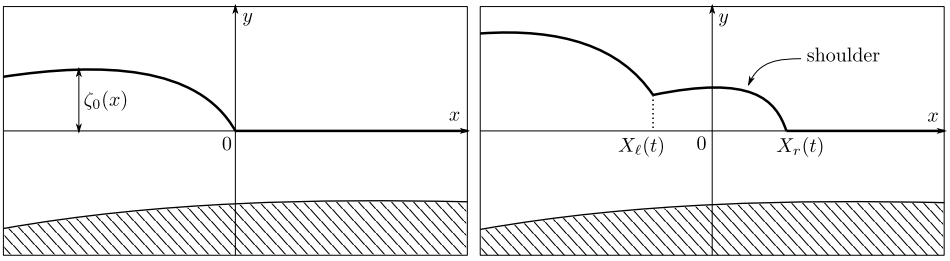

Figure 1.4: Sketch of initial conditions of class (1.24) (left) and a snapshot of their evolution at an instant $t > 0$ prior to any shock development (right). The shoulder part of the solution, not present at the initial time, is enclosed by the two moving points $x = X_r(t)$ and $x = X_\ell(t)$ for $t > 0$.

in region of the shoulder is half that of the neighboring region $\mathcal{L}$ (see Figure 1.3). Thus, according to (1.34), the initial slope of the shoulder part $\zeta_{\text{in}}'(0^-)$ equals the algebraic mean of the slope values on the two sides. As $\zeta_1 = \dot{X}_r u_1$, we also obtain the corresponding initial condition for u_1,

$$u_1(0) = \frac{\zeta_{\text{in}}'(0^-)}{2\dot{X}_r(0)} = \frac{\zeta_{\text{in}}'(0^-)}{2\sqrt{-b(0)}}. \tag{1.35}$$

Here equation (1.13) has been used in the last equality. Thus, together with these initial conditions, (1.20) (or (1.22)) determine the onset of a gradient catastrophe at the wavefront $x = X_r(t)$. The gradient blow-up rate depends on the bottom shape $b(x)$ as well as the given initial data $\zeta_{\text{in}}(x)$. Of particular relevance is the sign of the surface slope $\zeta_{\text{in}}'(0^-)$ near the singular point $x = 0$, which markedly affects the solution behaviour.

1.2.2 The case of a flat bottom

In this section we examine the special case $\frac{\partial b}{\partial x} = 0$, which corresponds to a horizontal seabed. Under these conditions, the SWE with initial conditions (1.23)–(1.24) can be solved using the method of characteristics [12]. This allows us to compare check the consistency of the assumptions and results of the previous section in a particular case where the exact solution is available. We start by recalling the problem set-up and solution [12]. In this setting, we use the form (1.1) of the SWE, and assign initial conditions on the depth function by

$$\eta(x,0) = \begin{cases} \eta_{\text{in}}(x) & \text{for } x < 0, \\ Q & \text{for } x > 0, \end{cases} \tag{1.36}$$

where $Q > 0$ is a constant. We insist that the velocity field is everywhere zero at the initial time. For $t > 0$, the solution is composed of the three regions represented in Figure 1.2. To determine the solution within the shoulder region, we write the SWE (1.1) in the characteristic form,

$$\partial_t R_\pm + \lambda_\pm \partial_x R_\pm = 0, \tag{1.37}$$

where the characteristic velocities $\lambda_\pm$ and the Riemann invariants $R_\pm$ are respectively defined by

$$\lambda_\pm = u \pm \sqrt{\eta}, \qquad R_\pm = u \pm 2\sqrt{\eta}. \tag{1.38}$$

The basic property of Riemann invariants is

$$R_\pm = \text{constant} \qquad \text{along} \qquad \frac{dx}{dt} = \lambda_\pm. \tag{1.39}$$

Characteristics with tangent λ_- intersect the curve $x = X_r(t)$ (because it is a characteristic curve with tangent λ_+). Therefore, since the solution is constant for $x > X_r(t)$, the Riemann invariant R_- is constant throughout the regions $\mathcal{R}$ and $\mathcal{S}$ as well as on their common boundary[1], and takes the value

$$R_- = -2\sqrt{Q}. \tag{1.40}$$

Specifically, in the shoulder region we have

$$V = 2\sqrt{N} - 2\sqrt{Q}. \tag{1.41}$$

Characteristic curves of the family λ_+ satisfy, within the shoulder region,

$$\frac{dx}{dt} = V + \sqrt{N}. \tag{1.42}$$

[1]This is generally true for sufficiently small times, i.e., as long as shocks do not occur.

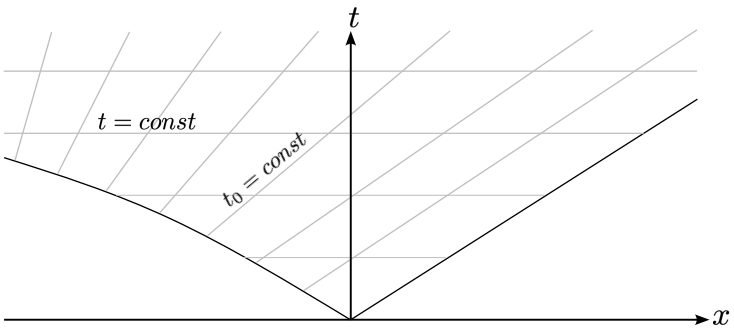

Figure 1.5: Space-time diagram of the shoulder region for small times and initial data $u(x,0) = 0$ with indication of the coordinate grid (t_0, t). The shoulder boundaries correspond to $t_0 = t$ and $t_0 = 0$.

The velocity V may be eliminated using 1.41, so this equation becomes

$$\frac{dx}{dt} = 3\sqrt{N} - 2\sqrt{Q}. \tag{1.43}$$

Note that the r.h.s. in this equation is constant because both R_+ and R_- are constant along the characteristics of the λ_+-family.

We assign initial conditions for this equation along the left boundary of the shoulder region, that is

$$x(t_0) = X_\ell(t_0) \qquad \text{for} \qquad t = t_0. \tag{1.44}$$

Therefore, we obtain a parametric expression for positive characteristics,

$$x = X_\ell(t_0) + (3\sqrt{N} - 2\sqrt{Q})(t - t_0). \tag{1.45}$$

where t acts as the curve parameter, and t_0 acts as a label for the characteristic curves. Note that the right boundary of $\mathcal{S}$ is the positive characteristic labelled by $t_0 = 0$. As long as shocks do not occur, the parameters (t_0, t) can be used as a local coordinate system in the shoulder region (see Figure 1.5). In other words, we think of (1.45) as defining a change of variables $(t_0, t) \mapsto (x, t)$ in the shoulder region. Because the field variables N and V are constant along positive characteristics, we have, in the new coordinates $\frac{\partial N}{\partial t} = \frac{\partial V}{\partial t} = 0$, and

$$N = N(t_0), \qquad V = V(t_0). \tag{1.46}$$

Furthermore, as long as the solution is continuous, the value of the field variables is fixed by the solution η^-, u^- in the $\mathcal{L}$ region. Therefore, we obtain

$$N(t_0) = \eta^-(X_\ell(t_0), t_0), \qquad V(t_0) = u^-(X_\ell(t_0), t_0), \tag{1.47}$$

which represents the full solution in the shoulder region. Gradient catastrophes are identified by the condition

$$\infty = \frac{\partial N}{\partial x} \equiv \frac{\frac{\partial N}{\partial t_0}}{\frac{\partial x}{\partial t_0}}, \tag{1.48}$$

which corresponds to

$$\frac{\partial x}{\partial t_0} = 0 \qquad \text{with} \qquad \frac{\partial N}{\partial t_0} \neq 0. \tag{1.49}$$

It follows from (1.45) that the first time at which the characteristic t_0 intersects another characteristic of the same family is

$$t = t_0 + \frac{3\sqrt{N(t_0)} - 2\sqrt{Q} - \dot{X}(t_0)}{3\frac{d\sqrt{N}}{dt_0}}. \tag{1.50}$$

The infimum of (1.50) over t_0 provides the catastrophe time for the shoulder part of the solution [2]

We are now ready to show consistency of the assumptions and results of the previous section within the closed form solution obtained here. To begin with, we note that the gradient of the field variables ∇N and ∇V is continuous on the closure of $\mathcal{S}$ for sufficiently small times. Indeed, using (t_0, t) as coordinates,

$$\frac{\partial N}{\partial x} = \frac{\frac{dN}{dt_0}}{\frac{\partial x}{\partial t_0}}, \qquad \frac{\partial N}{\partial t} = -\frac{\frac{\partial x}{\partial t}}{\frac{\partial x}{\partial t_0}}\frac{dN}{dt_0}, \tag{1.51}$$

which shows that ∇N is continuous as long as $\frac{\partial x}{\partial t_0} \neq 0$, i.e., as long as shocks do not arise. A similar result holds for V. Observe that $\frac{\partial x}{\partial t_0}$ is well defined on both the left boundary $t_0 = t$ and the right boundary $t_0 = 0$ of the shoulder:

$$\left.\frac{\partial x}{\partial t_0}\right|_{t_0=t} = \dot{X}_\ell(t) - 3\sqrt{N(t)} + 2\sqrt{Q}, \tag{1.52}$$

$$\left.\frac{\partial x}{\partial t_0}\right|_{t_0=0} = -2\sqrt{Q} + 3t\left.\frac{\mathrm{d}\sqrt{N(t_0)}}{\mathrm{d}t_0}\right|_{t_0=0}. \tag{1.53}$$

Furthermore, since $\dot{X}_\ell(0) = -\sqrt{Q}$ and $N(0) = Q$,

$$\frac{\partial x}{\partial t_0}(0,0) = -2\sqrt{Q}. \tag{1.54}$$

[2] When computing this infimum, one has must ensure that (1.45) evaluated at (1.50) falls within the shoulder region.

Thus we see that x_{t_0} is continuous and different from zero up to the boundaries of the shoulder domain for sufficiently small times (i.e., as long as shocks do not occur), and so are the gradients ∇N and ∇V.

Secondly, in this example a direct computation can be performed of the water surface's slope in the shoulder region at the initial time. Indeed, by using (1.47), we get

$$\left.\frac{dN}{dt_0}\right|_{t_0=0} = \left.\frac{\mathrm{d}\eta^-(X_\ell(t_0),t_0)}{\mathrm{d}t_0}\right|_{t_0=0} = \frac{\partial\eta^-}{\partial t}(0,0) + \dot{X}_\ell(0)\frac{\partial\eta^-}{\partial x}(0,0). \tag{1.55}$$

On the other hand, the initial condition $u(x,0) = 0$, combined with the continuity equation, implies $\frac{\partial\eta^-}{\partial t}(0,0) = 0$, so

$$\left.\frac{dN}{dt_0}\right|_{t_0=0} = \dot{X}_\ell(0)\frac{\partial\eta^-}{\partial x}(0,0) = -\sqrt{Q}\,\eta'_{\mathrm{in}}(0). \tag{1.56}$$

Combining (1.54) and (1.56), we conclude that

$$\frac{\partial N}{\partial x}(0,0) = \frac{\frac{dN}{dt_0}}{\frac{\partial x}{\partial t_0}} = \frac{\eta'_{\mathrm{in}}(0)}{2}, \tag{1.57}$$

in accordance with (1.34).

1.3 Dry points

In this section, we consider a family of initial data for (1.1) of the kind

$$\eta(x,0) = \begin{cases} \eta_{\mathrm{in}}(x) & \text{for } x < 0, \\ 0 & \text{for } x > 0, \end{cases} \tag{1.58}$$

with

$$u(x,0) = 0, \qquad \forall x \in \mathbb{R}. \tag{1.59}$$

We further require $\eta_{\mathrm{in}}(0) = 0$ in order to ensure continuity of the initial data. From a physical point of view, this setup mimics a shoreline placed at $x = 0$ at the initial time. At dry points ($\eta = 0$), the SWEs become parabolic, and the characteristic velocities in the (x,t)-plane coincide,

$$\lambda_\pm = u. \tag{1.60}$$

For this reason, singular points found in the dry region do not split and give rise to a shoulder as hyperbolic singular points would. Since generally not all

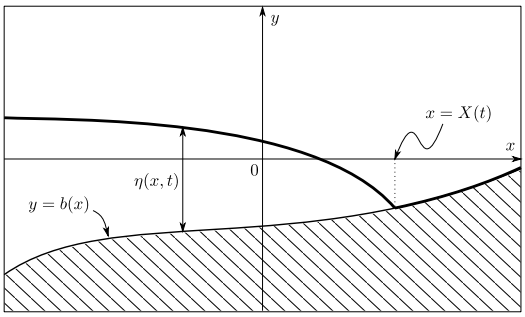

Figure 1.6: Schematic of moving dry point $x = X(t)$, separating a fluid-filled region on its left, where the water surface is strictly above the bottom, and a dry region to its right, where surface and bottom curves coincide.

derivatives of $\eta(x, 0)$ will be continuous at the shoreline, this will represent a singular point. After the initial instant, the shoreline, which we will denote by $x = X(t)$, will be advected by the velocity field.

In the terminology of gas dynamics often used for hyperbolic systems, $\eta(x, t)$ plays the role of a gas density, and the dry state on one side of the shoreline is understood as a vacuum. For this reason, the term "vacuum boundary" will also be used when referring to $x = X(t)$. We consider the setup depicted in Figure 1.6, where the shoreline $x = X(t)$ separates a fluid-filled region to its left from a dry region on its right. In the dry region, we have by definition $\eta = 0$, while the velocity field must satisfy the inhomogeneous Hopf equation,

$$\frac{\partial u}{\partial t} + u\frac{\partial u}{\partial x} + \frac{db}{dx} = 0. \tag{1.61}$$

To study the local behavior of the solution near the shoreline, we adopt the co-moving coordinate system (1.4), so that the SWE (1.1) read

$$\frac{\partial \eta}{\partial t} - \dot{X}\frac{\partial \eta}{\partial \xi} + \frac{\partial u\eta}{\partial \xi} = 0, \qquad \frac{\partial u}{\partial t} + (u - \dot{X})\frac{\partial u}{\partial \xi} + \frac{\partial}{\partial \xi}(\eta + b) = 0. \tag{1.62}$$

Next, we introduce the wavefront expansion of the solution in the wet region (i.e., $\xi < 0$). We consider a power series representation for η, u and b in the form

$$\eta(X(t) + \xi, t)\big|_{\xi<0} = \eta_0(t) + \eta_1(t)\xi + \eta_2(t)\xi^2 + \dots \tag{1.63}$$

$$u(X(t) + \xi, t)\big|_{\xi<0} = u_0(t) + u_1(t)\xi + u_2(t)\xi^2 + \dots \tag{1.64}$$

$$b(X(t) + \xi)\big|_{\xi<0} = b_0(t) + b_1(t)\xi + b_2(t)\xi^2 + \dots \tag{1.65}$$

with coefficients defined by

$$u_k(t) := \lim_{\xi\to 0^-} \frac{1}{k!}\frac{\partial^k u}{\partial \xi^k}(\xi, t), \qquad \eta_k(t) := \lim_{\xi\to 0^-} \frac{1}{k!}\frac{\partial^k \eta}{\partial \xi^k}(\xi, t), \tag{1.66}$$

n	(I)	(II)
0	$0 = 0$	$\dot{u}_0 + b_1 + \eta_1 = 0$
1	$\dot{\eta}_1 + 2u_1\eta_1 = 0$	$\dot{u}_1 + 2b_2 + u_1^2 + 2\eta_2 = 0$
2	$\dot{\eta}_2 + 3u_2\eta_1 + 3u_1\eta_2 = 0$	$\dot{u}_2 + 3b_3 + 3u_1u_2 + 3\eta_3 = 0$
3	$\dot{\eta}_3 + 4u_3\eta_1 + 4u_2\eta_2 + 4u_1\eta_3 = 0$	$\dot{u}_3 + 4b_4 + 2u_2^2 + 4u_1u_3 + 4\eta_4 = 0$
$\vdots$	$\vdots$	$\vdots$

Table 1.1: The first equations (I)–(II) for the unknown coefficients of the formal series (1.63)–(1.64) for $u(X(t)+\xi,t)$, $\eta(X(t)+\xi,t)$ and $b(X(t)+\xi)$.

$$b_k(t) := \frac{1}{k!}\frac{\partial^k b}{\partial \xi^k}(0,t) = \frac{1}{k!}\frac{d^k b}{dx^k}(X(t)). \tag{1.67}$$

We set $\eta_0 = 0$ in order to ensure continuity of the water surface at the shoreline. Inserting the power expansions (1.63)–(1.65) in equations (1.62), and collecting terms of the same order $O(\xi^n)$, we obtain the following infinite hierarchy of ODEs: for $n = 0$,

$$\dot{u}_0 + b_1 + \eta_1 = 0\,, \tag{1.68}$$

and for $n > 0$,

$$\dot{\eta}_n + (n+1)(u_0 - \dot{X})\eta_{n+1} + (n+1)\sum_{k=1}^{n} u_k\eta_{n+1-k} = 0, \tag{1.69}$$

$$\dot{u}_n + (n+1)(u_0 - \dot{X})u_{n+1} + (n+1)(\eta_{n+1} + b_{n+1}) + \sum_{k=1}^{n} k u_l u_{n+1-k} = 0\,. \tag{1.70}$$

Note that for $n = 0$ system (1.62) yields a single equation, as the η-equation in (1.62) is automatically satisfied and hence provides no information. Since $\dot{X} = u_0$, the hierarchy simplifies to

$$\dot{\eta}_n + (n+1)\sum_{k=1}^{n} u_k\eta_{n+1-k} = 0, \tag{I}$$

$$\dot{u}_n + (n+1)(\eta_{n+1} + b_{n+1}) + \sum_{k=1}^{n} k\, u_l u_{n+1-k} = 0. \tag{II}$$

Table 1.1 shows the explicit form of the first few equations in this hierarchy.

Remark 1.3.1. A closer look to this hieararchy of ODEs reveals some interesting features [10]:

1. Using $u_0 = \dot{X}$, equation (1.68) can be written as

$$\ddot{X} + b_1 + \eta_1 = 0\,. \tag{1.71}$$

This relates the acceleration of the wavefront (the vacuum boundary) $x = X(t)$ to the slope of the water surface behind it, which is precisely $b_1 + \eta_1$.

2. A truncation of the infinite hierarchy (I)-(II) to some order $n = N$ would correspond to a reduction of the continuum governed by the SWE to a finite number of degrees of freedom dynamics, with η and u being polynomial functions of x, respectively of order $N + 1$ and N. To this end, it is clear that a necessary condition for this to happen is that the bottom topography be a polynomial of degree N, as opposed to an infinite power series. This is reflected by the structure of the hierarchy (II), which would lose the terms $\{b_n\}$ (generated by the bottom topography for $n > N$) that make equations (II) inhomogeneous. Homogeneity would allow to set the corresponding series coefficients $\{\eta_{n+1}, u_n\}$ to zero if so initially, thereby reducing the power series solutions to mere ξ-polynomials. However, the very same structure of (II) shows that the condition of polynomial bottom profiles in general cannot be sufficient for an exact truncation of the series: even in the absence of the $\{b_n\}$ terms the equations in hierarchy (II) for $n > N$ are not truly homogeneous, since functions of lower index series-coefficient $\{(u_n, \eta_n)\}$ for $n < N$ enter themselves as inhomogeneous forcing functions in all the remaining $n > N$ infinite system.

3. The case of a quadratic bottom profile,

$$b(x) = c_0 + c_1 x + c_2 x^2/2 \tag{1.72}$$

for some constants c_0, c_1 and c_2, say, is clearly special (and often the one considered in the literature). In fact, for this case $b_1 = c_1 + c_2\, X(t)$, $b_2 = c_2$ (and of course $b_n = 0$ for $n > 2$). With null initial data $\eta_{n+1}(0)$ and $u_n(0)$ for $n > 1$, equations (I)-(II) are consistent with $\eta_{n+1}(t) = 0$ and $u_n(t) = 0$ for $t > 0$, $n > 1$, and hence the hierarchy truncates to a finite, closed system for the four unknowns $X(t), \eta_1(t), \eta_2(t)$, and $u_1(t)$,

$$\begin{cases} \ddot{X} + c_2 X + c_1 + \eta_1 = 0\,, \\ \dot{\eta_1} + 2u_1\eta_1 = 0\,, \\ \dot{\eta_2} + 3u_1\eta_2 = 0\,, \\ \dot{u_1} + u_1^2 + 2\eta_2 + c_2 = 0\,. \end{cases} \tag{1.73}$$

4. For $n = 1$ equation (I) gives

$$\dot{\eta}_1 + 2u_1\eta_1 = 0\,; \tag{1.74}$$

this implies that if the initial conditions are such that $\eta_1(0) = 0$, then $\eta_1(t) = 0$ at all subsequent times, at least for as long as the solution maintains the regularity assumed for the convergence of the power series expressions (1.63)–(1.64) for all the variables involved. Note that since $\eta\big|_{\xi=0}$ is the layer thickness at the front $\xi = 0$, the condition

$$\eta_1 \equiv \left.\frac{\partial\eta}{\partial\xi}\right|_{\xi=0} = 0 \tag{1.75}$$

implies that the derivative of the free surface matches that of the bottom at the dry point, that is, the free surface is tangent to the bottom there.

This last point in Remark 1.3.1 plays an important role in the classification and properties of the solutions with vacuum points, to which we turn next. Specifically, we analyze below the two cases $\eta_1 = 0$ and $\eta_1 < 0$ separately; in the literature these two different cases are commonly referred to as the "nonphysical" and "physical" vacuum points, respectively (see, e.g., [56]), and we will henceforth conform to this terminology.

1.3.1 Nonphysical vacuum points

We first consider the case $\eta_1(0) = 0$, for which the water surface is tangent to the bottom at the vacuum boundary. From equation (1.71) it follows that the motion of the wavefront is solely determined by the bottom shape as solution to the problem

$$\ddot{X} + b'(X(t)) = 0, \qquad X(0) = x_0, \qquad \dot{X}(0) = u_0(0). \tag{1.76}$$

Upon multiplying this equation by $\dot{X}(t)$, it can be integrated once, to get

$$\frac{\dot{X}^2}{2} + b(X(t)) = \text{constant}. \tag{1.77}$$

Thus, the motion of a nonphysical vacuum point turns out to be the same as that of a (unit mass) particle located at x in a potential $b(x)$: the particle is repelled by local maxima of the bottom topography, and is attracted by local minima. This motion enters the equations of hierarchy (II) by providing the $\{b_n(t)\}$ terms, which drive the evolution of the u- and η-coefficients by

entering their respective equation as prescribed forcing functions of time, since (1.76) is no longer coupled to the $\{u_n, \eta_n\}$ equations.

The special case of a quadratic form for bottom profiles is further simplified for non-physical vacuum. In particular, if $c_2 = 0$, i.e., the bottom is a straight line, the first equation in system (1.73) reduces to $\ddot{X} + c_1 = 0$ and the motion of the vacuum point $X(t)$ is that of uniform acceleration. If the bottom has a symmetric parabolic shape, $c_1 = 0$ and the same equation becomes $\ddot{X} + c_2 X = 0$. Thus, the motion of the non-physical vacuum point $X(t)$ depends on the concavity of the parabolic bottoms: if it is upward, the motion is oscillatory harmonic, while if it is downward the point $X(t)$ is exponentially repelled from the origin at $x = 0$.

For general bottom profiles that can be expressed as (convergent) power series, the case of non-physical vacuum yields a remarkable property for the infinite hierarchy (I)-(II). When $\eta_1 = 0$, the coupling term $u_2\eta_1$ in equation $(2, \mathrm{I})$ of Table 1.1 is suppressed and equations $(1, \mathrm{II})$ and $(2, \mathrm{I})$ of Table 1.1, become a *closed* system of two nonlinear differential equations for the two unknowns $u_1(t)$ and $\eta_2(t)$,

$$\dot{u}_1 + u_1^2 + 2\eta_2 + 2b_2 = 0, \qquad \dot{\eta}_2 + 3u_1\eta_2 = 0. \tag{1.78}$$

As remarked above, the function $b_2(t)$ can be thought of as an assigned time dependent forcing function, defined by

$$b_2(t) = \frac{1}{2}\, b''(X(t)), \tag{1.79}$$

and hence determined by the solution $X(t)$ satisfying the uncoupled equation (1.76). System (1.78) admits an immediate reduction: the first equation is of Riccati type, hence the substitution

$$u_1 = \frac{\dot{\phi}}{\phi} \tag{1.80}$$

for a new dependent variable $\phi(t)$ allows the reduction of system (1.78) to a single second order ODE,

$$\ddot{\phi} + \frac{2C}{\phi^2} + 2\, b_2\, \phi = 0\,, \tag{1.81}$$

since the $\dot{\eta}_2$ equation can be integrated at once,

$$\dot{\eta}_2 + \frac{3\dot{\phi}}{\phi}\eta_2 = 0 \quad \Rightarrow \quad \eta_2 = \frac{C}{\phi^3}\,, \tag{1.82}$$

for some constant C.

Remark 1.3.2. A few comments are now in order [10]:

1. A glance at Table (1.1) and at system (I)-(II) shows that beyond (1.78) the equations of the hierarchy constitute a recursive system of *linear* differential equations for the index-shifted pair of unknowns $\{u_n, \eta_{n+1}\}$. In fact, the condition $\eta_1 = 0$ eliminates the term containing u_{n+1} from the summation (II) making the system closed at any order n with respect to all the dependent variables up to that order, and, more importantly, past the first equation pair the system is linear, as its coefficients are determined only by the lower index variables u_i, η_j, with $i < n$ and $j < n+1$. For this reason, the possible occurrence of movable singularities, determined by the initial conditions, is entirely governed by the leading order nonlinear pair of equations (1.78). (For the present case of nonphysical vacuum, this extends to non-flat bottoms an analogous result in [12]).

2. If one assumes that u, η and the bottom topography at the initial time are in fact (one-sided) analytic functions admitting the expansion (1.63)–(1.65), then the Cauchy–Kovalevskaya Theorem (see, e.g. [37]) assures that the solution of the initial value problem of system (1.62) exist and is analytic for some finite time determined by the initial interval of convergence, i.e., by the initial values of the series' coefficients. Depending on these initial data, the maximum time of existence could then be completely determined by the reduced system (1.78) and 1.79), since, as per the previous comment, the infinite system of equations past the (u_1, η_2)-pair is linear and so its singularities coincide with those of the forcing functions, which in turn are entirely determined by this pair.

3. Equation (1.81) is isomorphic to that of a point (unit) mass subject to a force field $-(2C/\phi^2 + b_2\phi)$, which in general will be time-dependent through b_2. This can have interesting consequences. For instance, the coefficient b_2 can be time-periodic by the choice

$$b(x) = c_0 + \frac{c_2}{2}x^2 + \frac{c_4}{4}x^4\,, \tag{1.83}$$

which makes equation (1.76) for $X(t)$ that of a Duffing oscillator [81],

$$\ddot{X} + c_2 X + c_4 X^3 = 0\,. \tag{1.84}$$

As well known (see e.g. [81]) this equation has periodic solutions depending on the constants c_1 and c_2 and on its initial conditions. In

this case, for some classes of initial data, equation (1.81) can be viewed as that of a parametrically forced nonlinear oscillator, and resonances due to the periodic forcing $b_2(t) = c_2 + 3c_4\big(X(t)\big)^2$ from the solutions of (1.84) could arise, which in turn could generate nontrivial dynamics. This would further enrich the types of time evolution of PDE solutions supported by this class of bottom profiles with nonphysical vacuum initial data.

Next, we will switch our focus to the case of a physical vacuum, which is significantly different as some of the properties of its nonphysical counterpart cease to hold.

1.3.2 Physical vacuum points

When the surface of the water intersects the seabed with a finite angle other than zero, we speak of a *physical vacuum point*. In this case, $\eta_1(0) \neq 0$, and equation (1.71) is no longer sufficient to determine the motion of the wavefront $X(t)$. As a consequence, the whole hierarchy of equations (I)–(II), for the unknowns $X(t), u_n(t), \eta_n(t)$, $n = 0, 1, \dots$ is now completely coupled as (I)–(II) involve variables of order $n+1$ at any fixed $n \geq 0$.

This issue does not occur in the hyperbolic setup considered in Section 1.1, where the singularity propagates in a constant state background. Indeed, whether $\zeta_1 = 0$ or $\zeta_1 \neq 0$, equations (1.12) can always determine the motion of the wavefront $X(t)$. In fact, the coefficient u_0, which is zero due to the quiescent conditions established downstream of the wave front, does not enter the equations (1.12).

In the present setting, however, the lack of information about the velocity field in the dry region makes the coefficient u_0 unknown a priori. Note that this is also true for non-physical vacuum points; however, thanks to the condition $\eta_1 = 0$, (1.68) can be used to determine the motion of the wave front and, consequently, its velocity u_0.

There is no preferential way to assign the velocity field in the dry region as a particular solution to (1.61). Moreover, even if the velocity field in the dry region was known, this would be useless to determine u_0. Indeed, the velocity field is generically discontinuous at physical dry boundary. This result, already proved in [13] (§ 3.2) for a horizontal bottom, is extended here to more general topography:

Proposition 1.3.1. *If the water surface is transverse to the bottom at the vacuum point $x = X(t)$ and analytic for $x < X(t)$, and the velocity field u is initially continuous, then u is discontinuous at $x = X(t)$ in a neighbourhood of the initial time.*

Proof. To see this, Taylor expand the velocity field for $\xi > 0$,

$$u\big|_{\xi>0} = u_0^{\mathrm{r}}(t) + u_1^{\mathrm{r}}(t)\xi + u_2^{\mathrm{r}}(t)\xi^2 + \dots, \qquad u_k^{\mathrm{r}}(t) = \lim_{\xi\to 0^+} \frac{1}{k!}\frac{\partial^k u}{\partial \xi^k}(\xi, t). \quad (1.85)$$

The coefficients of this expansion evolve in time according to (1.61), which gives

$$\dot{u}_n^{\mathrm{r}} + (n+1)b_{n+1} + \sum_{k=1}^{n} k\, u_k^{\mathrm{r}} u_{n+1-k}^{\mathrm{r}} = 0. \qquad (\mathrm{II}^{\mathrm{r}})$$

For $n = 0$, (II) and (II$^{\mathrm{r}}$) yield

$$b_1 + \eta_1 + \dot{u}_0 = 0, \qquad b_1 + \dot{u}_0^{\mathrm{r}} = 0, \quad (1.86)$$

and these two equations together imply

$$\frac{d[\![u]\!]}{dt} := \dot{u}_0^{\mathrm{r}} - \dot{u}_0 = \eta_1 \neq 0, \quad (1.87)$$

where $[\![u]\!] := u_0^{\mathrm{r}} - u_0$ denotes the jump of the velocity field at the dry boundary. This means that , in the plane $(t, [\![u]\!])$, the graph of $[\![u]\!](t)$ is never tangent to the t-axis. Moreover, since η_1 has constant sign (it is negative in the situation considered so far), the velocity jump $[\![u]\!](t)$ can vanish vanish at most once. Hence, adjusting for a possible time shift, we see that the discontinuity of the velocity field at the vacuum/dry point has to emerge at $t = 0^+$. □

Another way of stating this result is that a shock wave always forms at a physical vacuum point for the velocity-like component of the system. However, as pointed out in [13], this is a non-standard kind of shock. Besides being uncoupled to the other dependent variable (in this case the water surface that maintains its initial continuity for a nonzero time interval) it also does not involve dissipation of conserved quantities, in general. It is indeed not too difficult to verify that the Rankine-Hugoniot conditions for mass, momentum and energy are all satisfied at the same time for this non-standard shock.

1.4 Summary of Chapter 1

In this chapter, we examined a class of singularities of the SWE model with variable seabed. Specifically, we considered first order singularities in the depth field and studied their temporal evolution. After a review of the traveling front type initial conditions (Section 1.1), widely studied in the literature

[40, 41], we considered the evolution of generic initial conditions containing first order singular points in the depth field. We have shown that singular points in the hyperbolic regime generally undergo splitting into a pair of traveling fronts, and we have derived the shock conditions at the leading front location through the wavefront local analysis (Section 1.2). We have validated our results in the particular case of a flat and horizontal bottom, where the general solution to the SWEs is available in closed form. Finally, we applied the same ideas to study first-order singular points that lie at the edge of the fluid-filled region (Section 1.3). Since the SWE system becomes parabolic at the dry points, the singularities present there do not undergo splitting and are advected by the fluid velocity. We then highlighted the fundamental differences between dry boundaries where the water surface is tangent to the seabed (nonphysical vacuum), and dry points where the water surface is transverse to the seabed (physical vacuum). Most importantly, the motion of nonphysical vacuum boundaries is solely dependent on the local shape of the seabed, and is not influenced by the adjacent mass of fluid. By contrast, the motion of physical vacuum boundaries depends on the motion of the fluid throughout its domain, and cannot therefore be determined by a local analysis.

Chapter 2

The semigeostrophic equations

Large-scale atmospheric flows are dominated by the Coriolis force and the pressure force. When these opposing forces balance each other exactly, the resulting equilibrium flow is called geostrophic. Real physical systems are usually found in nearly geostrophic conditions. However, the exact balance is only a rough approximation of reality, and does not allow predictions to be made. Several models for "nearly geostrophic" flows have been proposed over the years. The basic idea of all these models is that the acceleration of the fluid is small, being equal to the difference between two almost equal opposing forces. The common progenitors of all these models are the so-called *hydrostatic primitive equations* (HPEs), which descend from the Euler equations through a standard set of assumptions like those of shallow and hydrostatic atmosphere [91].

The hypothesis of nearly geostrophic equilibrium is handled differently by the various models. One of the most important example is represented by the so-called *semigeostrophic equations*. This is a model for subcontinental flows, and is derived from the HPEs through Hoskins' "geostrophic momentum approximation" [47].

Semigeostrophic equations have attracted much interest over the past fifty years due primarily to their ability to represent weather fronts (see for example [46, 19, 23]). Physically, a weather front is a (relatively) thin region in the atmosphere where the fluid thermodynamic properties change suddenly. From the mathematical point of view, a weather front in the semigeostrophic context is understood as a singular surface within the flow across which the field variables experience a jump discontinuity. In the seminal work [16], Chynoweth and Sewell gave the first characterization of semigeostrophic fronts in terms of catastrophe theory. Specifically, they advised a new method to model weather fonts using singular solutions to the semigeostrophic equations. By far, is not clear the extent to which the Chynoweth and Sewell

fronts share the properties of more classical constructions (say for example [19]). For this reason, we shall call them *Chynoweth–Sewell fronts*.

This chapter is structured as follows. We start with a review of the HPEs and the main hypotheses underlying their derivation [46, 91]. Next, we introduce the geostrophic momentum approximation and the semigeostrophic equations [47]. We proceed with a discussion on the vorticity-streamfunction formulation of the semigeostrophic equations [79] and the role of the Legendre transformation [16]. We conclude the chapter with a discussion on Chynoweth–Sewell fronts [16], and a consistent way to extend this notion to three spatial dimensions.

2.1 Overview on the parent model (HPEs)

In this section, we present the HPEs in the form given in [46] and review the main assumptions underlying their derivation. Atmospheric flows of geophysical interest are governed by the Euler equations in a rotating reference frame,

$$\frac{D\mathbf{u}}{Dt} + 2\boldsymbol{\Omega} \times \mathbf{u} + \frac{1}{\rho}\nabla p + \nabla\phi = 0, \tag{2.1}$$

$$\frac{\partial \rho}{\partial t} + \nabla \cdot (\rho \mathbf{u}) = 0, \tag{2.2}$$

$$\frac{D\hat{s}}{Dt} = 0. \tag{2.3}$$

The unknowns are the velocity field $\mathbf{u}$, the density ρ, the pressure p, and the specific entropy $\hat{s}$. The pseudo-vector $\boldsymbol{\Omega}$ represents the Earth's angular velocity, and the term $2\boldsymbol{\Omega}\times\mathbf{u}$ represents the Coriolis force. The given function ϕ, called the *geopotential*, combines the effects of gravity and the centrifugal force. The Earth's surface (i.e., the mean sea level) is modeled as a geoid, i.e., one of the level sets of the geopotential, which is customarily taken as $\phi = 0$. The operator D/Dt is the *material time derivative*. Its evaluation on a scalar function $F(t, x, y, z)$ yields the rate of change of F along the particles trajectories. In other words,

$$\frac{DF}{Dt} := \frac{d}{dt} F(t, \mathbf{r}(t, \mathbf{r}_0)), \tag{2.4}$$

where $\mathbf{r}$ represents the position vector, and $\mathbf{r}(t, \mathbf{r}_0)$ represents the trajectory of the particle found at $\mathbf{r}_0$ for $t = 0$.

Equations (2.1)–(2.3) involve more unknowns than variables and thus do not form a closed system. This issue is normally overcome by prescribing a

"caloric equation of state" relating pressure, density, and entropy. Assuming that the atmosphere consists of a single polytropic ideal gas, we are given a caloric equation of state in the form

$$\hat{s} = c_v \log \frac{p}{\rho^\gamma}, \qquad \gamma = \frac{c_p}{c_v}, \qquad R = c_p - c_v, \tag{2.5}$$

where c_p and c_v represent the specific heats of the gas (air) (see for example formula (6.39) of [92]).

Before introducing any approximation, we need to specify the geometry of the fluid domain under consideration. We shall not consider the whole Earth's atmosphere as our domain, but rather select a portion of the atmosphere in the northern hemisphere. The spatial extension of this domain is limited by the need to represent it globally with a co-rotating Cartesian frame. In practice, it is customary to consider a portion of the atmosphere of sufficiently small extension to be able to consider the sea level ($\phi = 0$) on which it lies flat.

The co-rotating Cartesian frame is built as follows. Let (x, y, h) a cartesian coordinate system based at a point on the sea level $\phi = 0$ with the h-axis directed along $\nabla\phi$. The remaining two coordinate axes (x, y) form a right-handed system with x increasing eastwards and y increasing northwards. The meaning of (x, y, h) is that of "linearized" longitude, latitude, and elevation above the sea level respectively. In these coordinates, the geopotential ϕ is usually approximated as

$$\phi = gh, \tag{2.6}$$

where g is a constant. We denote the compenents of the relative fluid velocity in this frame by

$$\mathbf{u} = (u, v, \dot{h}). \tag{2.7}$$

Moreover, the Earth's angular velocity reads

$$\mathbf{\Omega} = (0, \Omega\cos(\varphi), \Omega\sin(\varphi)), \tag{2.8}$$

so that the Coriolis force becomes

$$2\mathbf{\Omega} \times \mathbf{u} = 2(w\Omega\cos\varphi - v\Omega\sin\varphi, u\Omega\sin\varphi, -u\Omega\cos\varphi). \tag{2.9}$$

Here, Ω represents the Earth spin frequency, and φ represents the latitude.

The Earth angular velocity is simplified by a first set of assumptions: (i) the atmosphere can be safely assumed "shallow", since the horizontal length scale is much bigger than the vertical scale in geophysical flows, and this amounts to neglecting the $\cos(\varphi)$ term in (2.8) (see [91]); (ii) on horizontal scales of the order of $\sim 10^3$ km, it is acceptable to assume $f := 2\Omega\sin(\varphi)$

constant across the fluid domain ("f-plane approximation"). Under these assumptions, the Earth angular velocity becomes

$$\mathbf{\Omega} = (0, 0, f/2), \tag{2.10}$$

and the Coriolis force becomes

$$2\mathbf{\Omega} \times \mathbf{u} = (-fv, fu, 0). \tag{2.11}$$

In meteorology, it is customary to use a a quantity known as *potential temperature* to keep track of entropy. The potential temperature is defined as the temperature a parcel of air would have at the current entropy and the reference pressure. In other words,

$$\theta := \left.\frac{\partial \hat{h}}{\partial \hat{s}}\right|_{p=p_0}, \tag{2.12}$$

where $\hat{h}(\hat{s}, p) := \hat{e} + p/\rho$ is the specific enthalpy of the fluid. For a polytropic ideal gas, we have [92]

$$\hat{h}(\hat{s}, p) = \frac{\gamma}{\gamma - 1} p^{\frac{\gamma-1}{\gamma}} e^{\hat{s}/c_p}, \tag{2.13}$$

whereby,

$$\theta = \frac{1}{R} p_0^{\frac{\gamma-1}{\gamma}} e^{\hat{s}/c_p}. \tag{2.14}$$

Because θ is a function of the entropy alone, it is advected by an isentropic flow. Therefore, equation (2.3) may be equivalently written as

$$\frac{D\theta}{Dt} = 0. \tag{2.15}$$

The most important hypothesis underlying the derivation of the HPEs is that of a hydrostatic atmosphere. It amounts to neglecting the vertical component of the fluid acceleration, i.e.,

$$\frac{1}{\rho}\frac{\partial p}{\partial h} + \frac{\partial \phi}{\partial h} = 0. \tag{2.16}$$

and, using (2.6), may be written

$$\frac{\partial p}{\partial h} = -\rho g. \tag{2.17}$$

Since ρ and g are strictly positive quantities, equation (2.17) implies that p is a monotone function of h and so there exists the inverse function. Therefore,

it makes sense to use p (or a monotone function thereof) as the "vertical" coordinate in place of h. Because p is a function of space and time, the coordinate change that we wish to accomplish is a time-depending one. This aspect poses some complications, e.g., the relative velocity and acceleration do not transform as vector fields. This issue is overcome in classical literature with an extensive use of the chain rule (see for example [50, 91]).

In this manuscript, we follow the work of Hoskins and Bretherton [46], where the physical elevation h is replaced by a monotone function of p known as the *pseudo-height* and defined as

$$z = z_a \left[1 - \left(\frac{p}{p_0} \right)^{\frac{\gamma-1}{\gamma}} \right]. \tag{2.18}$$

Here, z_a represents the pseudo-height (or thickness) of the atmosphere, which depends on reference values for the pressure p_0 and density ρ_0[1],

$$z_a = \frac{\gamma}{\gamma - 1} \frac{p_0}{\rho_0 g}. \tag{2.19}$$

Remark 2.1.1. *The physical significance of the pseudo-height is clarified by observing that $z = h$ in an hydrostatic atmosphere with uniform entropy. Also, z_a represents the actual thickness of the atmosphere in these conditions. To see this, set $\hat{s} = const.$ in (2.5), whereby*

$$\frac{p}{\rho^\gamma} = \frac{p_0}{\rho_0^\gamma}. \tag{2.20}$$

Next, use this equation to eliminate ρ in (2.17) to get

$$\left(\frac{p_0}{p} \right)^{1/\gamma} \frac{\partial p}{\partial h} = -\rho_0 g. \tag{2.21}$$

Upon setting $p = p_0$ and $\rho = \rho_0$ at $h = 0$, integration of both sides yields,

$$h = \frac{\gamma}{\gamma - 1} \frac{p_0}{\rho_0 g} \left[1 - \left(\frac{p}{p_0} \right)^{\frac{\gamma-1}{\gamma}} \right], \tag{2.22}$$

which is precisely (2.18).

The change of variables we wish to accomplish is

$$(t, x, y, h) \mapsto (t, x, y, z). \tag{2.23}$$

[1] p_0 and ρ_0 represent the average value of the pressure and density at the sea level (over the surface $\phi = 0$).

It is implied that p will no longer be a dependent variable, but rather a known function of z. Its place in the set of dependent variables is taken by h, or, equivalently, by ϕ. It must be noted the Jacobian relation

$$\frac{\partial z}{\partial h} = \frac{\partial(t,x,y,z)}{\partial(t,x,y,h)} = \left(\frac{\partial(t,x,y,h)}{\partial(t,x,y,z)}\right)^{-1} = \left(\frac{\partial h}{\partial z}\right)^{-1}. \tag{2.24}$$

We start with the hydrostatic relation (2.16), which, by a straightforward application of the chain rule, is shown to become

$$\frac{1}{\rho}\frac{\partial p}{\partial z} + \frac{\partial \phi}{\partial z} = 0. \tag{2.25}$$

Moreover, using (2.18) and recalling (2.14), it is possible to show that

$$\frac{1}{\rho}\frac{\partial p}{\partial z} = -g\frac{\theta}{\theta_0}, \tag{2.26}$$

so the hydrostatic balance condition (2.25) may be written

$$g\frac{\theta}{\theta_0} = \frac{\partial \phi}{\partial z}. \tag{2.27}$$

The change of variable for the other equations of the system (2.1)–(2.3) is explicitly worked out in [50]. We simply note that the relative fluid velocity becomes

$$\mathbf{u} = (u, v, w), \tag{2.28}$$

where

$$w := \frac{Dz}{Dt} = \frac{\partial z}{\partial t} + u\frac{\partial z}{\partial x} + v\frac{\partial z}{\partial y} + \dot{h}\frac{\partial z}{\partial h}, \tag{2.29}$$

and the continuity equation (2.2) becomes

$$\frac{\partial r}{\partial t} + \frac{\partial ru}{\partial x} + \frac{\partial rv}{\partial y} + \frac{\partial rw}{\partial z} = 0. \tag{2.30}$$

Here, the quantity

$$r := \rho\frac{\partial h}{\partial z} \tag{2.31}$$

is known as the *pseudo-density*, and can be shown to be a function of z only. Indeed, from (2.18) it follows

$$\frac{\partial z}{\partial h} = \frac{\rho}{\rho_0}\left(\frac{p}{p_0}\right)^{-1/\gamma}, \tag{2.32}$$

and therefore

$$r \equiv \rho \frac{\partial h}{\partial z} = \rho_0 \left(\frac{p}{p_0} \right)^{1/\gamma} = \rho_0 \left(1 - \frac{z}{z_a} \right)^{\frac{1}{\gamma - 1}}. \tag{2.33}$$

Using this result in the continuity equation (2.30) yields

$$r \left(\frac{\partial u}{\partial x} + \frac{\partial v}{\partial y} + \frac{\partial w}{\partial z} \right) + w \frac{\partial r}{\partial z} = 0. \tag{2.34}$$

Hoskins [46] shows that neglecting the term $\partial r / \partial z$ in the continuity equation is a form of Boussinesq approximation, and is acceptable on the typical scale of validity of the other assumptions. Thus, the continuity equations reduces to the nondivergence statement on the new relative velocity,

$$\frac{\partial u}{\partial x} + \frac{\partial v}{\partial y} + \frac{\partial w}{\partial z} = 0. \tag{2.35}$$

Remark 2.1.2. *Despite the fact that they are denoted the same way, the relative fluid velocities (2.7) and (2.28) are not the same vector field. By this we mean that they are not pushed forward to one another by the change of variables (2.23). This property is restored if a 4-dimensional spacetime view is taken, and the fluid velocity is augmented by a unit component in the time direction.*

The HPEs given in [47] are

$$\frac{Du}{Dt} - fv + \frac{\partial \phi}{\partial x} = 0, \tag{2.36}$$

$$\frac{Dv}{Dt} + fu + \frac{\partial \phi}{\partial y} = 0, \tag{2.37}$$

$$g \frac{\theta}{\theta_0} = \frac{\partial \phi}{\partial z}, \tag{2.38}$$

$$\frac{\partial u}{\partial x} + \frac{\partial v}{\partial y} + \frac{\partial w}{\partial z} = 0, \tag{2.39}$$

$$\frac{D\theta}{Dt} = 0. \tag{2.40}$$

They form a closed system of five equations in the five unknowns (u, v, w, ϕ, θ).

2.2 The geostrophic momentum approximation

A geophysical flow is said to be in geostrophic equilibrium if pressure forces are exactly balanced by the Coriolis force. In these conditions, the net force

acting on parcels is zero and they experience no acceleration. In other words,

$$u = -\frac{1}{f}\frac{\partial \phi}{\partial y} =: u_g, \qquad v = \frac{1}{f}\frac{\partial \phi}{\partial x} =: v_g, \tag{2.41}$$

where u_g and v_g are respectively called the zonal and the meridional component of the *geostrophic wind*. In general flow regimes, the actual velocity field can be decomposed in its geostrophic and ageostrophic parts,

$$u = u_g + u_a, \qquad v = v_g + v_a, \tag{2.42}$$

and typically $|u_a| \ll |u_g|$ and $|v_a| \ll |v_g|$. The semigeostrophic equations are obtained from the HPEs by the so called *geostrophic momentum approximation*. Formally, this amounts to replacing u and v by their respective geostrophic parts in the acceleration terms appearing in (2.36), (2.37), but neither in D/Dt nor in the Coriolis term,

$$\frac{Du_g}{Dt} - fv + \frac{\partial \phi}{\partial x} = 0, \tag{2.43}$$

$$\frac{Dv_g}{Dt} + fu + \frac{\partial \phi}{\partial y} = 0, \tag{2.44}$$

$$g\frac{\theta}{\theta_0} = \frac{\partial \phi}{\partial z}, \tag{2.45}$$

$$\frac{\partial u}{\partial x} + \frac{\partial v}{\partial y} + \frac{\partial w}{\partial z} = 0, \tag{2.46}$$

$$\frac{D\theta}{Dt} = 0. \tag{2.47}$$

The geostrophic momentum approximation is justified by Hoskins [47] using the following argument. The momentum balance equations (2.36) – (2.37) may be written in the form

$$u = u_g - \frac{1}{f}\frac{Dv_g}{Dt} - \frac{1}{f^2}\frac{D^2u}{Dt^2}, \tag{2.48}$$

$$v = v_g + \frac{1}{f}\frac{Du_g}{Dt} - \frac{1}{f^2}\frac{D^2v}{Dt^2}, \tag{2.49}$$

which can be concatenated to express u and v as a series in f^{-1} with coefficients depending on the geostrophic wind and its time derivatives,

$$u = u_g - \frac{1}{f}\frac{Dv_g}{Dt} - \frac{1}{f^2}\frac{D^2u_g}{Dt^2} + \frac{1}{f^3}\frac{D^3v_g}{Dt^3} + \ldots, \tag{2.50}$$

$$v = v_g + \frac{1}{f}\frac{Du_g}{Dt} - \frac{1}{f^2}\frac{D^2v_g}{Dt^2} - \frac{1}{f^3}\frac{D^3u_g}{Dt^3} + \dots. \tag{2.51}$$

For subcontinental mid-latitude atmospheric flows, the Coriolis parameter is usually large ($f \approx 10^{-4}s^{-1}$). This means that each of the terms in the above expansion is much smaller than the preceding one, and truncation at any finite order makes sense. In particular, the geostrophic momentum approximation is equivalent to retaining terms up to $O(f^{-1})$,

$$u \cong u_g - \frac{1}{f}\frac{Dv_g}{Dt}, \qquad v \cong v_g + \frac{1}{f}\frac{Du_g}{Dt}, \tag{2.52}$$

which precisely corresponds to (2.43), (2.44).

The semigeostrophic equations admit two important Lagrangian invariants. The first one is the total geostrophic energy,

$$\frac{D}{Dt}(K_g + V) = 0, \tag{2.53}$$

which consists of the sum of the geostrophic kinetic energy $K_g = \frac{1}{2}(u_g^s + v_g^2)$ and the potential energy $V = -gz\theta/\theta_0$. The second quantity is the so called geostrophic potential vorticity q_g (or simply *potential vorticity*),

$$\frac{Dq_g}{Dt} = 0, \tag{2.54}$$

which represents the geostrophic counterpart of Ertel's potential vorticity, and is defined by and is defined by

$$q_g = \boldsymbol{\zeta}_g \cdot \nabla\theta. \tag{2.55}$$

Here,

$$\boldsymbol{\zeta}_g = \left(-\frac{\partial v_g}{\partial z} + \frac{\partial(u_g, v_g)}{\partial(y,z)}, \frac{\partial u_g}{\partial z} + \frac{\partial(u_g, v_g)}{\partial(z,x)}, 1 + \frac{\partial v_g}{\partial x} - \frac{\partial u_g}{\partial y} + \frac{\partial(u_g, v_g)}{\partial(x,y)}\right), \tag{2.56}$$

represents the geostrophic *absolute vorticity*.

2.3 Dimensionless variables

In this manuscript, we adopt a dimensionless set of variables, introduced in [85], which clears the semigeostrophic equations from all physical constants. We take $f^{-1}, L, f^2L^2/g, f^2L^2, \theta_0$ as measure units for time, horizontal length, vertical length, geopotential, and potential temperature respectively, with L

being some unspecified horizontal length scale. Using the same notation for a variable and its dimensionless counterpart, the semigeostrophic system (2.43) – (2.47) becomes

$$\frac{Du_g}{Dt} - v + \frac{\partial \phi}{\partial x} = 0, \tag{2.57}$$

$$\frac{Dv_g}{Dt} + u + \frac{\partial \phi}{\partial y} = 0, \tag{2.58}$$

$$\theta = \frac{\partial \phi}{\partial z}, \tag{2.59}$$

$$\frac{\partial u}{\partial x} + \frac{\partial v}{\partial y} + \frac{\partial w}{\partial z} = 0, \tag{2.60}$$

$$\frac{D\theta}{Dt} = 0, \tag{2.61}$$

where

$$u_g = -\frac{\partial \phi}{\partial y}, \qquad v_g = \frac{\partial \phi}{\partial x}. \tag{2.62}$$

2.4 Vorticity-streamfunction formulation

The semigeostrophic equations can be cast in a way which is formally analogous to the vorticity-streamfunction formulation for 2D Euler flows. In this section, we introduce the vorticity-streamfunction problem for the semigeostrophic equations in physical variables, and later discuss the advantages brought by the (partial) Legendre transform and the use of dual variables. In this subject, the following notation is classically used,

$$X := x + v_g, \qquad Y := y - u_g, \qquad Z := \theta, \tag{2.63}$$

with X and Y physically representing the two horizontal components of the absolute momentum associated with the geostrophic wind. Using these variables, one may write the evolution equations (2.57), (2.58) and (2.61) in the form,

$$\frac{DX}{Dt} = u_g, \qquad \frac{DY}{Dt} = v_g, \qquad \frac{DZ}{Dt} = 0. \tag{2.64}$$

Moreover, equations (2.62) and (2.59) may be written, using (2.63), as

$$X = \frac{\partial P}{\partial x}, \qquad Y = \frac{\partial P}{\partial y}, \qquad Z = \frac{\partial P}{\partial z}, \tag{2.65}$$

where

$$P := \frac{x^2}{2} + \frac{y^2}{2} + \phi, \tag{2.66}$$

is called the *modified geopotential*. Combining the definition of q_g (2.55) with (2.63) and (2.65), one can express the potential vorticity in terms of the modified geopotential alone. This relation occurs in the peculiar form of a Monge–Ampère equation,

$$\det \mathrm{Hess}\,(P) = q_g. \tag{2.67}$$

Remark 2.4.1. *A widely accepted definition for a 2-dimensional Monge–Ampère equation can be found in p. 324 of [18] (see also [55]). This definition is consistently extended to equations having three or more independent variables as follows. A Monge–Ampère equation is a nonlinear partial second order of the second order in which the highest (second) order derivatives only appear as combinations of the minors of the Hessian matrix of the dependent variable [55]. Equation (2.67) fits in this definition because all the second derivatives of the dependent variable $P(x, y, z)$ appear in a minor (the whole matrix determinant) of the Hessian of P.*

If P is regarded as the "streamfunction" and q_g as the "vorticity", equation (2.67) is a nonlinear analogue of the familiar Poisson equation found in 2D Euler flows. Also, equation (2.54) replaces the vorticity equation found in the same context. Equations (2.67) and (2.54) can be considered as a closed system of two equations in two unknowns P, q_g provided that we can express the material time derivative operator in (2.54) in terms of P. To this aim, use (2.65) to write equations (2.64) in the matrix form

$$\frac{D\nabla P}{Dt} = \mathbf{u}_g, \tag{2.68}$$

where we have denoted

$$\nabla P := (\partial_x P, \partial_y P, \partial_z P), \qquad \mathbf{u}_g := \Big(y - \partial_y P, \partial_x P - x, 0\Big). \tag{2.69}$$

More explicitly, equation (2.68) reads

$$\frac{\partial}{\partial t}\nabla P + \mathrm{Hess}\,(P)\mathbf{u} = \mathbf{u}_g, \tag{2.70}$$

where $\mathrm{Hess}\,(P) := \nabla\nabla P$ is the Hessian matrix of P with respect to the space variables. Assuming that $\mathrm{Hess}\,(P)$ is invertible,

$$\mathbf{u} = \mathrm{Hess}\,(P)^{-1}\left(\mathbf{u}_g - \frac{\partial \nabla P}{\partial t}\right). \tag{2.71}$$

Now use this relation in (2.54), written in the form

$$\frac{\partial q_g}{\partial t} + \mathbf{u} \cdot \nabla q_g = 0, \tag{2.72}$$

to obtain

$$\frac{\partial q_g}{\partial t} + \left[\mathrm{Hess}\,(P)^{-1} \left(\mathbf{u}_g - \frac{\partial \nabla P}{\partial t} \right) \right] \cdot \nabla q_g = 0. \tag{2.73}$$

Equations (2.67) and (2.73) form a closed system in the two unknowns P and q_g. An important simplification is obtained in the special case $q_g = \textit{constant}$, in which equation (2.54) is identically satisfied, and the semigeostrophic equations reduce to just the Monge–Ampère equation (2.67) to be solved for the unknown P. The geopotential P may still depend on time, although (2.67) says nothing about this dependence. Time-dependence is in fact specified by the boundary conditions. To clarify this point, we limit our discussion to rigid impermeable boundaries, on which $\mathbf{u} \cdot \mathbf{n} = 0$ with $\mathbf{n}$ representing the normal to the boundary. Using (2.71), we can express this condition as

$$\left[\mathrm{Hess}\,(P)^{-1} \left(\mathbf{u}_g - \frac{\partial \nabla P}{\partial t} \right) \right] \cdot \mathbf{n} = 0. \tag{2.74}$$

The vorticity-streamfunction formulation of the semigeostrophic equations achieves a clear distinction between the model kinematics, encoded in (2.67), and its dynamics, encoded in (2.73). Because of this, we will sometimes call (2.67) and (2.73) the *kinematic* and the *dynamic* equation respectively.

2.4.1 Legendre transformations of P

The first two equations in (2.63) may be interpreted as a change of variables $(x, y) \mapsto (X, Y)$ known as the *geostrophic momentum transformation*. Hoskins [47] noted that the system (2.67)–(2.73) simplifies considerably after the geostrophic momentum transformation is effected, i.e., treating (X, Y, z) as the spatial coordinates. Later, Chynoweth and Sewell [16] recognised that the geostrophic momentum transformation is a form of partial Legendre transform. Indeed, they identified a quartet of Legendre transformations of P, formally analogous to that of the internal energy found in classical thermodynamics[2]. The two pairs of dual variables in the semigeostrophic

[2]The quartet of Legendre dual potentials of classical thermodynamics are the internal energy $\hat{e}$, the enthalpy $\hat{h}$, the Gibbs free energy, and the Helmholtz free energy. The thermodynamic potentials are connected by two pairs of "dual variables", namely, $\Theta \leftrightarrow \hat{s}$ and $p \leftrightarrow \rho^{-1}$, where Θ represents the absolute temperature.

theory are

$$(x, y) \leftrightarrow (X, Y), \qquad \text{and} \qquad z \leftrightarrow Z. \tag{2.75}$$

These are used to define the three dual potentials to P, namely, $R(X, Y, Z)$, $S(X, Y, z)$, and $T(x, y, Z)$.

Remark 2.4.2. *In this section, we suppress the time dependence in P and its dual potentials to highlight the duality structure. We will explicitly flag the time dependence later in the thesis as needed.*

The full Legendre transform R of P is obtained from

$$R = Xx + Yy + Zz - P, \tag{2.76}$$

where x, y, and z are found by inverting

$$X = \frac{\partial P(x, y, z)}{\partial x}, \quad Y = \frac{\partial P(x, y, z)}{\partial y}, \quad Z = \frac{\partial P(x, y, z)}{\partial z}. \tag{2.77}$$

Similarly, the partial Legendre transform S of P is defined by

$$S = Xx + Yy - P, \tag{2.78}$$

where x and y are found by inverting

$$X = \frac{\partial P(x, y, z)}{\partial x}, \quad Y = \frac{\partial P(x, y, z)}{\partial y}. \tag{2.79}$$

Alternatively, the partial Legendre transform T of P is found from

$$T = P - Zz, \tag{2.80}$$

where z is found by inverting

$$Z = \frac{\partial P(x, y, z)}{\partial z}. \tag{2.81}$$

We use the terminology *Legendre map* to indicate either

$$(x, y, z) \mapsto (X, Y, Z) = \left(\frac{\partial P}{\partial x}, \frac{\partial P}{\partial y}, \frac{\partial P}{\partial z}\right), \tag{2.82}$$

$$(x, y, z) \mapsto (X, Y, z) = \left(\frac{\partial P}{\partial x}, \frac{\partial P}{\partial y}, z\right), \tag{2.83}$$

or

$$(x, y, z) \mapsto (x, y, Z) = \left(x, y, \frac{\partial P}{\partial z}\right), \tag{2.84}$$

depending on the particular dual potential at hand. In each case, the inverse Legendre map is obtained by considering the differential of equations (2.82)–(2.80). For example, the differential of (2.76) gives

$$\frac{\partial R}{\partial X}dX + \frac{\partial R}{\partial Y}dY + \frac{\partial R}{\partial Z}dZ = \tag{2.85}$$

$$= Xdx + xdX + Ydy + ydY + Zdz + zdZ - \frac{\partial P}{\partial x}dx - \frac{\partial P}{\partial y}dy - \frac{\partial P}{\partial z}dz. \tag{2.86}$$

Now, using (2.65), one obtains

$$\frac{\partial R}{\partial X}dX + \frac{\partial R}{\partial Y}dY + \frac{\partial R}{\partial Z}dZ = xdX + ydY + zdZ, \tag{2.87}$$

whereby,

$$\frac{\partial R}{\partial X} = x, \quad \frac{\partial R}{\partial Y} = y, \quad \frac{\partial R}{\partial Z} = z. \tag{2.88}$$

Therefore, the inverse Legendre map of (2.82) is

$$(X, Y, Z) \mapsto (x, y, z) = \left(\frac{\partial R}{\partial X}, \frac{\partial R}{\partial Y}, \frac{\partial R}{\partial Z}\right). \tag{2.89}$$

Similarly, taking the differential of (2.78) gives

$$\frac{\partial S}{\partial X} = x, \qquad \frac{\partial S}{\partial Y} = y, \qquad \frac{\partial S}{\partial z} = -\frac{\partial P}{\partial z} \equiv -Z, \tag{2.90}$$

and defines the inverse Legendre map as

$$(X, Y, z) \mapsto (x, y, z) = \left(\frac{\partial S}{\partial X}, \frac{\partial S}{\partial Y}, z\right). \tag{2.91}$$

Finally, taking the differential of (2.80) gives

$$\frac{\partial T}{\partial x} = \frac{\partial P}{\partial x} \equiv X, \qquad \frac{\partial T}{\partial y} = \frac{\partial P}{\partial y} \equiv Y, \qquad \frac{\partial T}{\partial Z} = -z, \tag{2.92}$$

and

$$(x, y, Z) \mapsto (x, y, z) = \left(x, y, -\frac{\partial T}{\partial Z}\right). \tag{2.93}$$

The local existence of the inverse maps (2.89), (2.91), and (2.93) is ensured respectively by the conditions

$$\frac{\partial(X, Y, Z)}{\partial(x, y, z)} \neq 0, \qquad \frac{\partial(X, Y)}{\partial(x, y)} \neq 0, \qquad \frac{\partial Z}{\partial z} \neq 0. \tag{2.94}$$

Each of the dual potentials (2.76)–(2.80) satisfies a different form of the Monge–Ampère equation (2.67). In order to see this, use (2.65) to write equation (2.67) in the form

$$\frac{\partial(X,Y,Z)}{\partial(x,y,z)} = q_g. \tag{2.95}$$

This may be written

$$\frac{\partial(x,y,z)}{\partial(X,Y,Z)} = \frac{1}{q_g}, \tag{2.96}$$

which, using (2.88), gives the Monge–Ampère equation satisfied by R,

$$\det \mathrm{Hess}\,(R) = \frac{1}{q_g}, \tag{2.97}$$

where $\mathrm{Hess}\,(R)$ represent the Hessian matrix of R with respect to (X,Y,Z). Alternatively, multiply (2.95) by

$$\frac{\partial(x,y,z)}{\partial(X,Y,z)} \tag{2.98}$$

to obtain

$$\frac{\partial Z}{\partial z} = q_g \frac{\partial(x,y)}{\partial(X,Y)}. \tag{2.99}$$

Next, use (2.90) allows us to obtain the Monge–Ampère equation satisfied by S,

$$q_g\left(\frac{\partial^2 S}{\partial X^2}\frac{\partial^2 S}{\partial Y^2} - \left(\frac{\partial^2 S}{\partial X \partial Y}\right)^2\right) + \frac{\partial^2 S}{\partial z^2} = 0. \tag{2.100}$$

Finally, multiplying (2.95) by

$$\frac{\partial(x,y,z)}{\partial(x,y,Z)} \tag{2.101}$$

yields

$$\frac{\partial(X,Y)}{\partial(x,y)} = q_g \frac{\partial z}{\partial Z}, \tag{2.102}$$

which, using (2.92), becomes the Monge–Ampère equation satisfied by T,

$$\frac{\partial^2 T}{\partial x^2}\frac{\partial^2 T}{\partial y^2} - \frac{\partial^2 T}{\partial x \partial y} + q_g \frac{\partial^2 T}{\partial Z^2} = 0. \tag{2.103}$$

Equations (2.100) and (2.103) are known as the *Chynoweth–Sewell equations*. Unlike equations (2.67) and (2.97), the Chynoweth–Sewell equations achieve

a separation between the "horizontal" and the "vertical" derivatives, which makes easier to guess particular solutions. For example, a class of polynomial solutions to (2.103) has been analysed in [30] for constant q_g. Regarding the vorticity-stream function problem, this takes the simplest form in R, which has made it possible to prove its well-posedness in these variables [4]. On the other hand, when specific configurations of the fluid domain are considered, using S makes the vorticity-streamfunction problem more tractable. Below, we review the vorticity-streamfunction problem with impermeable boundaries in R and S.

2.4.2 Vorticity-streamfunction system in R-variables

When (X, Y, Z) are considered as the independent variables, equation (2.54) reads

$$\frac{Dq_g}{Dt} = \frac{\partial q_g}{\partial t} + \frac{DX}{Dt}\frac{\partial q_g}{\partial X} + \frac{DY}{Dt}\frac{\partial q_g}{\partial Y} + \frac{DZ}{Dt}\frac{\partial q_g}{\partial Z} \tag{2.104}$$

$$= \frac{\partial q_g}{\partial t} + u_g\frac{\partial q_g}{\partial X} + v_g\frac{\partial q_g}{\partial Y} = 0, \tag{2.105}$$

where (2.64) has been used. Here, the geostrophic wind is expressed in terms of R using (2.63) and (2.88), which brings the previous equation into

$$\frac{\partial q_g}{\partial t} + \left(\frac{\partial R}{\partial Y} - Y\right)\frac{\partial q_g}{\partial X} + \left(X - \frac{\partial R}{\partial X}\right)\frac{\partial q_g}{\partial Y} = 0. \tag{2.106}$$

Equations (2.97) and (2.106) form a closed system which is formally analogous to (2.67) and (2.54), and represents the full Legendre transform of the vorticity-streamfunction system. One advantage of the dual formulation is immediately apparent: the transport of vorticity equation (2.106) is significantly simpler than its counterpart in physical variables (2.54). However, an additional layer of difficulty now affects the treatment of boundaries. If the physical domain has rigid impermeable boundaries, these become free boundaries in (X, Y, Z)-variables.

To see this, assume that the boundaries are represented by the zero set of a function,

$$F(x, y, z) = 0. \tag{2.107}$$

Using (2.88) written in the form

$$\mathbf{x} = \nabla R, \tag{2.108}$$

with $\nabla R := (\partial_X R, \partial_Y R, \partial_Z R)$ and $\mathbf{x} := (x, y, z)$, the free boundaries in dual variables are identified by

$$F(\nabla R) = 0. \tag{2.109}$$

Since R is one of the problem's unknowns, the boundaries (2.109) are not a priori known. The impermeability condition reads, in physical variables,

$$\mathbf{u} \cdot \nabla F = 0, \tag{2.110}$$

and, since $\partial F/\partial t = 0$, it trivially implies

$$\frac{DF}{Dt} = 0. \tag{2.111}$$

This equation is clearly invariant under time-dependent changes of coordinates. Therefore, after the transformation $(t, x, y, z) \mapsto (t, X, Y, Z)$ is effected, (2.111) becomes

$$\frac{\partial F(\nabla R)}{\partial t} + u_g \frac{\partial F(\nabla R)}{\partial X} + v_g \frac{\partial F(\nabla R)}{\partial Y} = 0, \tag{2.112}$$

where now $\partial F/\partial t$ is generally nonzero because it has to be taken at (X, Y, Z) fixed. Equations (2.109) and (2.112) are the pair of boundary conditions that must be enforced on the free boundaries to define the vorticity-streamfunction problem in dual variables.

2.4.3 Vorticity-streamfunction system in S-variables

In particular arrangements of the fluid domain, the partial Legendre transform of P becomes preferable. This is the case for the so called *Eady problem* (see Chapter 5), in which the fluid domain consists of a strip $0 < z < const.$ In these conditions, the partial transform $(x, y, z) \mapsto (X, Y, z)$ brings most of the advantages of the full transform, while keeping the boundaries fixed. The dual potential S satisfies the *Chynoweth–Sewell equation* (2.100). On the other hand, the vorticity transport equation becomes

$$\frac{Dq_g}{Dt} = \frac{\partial q_g}{\partial t} + \frac{DX}{Dt}\frac{\partial q_g}{\partial X} + \frac{DY}{Dt}\frac{\partial q_g}{\partial Y} + \frac{Dz}{Dt}\frac{\partial q_g}{\partial Z} \tag{2.113}$$

$$= \frac{\partial q_g}{\partial t} + u_g \frac{\partial q_g}{\partial X} + v_g \frac{\partial q_g}{\partial Y} + w\frac{\partial S}{\partial q_g} = 0, \tag{2.114}$$

where now q_g is understood as a function of (X, Y, z) and time. The geostrophic wind is expressed in terms of S by (2.63) and (2.78), which brings the vorticity transport equation into the form

$$\frac{\partial q_g}{\partial t} + \left(\frac{\partial S}{\partial Y} - Y\right)\frac{\partial q_g}{\partial X} + \left(X - \frac{\partial S}{\partial X}\right)\frac{\partial q_g}{\partial Y} + w\frac{\partial q_g}{\partial z} = 0. \tag{2.115}$$

Note that equations (2.100) and (2.115) do not form a closed system because w still appears in (2.115). The third equation in (2.64), together with the last in (2.90), is still needed to express w in terms of S. This gives

$$w = -\frac{\frac{\partial^2 S}{\partial z \partial t} + \left(\frac{\partial S}{\partial Y} - Y\right)\frac{\partial^2 S}{\partial X \partial z} + \left(X - \frac{\partial S}{\partial X}\right)\frac{\partial^2 S}{\partial Y \partial z}}{\frac{\partial^2 S}{\partial z^2}}. \tag{2.116}$$

Using the same argument that led to (2.112), we can see that the impermeability condition on physical boundaries implies that the dual boundaries are transported. Boundaries of the form $z = const.$ are not affected by the partial Legendre transform, so the transport condition reads

$$0 = \frac{Dz}{Dt} \equiv w. \tag{2.117}$$

This constraint is combined with (2.116) to obtain a time-dependent boundary condition on S on boundaries of the form $z = constant$,

$$\frac{\partial^2 S}{\partial z \partial t} + \left(\frac{\partial S}{\partial Y} - Y\right)\frac{\partial^2 S}{\partial X \partial z} + \left(X - \frac{\partial S}{\partial X}\right)\frac{\partial^2 S}{\partial Y \partial z} = 0. \tag{2.118}$$

2.5 Chynoweth–Sewell fronts

Much of the current interest in the semigeostrophic equations is motivated by their ability to represent weather fronts. Physically speaking, a front is a "thin" region within atmosphere characterized by large vorticity and small acceleration where the fluid velocity and temperature vary quickly (see [47, 16]). For the purpose of mathematical modelling, fronts may be understood as surfaces in the fluid domain across which the fluid velocity and temperature experience a jump discontinuity. In the seminal paper [16], Chynoweth and Sewell proposed a mathematical model for fronts based on semigeostrophic equations and the singularities of the Legendre map in two space dimensions (x, z). After one of the dual potentials (R, S or T) is assigned, the physical potential P is recovered by the inverse Legendre transform. This may be singular, and result in a multivalued P. In specific conditions (see also [54]), it is possible to excise a single valued function from the graph of P with discontinuous first derivatives across one or more lines in the (x, z)-plane. These singular lines are then interpreted as fronts, as the momentum and temperature fields experience a jump discontinuity across them (cf. equations (2.65)).

Among all the weak solutions built this way, some are not physically achievable. In three spatial dimensions, Cullen *et al.* [24] proved that a

necessary condition for static stability of semigeostrophic flows is that the geopotential P be a convex function of space. This convexity principle is named after Cullen, Norbury, and Purser (*CNP principle*), and is a constrain that every solution (weak or classical) must obey. Is instructive to think of the CNP principle as the semigeostrophic analogue of the "entropy condition" of shock theory, which is used to characterize physically consistent weak solutions to the gas dynamics equations. The CNP principle is implemented in the Chynoweth and Sewell construction by requiring that whatever is left after surgery on the graph of P is a convex function of (x, z).

Using the same mathematical ideas, we introduce a notion of three-dimensional fronts by applying Chynoweth and Sewell's reasoning in three spatial dimensions. We use the terminology *Chynoweth–Sewell fronts* to identify both 2D and 3D fronts built this way.

2.5.1 The convex envelope algorithm

As pointed out in [16], convexity of P carries over in different ways to its Legendre dual potentials. A convex $P(x, y, z)$ corresponds to $R(X, Y, Z)$ being convex, $S(X, Y, z)$ being saddle shaped (convex in (X, Y) and concave in z), and $T(x, y, Z)$ being saddle shaped (convex in (x, y) and concave in Z). This observation allows one to change viewpoint and perform surgery on the dual potential rather than P. We apply these ideas to build Chynoweth–Sewell fronts in three dimensions. Our approach reduces to the original set of equations in [16] when a particular class of solutions is considered. In view of the application to the Eady problem in Chapter 5, we work with the partial Legendre transform $S(X, Y, z)$.

Fix t in (2.100) and assume q_g to be given. Let $S(X, Y, z)$ be a given regular solution to (2.100). For every fixed $z = constant$, build the convex envelope $\check{S}(\,\cdot\,,\,\cdot\,, z)$ of $S(\,\cdot\,,\,\cdot\,, z)$. Therefore, $\check{S}(X, Y, z)$ is convex in (X, Y) and concave in z. Thus, the partial Legendre transform of $\check{S}$ with respect to (X, Y) yields a convex function $\check{P}(x, y, z)$. Moreover, if $\check{S} \neq S$, $\nabla\check{P}$ is discontinuous across one or more singular surfaces in $\mathbb{R}^3$ which are interpreted as fronts. In other words,

Definition 2.5.1. Chynoweth–Sewell fronts are the image, under the Legendre map, of the set in (X, Y, z)-space where $S(\,\cdot\,,\,\cdot\,, z)$ is concave.

Remark 2.5.1. *The convex envelope of a given regular function is obtained as follows. Let $S(X, Y)$ be a given regular function which is everywhere convex except in some bounded domain $D \subset \mathbb{R}^2$. Finding its convex envelope $\check{S}(X, Y)$ amounts to solving a free-boundary value problem where the Monge–*

Ampère equation

$$\frac{\partial^2\sigma}{\partial X^2}\frac{\partial^2\sigma}{\partial Y^2} - \left(\frac{\partial^2\sigma}{\partial X\partial Y}\right)^2 = 0 \tag{2.119}$$

holds in D, and the boundary conditions

$$\sigma = S, \qquad \nabla\sigma = \nabla S, \tag{2.120}$$

hold on the unknown boundary ∂D. Once a solution s is found, the convex envelope is obtained piecewise as

$$\check{S}(X,Y) = \begin{cases} S(X,Y), & \text{if } (X,Y) \ni D, \\ \sigma(X,Y), & \text{if } (X,Y) \in D. \end{cases} \tag{2.121}$$

If the function $S(X,Y)$ is concave in several regions $D_1, ..., D_n$, then one has to solve n free-boundary value problems similar to the one just described to find the convex envelope of S.

2.5.2 Cylindrical solutions

Finding the convex envelope of $S(\,\cdot\,,\,\cdot\,,z)$ is much simpler if the function S has a trivial dependence on the variable Y. As we will show in Chapter 5, this precisely occurs for Eady waves travelling in the X-direction, which have the form

$$S = \frac{Y^2}{2} + CYz + S'(X,z), \qquad C \in \mathbb{R}. \tag{2.122}$$

Here, S' solves a the *2D Chynoweth–Sewell equation*,

$$q_g\frac{\partial^2 S}{\partial X^2} + \frac{\partial^2 S}{\partial z^2} = 0. \tag{2.123}$$

For reasons that will be clear at the end of this section (see also Section 3.4), we call (2.122) the *cylindrical solutions*. When S is cylindrical, a solution to equation (2.119) can be sought in the form

$$\sigma = \frac{Y^2}{2} + CYz + \sigma'(X,z). \tag{2.124}$$

In this case, equation (2.119) implies that σ is affine in X, while the second of (2.120) yields $\partial_X\sigma = \partial_X S$. Therefore, the solution to the convex envelope problem reduces to the Chynoweth and Sewell algorithm [16]. Namely, suppose that, for a fixed z, there exists a region $X_1(z) \le X \le X_2(z)$ where

$S'(\,\cdot\,,z)$ is concave. The boundary points $X_1(z), X_2(z)$ of this region are found from the system

$$\left.\frac{\partial S'}{\partial X}\right|_{X_1} = \frac{S'|_{X_2} - S'|_{X_1}}{X_2 - X_1}, \qquad \left.\frac{\partial S'}{\partial X}\right|_{X_2} = \frac{S'|_{X_2} - S'|_{X_1}}{X_2 - X_1}, \tag{2.125}$$

and the convex envelope $\check{S}'(\,\cdot\,,z)$ is obtained as

$$\check{S}'(X,z) = \begin{cases} S'(X,z), & \text{if } X < X_1(z) \text{ or } X > X_2(z), \\ S'(X_1,z) + \frac{\partial S'}{\partial X}(X_1,z)(X - X_1), & \text{if } X_1(z) < X < X_2(z). \end{cases} \tag{2.126}$$

The domain in (X,Y,z)-space where S is concave has always the form

$$\bigcup_z [X_1(z), X_2(z)] \times \mathbb{R}, \tag{2.127}$$

($\mathbb{R}$ stands for the Y-axis). The image of this 3D domain under the inverse Legendre map (2.91) is a 2D surface that represent a Chynoweth–Sewell front in the physical space. A front obtained this way is always a cylindrical surface, meaning that each section $y = \textit{constant}$ looks the same.

2.6 Summary of Chapter 2

In this chapter we introduced the semigeostrophic equations, a famous model for numerical weather prediction at the subcontinental scale. We reviewed their derivation in Sections 2.1 and 2.2. We then revised the rewriting of the system of equations in the form of an advection equation for the vorticity coupled with a Monge–Ampère equation for the stream function (the geopotential), which makes a clear distinction between the dynamics and kinematics of semigeostrophic equations (Section 2.4). Next, we have introduced the so-called "geostrophic momentum transformation", a change of variables that facilitates the analysis of the system of equations, using the language of the Legendre transformation. Most importantly, the geostrophic momentum transformation allows the vorticity-streamfunction system to be simplified as much as possible, and facilitates their analysis in a particular case of physical interest discussed later in the thesis. Finally, we shifted attention to atmospheric fronts in Section 2.5, the most important singularities that semigeostrophic equations are capable of supporting. After a review of Chynoweth and Sewell's work on the topic, we introduced a class of solutions that allows the Chynoweth and Sewell construction to be extended to three spatial dimensions.

Chapter 3

Monge–Ampère geometry

Because of mathematical structures such as the Legendre duality and the Monge–Ampère equation (2.67), the semigeostrophic equations admit of treatment by symplectic geometry, and more specifically, Monge–Ampère geometry (see for example [55] and references therein). The geometry of Monge–Ampère equations was explored by Lychagin and his school with the main objective of classifying all the possible equations of this kind. The applications of this theory to fluid dynamics are now numerous, and have strengthened the connection between fluid dynamics and the geometry of differential equations. Delahaies and Roulstone [27] have explored the implications of Monge–Ampère geometry on the shallow water semigeostrophic equations, while Roulstone *et al.* [78] and Banos *et al.* [7] have conducted similar studies for the Euler equations. This and the following chapters follow the same line of research, and investigate the relevance of Monge–Ampère geometry to semigeostrophic equations.

The geometric theory of differential equations provides a useful point of view on singularities of solutions. The key is to interpret a differential equation as a pair of differential forms on a suitable ambient space, which in all the cases considered in this manuscript consists of the cotangent bundle to the space of independent variables. The (generalized) solutions are seen as submanifolds in this bundle, while their projection onto the basis defines the (possibly multivalued) physical fields. This projection operation can be singular, depending on how the solution is placed with respect to bundle structure. Because we only allow for smooth generalized solutions, any singularity that may appear in the physical fields is due to the projection operation. This point of view paves the way for catastrophe theory, which can be used to classify such singularities, and dates back to the work of Vinogradov and Kupershmidt on Hamilton-Jacobi theory (§8 of [88]). We refer to [62] for further examples of application of these ideas. In this the-

sis, we shall only consider a special class of Monge–Ampère equations called *symplectic*. The coefficients of a symplectic Monge–Ampère equation can only depend on the independent variables and the gradient of the dependent variable. Equation (2.67) is an example of symplectic Monge–Ampère equation in three independent variables provided that q_g is understood as a function of (x, y, z), time, and possibly ∇P. In the symplectic setting, all the generalized solutions are Lagrangian submanifolds of the cotangent bundle. Arnold's theory of Lagrangian singularities is therefore naturally called into question (see [1] for reference). This viewpoint is at the core of Ishikawa and Machida's work on singularities of Hessian-type Monge–Ampère equations [49, 51]. Kossowski [54] has independently proposed the same formalism for studying singularities of general symplectic Monge–Ampère equations in two independent variables (see ([30]) for the details).

This section is structured as follows. After recalling the basic ideas about Monge–Ampère geometry [55], we apply these ideas to the semigeostrophic equations and their solutions [30]. We describe a systematic way to compute the velocity field associated with a given generalized solution, and rephrase Chynoweth and Sewell's construction of weather fonts in the language of Monge–Ampère geometry.

3.1 Geometry of the phase space

For a given symplectic Monge–Ampère equation, we can identify the space of independent variables and denote it $\mathcal{M}$. Notice that for the Monge–Ampère equation (2.67, this is the Euclidean space $\mathbb{R}^3$ with coordinates (x, y, z). This particular case will be further developed in Section 3.2, and in this section we will retain some generality and refer to an unspecified set of independent variables $\mathcal{M}$. Next, the cotangent bundle $T^*\mathcal{M}$ to the space of independent variables $\mathcal{M}$ is considered. The cotangent bundle to any given $\mathcal{M}$ is naturally endowed with a symplectic structure, that is, a closed and non-degenerate differential 2-form ω. The realm of Monge–Ampère geometry is entered when $T^*\mathcal{M}$ is equipped with an n-form α ($n = \dim(\mathcal{M})$) called the *Monge–Ampère form*, which contains the information about the Monge–Ampère equation at hand. Borrowing terminology from classical mechanics, we shall call $T^*\mathcal{M}$ the *phase space*.

In order to understand how the Monge–Ampère form α encodes information about the corresponding Monge–Ampère equation, assume that $F : \mathcal{M} \to \mathbb{R}$ is a classical solution, that is, a smooth function that satisfies the given Monge–Ampère equation (which is defined on $\mathcal{M}$). Then, the image of the differential $dF : \mathcal{M} \to T^*\mathcal{M}$ can be understood as a submanifold

$L \subset T^*\mathcal{M}$, and one can show that the restriction of the symplectic form ω to this submanifold always vanish regardless of the function F that generated it,

$$\omega|_L = 0. \tag{3.1}$$

The Monge–Ampère n-form α is designed in such a way that if F is a solution to the given Monge–Ampère equation then also the restriction of α to the image of dF must vanish. Furthermore, when the condition $\alpha|_L = 0$ is expressed in local coordinates, it boils down to the original Monge–Ampère that F satisfies. This machinery is more easily understood in a specific example, and will be worked out in full detail in Section 3.2 for the semigeostrophic Monge–Ampère equation (2.67).

One of the biggest advantages brought by the geometric view on Monge–Ampère equations is that of an enlarged notion of a solution, which encompasses singular and multi-valued ones. In order for the conditions $\omega|_L = 0$ and $\alpha|_L = 0$ to hold, it is not required that the submanifold $L \subset T^*\mathcal{M}$ is the image of some differential dF of some function F. Therefore, one can define a *generalized solution* to the Monge–Ampère equation under consideration as a Lagrangian[1] submanifold $L \subset T^*\mathcal{M}$ that satisfies the additional condition $\alpha|_L = 0$. This notion of a solution is more general in the sense that it allows the submanifold L to have singular projection to the base manifold M, something precluded to classical solutions. This aspect essentially means that the coordinates of M cannot be globally taken as coordinates on L too. Rather, different sets of coordinates are needed on different patches of L, and the condition $\alpha|_L = 0$ results in a Monge–Ampère equation whose appearance depends on the particular coordinates adopted. In all cases, the Monge–Ampère equation obtained by expressing $\alpha|_L = 0$ in local coordinates is still equivalent to the original one in the sense of Lychagin and Roubtsov [55].

Although generalized solutions cannot be globally represented as the image of the differential dF of some function $F : \mathcal{M} \to T^*\mathcal{M}$, they always admit an alternative local representation in terms of a single function G called the *generating function*. Note that the canonical symplectic form can be written

$$\omega = d\lambda, \tag{3.2}$$

where λ is the tautological 1-form on $T^*\mathcal{M}$. If L is a Lagrangian submanifold, then $\lambda|_L$ is closed, and so there exist a function G on L such that, locally,

$$\lambda|_L = dG. \tag{3.3}$$

[1] A submanifold of a $2n$-dimensional symplectic manifold is said to be *Lagrangian* if it is n-dimensional and $\omega|_L = 0$

Once a coordinate set on L is selected, (3.3) reduces to an algebraic system of equations whose zero set in $T^*\mathcal{M}$ identifies (a patch of) the submanifold L. If L is a generalized solution, the coordinate expression of $\alpha|_L = 0$ ultimately boils down to a Monge–Ampère equation that the generating function G has to satisfy. In some cases, the equivalent equation satisfied by G is much simpler to solve than the original one or even linear [55]. Furthermore, generating functions allow us to study generalized solutions in the neighbourhood of a singularity.

A point $p \in L$ is said to be *singular* if the restriction $\pi_L := \pi|_L$ of the bundle projection,

$$\pi : T^*\mathcal{M} \to \mathcal{M}, \tag{3.4}$$

to the Lagrangian submanifold L is singular at p. We denote the subset of such points on L by ΣL, that is,

$$\Sigma L = \{p \in L : \det(d\pi_L)|_p = 0\}. \tag{3.5}$$

The image of the singular set ΣL by π_L is called the *caustics* of the map π_L. The shape and dimension of the caustics depend on how L is placed with respect to the bundle structure π.

In the language of catastrophe theory, the singularities of π_L are of *Lagrangian* kind. The classification of Lagrangian singularities and caustics up to small deformations of the Lagrangian submanifold L was pioneered by Arnold (see for example [1]). The list of generic Lagrangian singularities in the case most relevant to us ($n = 3$) is

$$A_2(\text{“fold”}), \quad A_3(\text{“cusp”}), \quad A_4(\text{“swallowtail”}), \tag{3.6}$$

$$D_4^+(\text{“purse”}), \quad D_4^-(\text{“pyramid”}). \tag{3.7}$$

3.1.1 Anatomy of the cusp singularity

The most important type of singularity for the present work is the cusp A_3. As we will show in Section 3.4, the cusp singularity is the basis of the modeling of weather fronts in semigeostrophic equations. We assume $n = 3$ throughout this section. This assumption forces any Lagrangian submanifold L to be three-dimensional. When a cusp singularity is present, the singular set ΣL is a (2-dimensional) regular surface in L. Within ΣL, two different kind of singular points are found, namely, fold points (A_2) and cusp points (A_3). Also, the rank of π_L drops by 1 everywhere on ΣL [2]. In order to distinguish fold from cusp points we have to resort to Arnold's theory, which

[2] meaning that $d\pi_L$ has everywhere 1D kernel.

establishes that the (1D) kernel of $d\pi_{_L}$ is transversal to ΣL at fold points and tangent to ΣL at cusp points. Writing the singular set ΣL as the zero set $f = 0$ of a smooth function $f : L \to \mathbb{R}$, Arnold's condition for cusp points may be written

$$\ker(d\pi_{_L}) \subset \ker(df), \tag{3.8}$$

where we accounted for the fact that $\ker(d\pi_{_L})$ is 1D and $\ker(df)$ is 2D by using the inclusion operator. Next, let ξ a vector field on L such that $\xi|_{\Sigma L}$ generates $\ker(d\pi_{_L})$, i.e.,

$$d\pi_{_L}(\xi) = 0 \quad \text{on} \quad \Sigma L. \tag{3.9}$$

Then, (3.8) may be written $df(\xi) = 0$, so that A_3 points may be characterized by

$$\begin{cases} f = 0, \\ df(\xi) = 0. \end{cases} \tag{3.10}$$

3.2 Semigeostrophic equations

In this section, we adapt the machinery of Monge–Ampère geometry introduced above to the special case of semigeostrophic equations, and, specifically, the kinematic equation (2.67), which we rewrite here for convenience,

$$\det \mathrm{Hess}\,(P) = q_g. \tag{3.11}$$

In this setting, the manifold of independent variables (excluding time) is $\mathcal{M} = \mathbb{R}^3$, and the phase space is $T^*\mathbb{R}^3$. We endow the phase space with coordinates (x, y, z, X, Y, Z) and we assume them to be canonical. Therefore, the symplectic form takes the standard form

$$\omega = \mathrm{d}X \wedge \mathrm{d}x + \mathrm{d}Y \wedge \mathrm{d}y + \mathrm{d}Z \wedge \mathrm{d}z. \tag{3.12}$$

It is easy to check that the Monge–Ampère form relating to (2.67) is

$$\alpha = dX \wedge dY \wedge dZ - q_g dx \wedge dy \wedge dz. \tag{3.13}$$

Indeed, for any smooth function $P : \mathbb{R}^3 \to \mathbb{R}$, we understand the differential $dP : \mathcal{M} \to T^*\mathcal{M}$ as the map

$$dP : (x, y, z) \mapsto (x, y, z, X, Y, Z) = (x, y, z, \partial_x P, \partial_y P, \partial_z P), \tag{3.14}$$

compatibly with (2.65) and the assumption that (x, y, z, X, Y, Z) are canonical coordinates. Thus, the restriction of α to the image of the differential dP reads

$$dP^*(\alpha) = d(\partial_x P) \wedge d(\partial_y P) \wedge d(\partial_z P) - q_g dx \wedge dy \wedge dz, \tag{3.15}$$

where * represents the pull-back operator, and results in

$$dP^*(\alpha) = (\det \mathrm{Hess}\,(P) - q_g)dx \wedge dy \wedge dz. \tag{3.16}$$

We next consider generalized solutions. Let L be a Lagrangian submanifold in $T^*\mathbb{R}^3$. For any point $p \in L$, there is always a 3-subset of $\{x, y, z, X, Y, Z\}$ that can be used as a set of coordinates on a suitably small neighbourhood of p (see for example [1]). Overall, there are $2^3 = 8$ possible 3-element subsets in $\{x, y, z, X, Y, Z\}$ and, therefore, as many classes of generating functions for Lagrangian submanifolds in $T^*\mathbb{R}^3$. The Legendre dual potentials of Chynoweth and Sewell [16],

$$R(X, Y, Z), \qquad S(X, Y, z), \qquad T(x, y, Z), \tag{3.17}$$

provide some physically relevant examples. We explicitly work out the description of a Lagrangian submanifold L in terms of S. The tautological 1-form on $T^*\mathbb{R}^3$ reads

$$\lambda = X dx + Y dy + Z dz. \tag{3.18}$$

Therefore, setting

$$G(X, Y, z) = Xx + Yy - S(X, Y, z) \tag{3.19}$$

in equation (3.3), we obtain,

$$Z\,\mathrm{d}z = x\,\mathrm{d}X + y\,\mathrm{d}Y - \frac{\partial S}{\partial X}\,\mathrm{d}X - \frac{\partial S}{\partial Y}\,\mathrm{d}Y - \frac{\partial S}{\partial z}\,\mathrm{d}z, \tag{3.20}$$

which in turn implies

$$x = \frac{\partial S}{\partial X}(X, Y, z), \qquad y = \frac{\partial S}{\partial Y}(X, Y, z), \qquad Z = -\frac{\partial S}{\partial z}(X, Y, z). \tag{3.21}$$

The combined zero set of equations (3.21) in $T^*\mathbb{R}^3$ identifies the Lagrangian submanifold L generated by S. Similarly, the choices

$$G(X, Y, Z) = Xx + Yy + Zz - R(X, Y, Z) \tag{3.22}$$

and

$$G(x, y, Z) = Zz + T(x, y, Z) \tag{3.23}$$

lead to a local description of as two more classes of Lagrangian submanifolds as the zero set of, respectively,

$$x = \frac{\partial R}{\partial X}(X, Y, Z), \qquad y = \frac{\partial R}{\partial N}(X, Y, Z), \qquad z = \frac{\partial R}{\partial Z}(X, Y, Z), \tag{3.24}$$

and

$$z = -\frac{\partial T}{\partial Z}(x, y, Z), \qquad X = \frac{\partial T}{\partial x}(x, y, Z), \qquad Y = \frac{\partial T}{\partial y}(x, y, Z). \tag{3.25}$$

Remark 3.2.1. *Notice that, in all cases (3.17), the restriction $\pi_{_L}$ of the bundle projection to L,*

$$\pi : (x, y, z, X, Y, Z) \mapsto (x, y, z), \tag{3.26}$$

coincides, when expressed in coordinates, with the inverse Legendre map (2.89), (2.91), or (2.93).

3.3 Reconstruction of the velocity field

Suppose that a particular generalized solution to (2.67) is known. In order to visualize the physical content of the solution it is crucial to be able to reconstruct the fluid velocity it induces on $\mathbb{R}^3$. Unlike elsewhere above, where we could ignore the time dependence, this will be crucial here to take into account the motion of the generalized solution in phase space. To emphasize this aspect, we will denote the time-dependent solution by L_t. We will perform all calculations explicitly in the case of most interest for us, i.e. when L_t is generated by a generating function $S(t, X, Y, z)$. By definition, the velocity field on $\mathbb{R}^3$ is

$$u = \frac{Dx}{Dt}, \qquad v = \frac{Dy}{Dt}, \qquad w = \frac{Dz}{Dt}. \tag{3.27}$$

As already noted, the projection map $\pi_{_L} : L \to \mathbb{R}^3$ coincides with the inverse Legendre map (2.91). Therefore, using (2.91), we may write

$$u = \frac{D(\partial_X S)}{Dt} = \frac{\partial^2 S}{\partial t \partial X} + u_g \frac{\partial^2 S}{\partial X^2} + v_g \frac{\partial^2 S}{\partial X \partial Y} + w \frac{\partial^2 S}{\partial X \partial z}, \tag{3.28}$$

$$v = \frac{D(\partial_Y S)}{Dt} = \frac{\partial^2 S}{\partial t \partial Y} + u_g \frac{\partial^2 S}{\partial X \partial Y} + v_g \frac{\partial^2 S}{\partial Y^2} + w \frac{\partial^2 S}{\partial Y \partial z}. \tag{3.29}$$

Also, w is directly provided by (2.116),

$$w = -\frac{\frac{\partial^2 S}{\partial z \partial t} + \left(\frac{\partial S}{\partial Y} - Y\right) \frac{\partial^2 S}{\partial X \partial z} + \left(X - \frac{\partial S}{\partial X}\right) \frac{\partial^2 S}{\partial Y \partial z}}{\frac{\partial^2 S}{\partial z^2}}. \tag{3.30}$$

Finally, the geostrophic wind (u_g, v_g) is expressed in terms of S by

$$u_g = \frac{\partial S}{\partial Y} - Y, \qquad v_g = X - \frac{\partial S}{\partial X}, \tag{3.31}$$

which descend from (2.63) and (2.90). Equations (3.28), (3.29), and (2.116), together with (3.31), provide a parametric representation of the velocity field induced on $\mathbb{R}^3$ by the generalized solution L.

We remark that the velocity **u** obtained by this algorithm is generally multivalued. Single valuedness is only guaranteed when L_t is a classical solution. If L_t contains a cusp A_3, then **u** will be three-valued somewhere in its domain. Single-valuedness may be restored by introducing a Chynoweth–Sewell front, as we clarify in the next section.

3.4 Monge–Ampère geometry and fronts

In Section (2.5), we introduced the notion of a Chynoweth–Sewell front and presented the convex envelope algorithm for its construction. In this section, we give a geometrical interpretation of this algorithm. Our goal is to highlight a similarity between Chynoweth–Sewell fronts and gas dynamical shocks, and in particular in the way these structures are constructed. We limit our discussion to the class of cylindrical solutions (2.122). The reason for this terminology should now be clear: the Lagrangian submanifold generated by (5.40) is cylindrical, meaning that all the sections $Y + Cz = constant$ are identical. This immediately follows from the definition (3.21) of L, which for (2.122) becomes

$$L = \{(X, Y, z) : x = \frac{\partial S'(X, z)}{\partial X}, y = Y + Cz, Z = -\frac{\partial S'(X, z)}{\partial z}\}. \tag{3.32}$$

We start by considering a Lagrangian submanifold L with generating function (2.122), and we assume that L contains a cusp point. The singular set ΣL is given by

$$f = \frac{\partial^2 S'}{\partial X^2} = 0. \tag{3.33}$$

A vector field ξ that generates $\ker(d\pi_{_L})$ on ΣL is found to be

$$\xi = \frac{\partial}{\partial X}. \tag{3.34}$$

Therefore, the second condition in (3.10) becomes

$$\frac{\partial f}{\partial X} = \frac{\partial^3 S'}{\partial X^3} = 0. \tag{3.35}$$

Equations (3.33) and (3.35) identify A_3 points on L. Because S' is independent of Y, the singular set (3.33) is a cylindrical surface, and all its sections $Y = const.$ look the same. We can therefore restrict our analysis to a single slice $Y = const.$ of L.

In the geometrical view, Chynoweth and Sewell's construction of fronts boils down to cutting the Lagrangian submanifold L along a suitably chosen

surface and discarding the multivalued piece. The precise geometry of the cut is determined by Chynoweth and Sewell's criterion. Note first that equations (2.125) can be written as

$$S'|_{X_2} - S'|_{X_1} = x(X_2 - X_1), \qquad x = \left.\frac{\partial S'}{\partial X}\right|_{X_1} = \left.\frac{\partial S'}{\partial X}\right|_{X_2}. \tag{3.36}$$

On the other hand, a straightforward application of the integration by parts yields

$$S'|_{X_2} - S'|_{X_1} - x(X_2 - X_1) = -\int_\gamma X dx, \tag{3.37}$$

where γ is the contour represented in Figure 3.1. Thus, the cutting surface is $\gamma \times \mathbb{R} \subset L$, where the contour γ is found from

$$\int_\gamma X dx = 0. \tag{3.38}$$

The geometrical meaning of this condition can be made more explicit by observing that, by Stokes' theorem,

$$0 = \int_{\Sigma_+ \cup \Sigma_-} dX \wedge dx = \int_{\Sigma_+} dX \wedge dx - \int_{\Sigma_-} dX \wedge dx, \tag{3.39}$$

where Σ_+, Σ_- are the regions depicted in Figure 3.1. Equation (3.39) says that, for each $z = const.$ (and $Y = const.$) slice of L, the two regions Σ_+, Σ_- have equal area. Figure 3.2 provides a schematic comparison between L and $\check{L}$.

Equation (3.39) is nothing but a statement of the classical Maxwell rule of shock theory in the context of semigeostrophic equations. The presence of a Maxwell rule suggests that Chynoweth–Sewell fronts, just as shocks, must obey some conservation law. Indeed, semigeostrophic flows satisfy the thermal wind balance, which may be expressed as

$$\frac{\partial X}{\partial z} = \frac{\partial Z}{\partial x}, \qquad \frac{\partial Y}{\partial z} = \frac{\partial Z}{\partial y}. \tag{3.40}$$

From the mathematical viewpoint, these conservation laws are just the compatibility condition which ensure that $(X, Y, Z) = \nabla P$ for some P. In the language of Monge–Ampère geometry, a conservation law is a $(n-1)$-form on $T^*\mathbb{R}^n$ whose pull-back to a solution is closed [62, 55]. The 2-forms corresponding to (3.40) are, respectively,

$$\beta_1 = (X dx + Z dz) \wedge dy, \qquad \beta_2 = dx \wedge (Y dy + Z dz). \tag{3.41}$$

As long as the class of solutions (2.122) is considered, the equal area rule (3.39) can be used to derive a Rankine-Hugoniot conditions corresponding to the conservation law β_1. First, note that for these solutions we always have $Y = y - Cz$. As a consequence, (X, y, z) can be used as coordinates on L in place of (X, Y, z). Next, consider the cylindrical surface in L given by

$$\Gamma \times [0, 1], \tag{3.42}$$

where Γ is a certain closed curve in the (X, z) plane and $y \in [0, 1]$. By Stokes theorem, we have

$$\int_{\Gamma\times[0,1]} \beta_1 = 0. \tag{3.43}$$

This implies

$$\oint_{\Gamma} X dx + Z dz = 0. \tag{3.44}$$

Next, suppose that $\Gamma = \gamma \cup \Gamma_+ \cup \Gamma_-$ as in Figure 3.2. Then, the above integral splits into three contributions,

$$\int_{\gamma} (X dx + Z dz) + \int_{\Gamma_+} (X dx + Z dz) + \int_{\Gamma_-} (X dx + Z dz) = 0. \tag{3.45}$$

Now, the first integral vanishes because of the equal area rule and the fact that $dz = 0$ on γ. Accounting for the fact that Γ_+ and Γ_- have the same projection onto the (x, z)-plane, we can write what is left of (3.45) as a single integral using z as parameter,

$$\int_{z_1}^{z_2} \left([\![X]\!] \frac{dx}{dz} + [\![Z]\!] \right) dz = 0, \tag{3.46}$$

where z_2 represent the z-coordinate of the A_3 point, and z_1 represents the plane where the curve γ lies. Finally, $[\![\cdot]\!]$ represents the classical jump operator. Since z_1 can be chosen arbitrarily, the previous equation implies the Rankine-Hugoniot condition,

$$\frac{dx}{dz} = -\frac{[\![Z]\!]}{[\![X]\!]}. \tag{3.47}$$

Note that this equation occurs in the papers [23, 25] where its origin is traced back to the work of Margules.

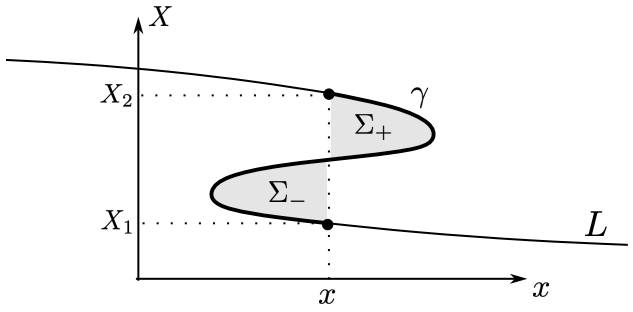

Figure 3.1: A slice through L for constant z and y. The front position x is chosen so as to make the areas of Σ_+ and Σ_- coincide. The curve γ has end points (x, X_1) and (x, X_2).

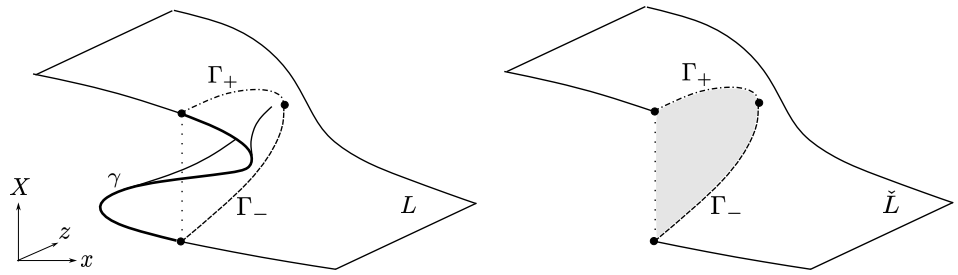

Figure 3.2: A slice through L for constant y. The three curves $\gamma, \Gamma_+, \Gamma_-$ form a closed loop. The curves Γ_+, Γ_- have the same projection onto the (x, z)-plane.

3.5 Summary of Chapter 3

After a review on the geometry of the Monge–Ampère equations and the theory of Lagrangian singularities (Section 3.1), we applied these ideas to study the kinematics of semigeostrophic equations which is encoded in the Monge–Ampère equation (2.67) (Section 3.4). The key message of this chapter is that singular solutions of semigeostrophic equations can be interpreted as Lagrangian submanifolds in a suitable phase space whose projection onto physical space is singular. Section 3.3 deals with the problem of recovering physical information from a generalized solution, and, specifically, on the velocity field that it induces in the fluid domain. In Section 3.4, we reinterpreted the construction of Chynoweth–Sewell fronts in the context of Monge–Ampère geometry as a surgery on the generalized solution. This procedure, familiar from gas dynamics, highlights the nature of Chynoweth–Sewell fronts as relatives of shocks in classical gas models.

Chapter 4

The Lychagin–Roubtsov metric

In [64], Lychagin and Rubtsov addressed the problem of classifying the Monge–Ampère forms on a three-dimensional phase space up to local symplectomorphisms. To this aim, they introduced a bilinear form g_α on $T^*\mathcal{M}$ associated to each Monge–Ampère form α. Then, they were able to show that the signature of g_α uniquely identifies the class to which α belongs. In some "nondegenerate" cases, the bilinear form g_α is a pseudo-Riemannian metric on $T^*\mathcal{M}$, which we call the *Lychagin–Roubtsov metric*. In a more recent work [30], the pull-back metric,

$$h_\alpha := g_\alpha|_L, \tag{4.1}$$

on generalized solutions of (2.67) was studied. The signature of h_α was the main object of investigation, and it was shown that it relates in a precise way to the symbol type of the Monge–Ampère equation at the solution L. Also in [30] a relation between h_α and the singular set ΣL was pointed out. The bilinear form g_α may be defined through

$$g_\alpha(\xi_1, \xi_2)\frac{\Omega^3}{3!} = \iota_{\xi_1}\alpha \wedge \iota_{\xi_2}\alpha \wedge \omega, \tag{4.2}$$

which holds for any pair of vector fields ξ_1, ξ_2 on $T^*\mathcal{M}$ (see [7]). As long as the kinematic equation (2.67) is concerned, g_α is a pseudo-Riemannian metric with signature $(3,3)$ over the phase space $T^*\mathbb{R}^3$. Indeed, for α and ω given by (3.13) and (3.12), formula (4.2) yields

$$g_\alpha = 2q_g(\,\mathrm{d}x\,\mathrm{d}X + \,\mathrm{d}y\,\mathrm{d}Y + \,\mathrm{d}z\,\mathrm{d}Z). \tag{4.3}$$

Now, since the potential vorticity is transported by the flow (cf. equation (2.54)), we can safely assume that

$$q_g > 0 \tag{4.4}$$

everywhere. Note that this assumption is compatible with the CNP convexity principle (see Section 2.5) because it is implied by the convexity of P (cf. equation (2.67)). Therefore, (4.3) is always nondegenerate. Unlike the ambient metric g_α, nothing can be said a priori about the pull-back metric (4.1) h_α, which depends on the solution L and the points on L. Generally speaking, h_α can be either Riemannian, pseudo-Riemannian or degenerate. We call h_α degenerate at a point $p \in L$ if there exists a tangent vector $\xi_1 \in T_pL$ such that $h_\alpha(\xi_1, \xi_2) = 0$ for every $\xi_2 \in T_pL$.

This chapter closely replicates the key sections of ([30]) pertaining the pull-back metric on solutions. We handle differently classical solutions, amenable for treatment through linearization of the Monge–Ampère operator, and generalized solutions, treated through generating functions. We draw these ideas together in §4.3, stating the relationship between elliptic-hyperbolic transitions, projection singularities and the pull-back of the Lychagin–Roubtsov metric.

4.1 Pull-back on classical solutions

We begin with recalling a classical definition from PDE theory (see for example [18]):

Definition 4.1.1 (Type of a linear equation)**.** A second order linear PDE with principal part

$$\sum_{i,j=1}^{n} b_{ij}(x) \frac{\partial^2 u}{\partial x_i \partial x_j} \tag{4.5}$$

is called *elliptic* if the eigenvalues of the symmetric matrix $B = [b_{ij}]$ have the same sign; *hyperbolic* if one eigenvalue has the opposite sign from the others; and *parabolic* if there is at least one zero eigenvalue.

The notion of an equation type has been generalized to nonlinear equations by Harvey and Lawson [43] as follows (see also §2 of [33] for a geometrical perspective).

Definition 4.1.2. The type of a nonlinear equation *at* a given solution is the type of its linearization about the solution.

We are thus led to consider the linearization of equation (2.67) about a fixed solution. Let $P + \delta P$ be a perturbation of some exact solution P to (2.67). Introducing this ansatz into equation (2.67) and using the Jacobi

formula for determinants leads, to the first order in δP, to the linear equation satisfied by the perturbation field,

$$\text{Tr } [\text{adj}(\text{Hess}\,(P))\text{Hess}\,(\delta P)] = 0. \tag{4.6}$$

Note that the coefficient matrix of this linear equation is

$$B = \text{adj}(\text{Hess}\,(P)), \tag{4.7}$$

where "adj" denotes the adjugate matrix.

The assumption that $q_g > 0$ implies that (4.6) is elliptic if P is (spatially) convex and hyperbolic if P is saddle shaped. Definition 4.1.2 allows us to bring this information to the nonlinear equation (2.67) as it stands. Also note that equation (2.67) is nowhere parabolic as long as classical solutions are considered. In fact, equation (2.67) itself prevents the eigenvalues of $\text{Hess}\,(P)$ (and thus those of B) from vanishing. We are now in a position to prove the following

Proposition 4.1.1. *Let P be a classical solution to (2.67) and let $L \subset T^*\mathbb{R}^3$ denote the graph of dP. Then, the pull-back Lychagin–Roubtsov metric on L,*

$$h_\alpha := (dP)^* g_\alpha, \tag{4.8}$$

has matrix representation

$$h_\alpha = 2\text{adj}(B) = 2q_g\text{Hess}\,(P), \tag{4.9}$$

where B is the linearization matrix (4.7). Moreover, h_α has signature $(3,0)$ if equation (2.67) is elliptic at the solution P and signature $(1,2)$ if (2.67) is hyperbolic at P.

Proof. By direct calculation. From equation (4.3) and

$$dP : (x,y,z) \mapsto \left(x, y, z, \frac{\partial P}{\partial x}, \frac{\partial P}{\partial y}, \frac{\partial P}{\partial z}\right), \tag{4.10}$$

it follows that

$$h_\alpha = (dP)^* g_\alpha = 2q_g \sum_{i,j=1}^{3} \frac{\partial^2 P}{\partial x_i \partial x_j}\, \mathrm{d}x_i\, \mathrm{d}x_j, \tag{4.11}$$

where $x_i = x, y, z$. Therefore, h_α has matrix representation

$$h_\alpha = 2q_g\text{Hess}\,(P). \tag{4.12}$$

On the other hand, equation (4.7) plus the algebraic identity

$$\mathrm{adj}(\mathrm{adj}(M)) = \det(M)^{n-2}M, \tag{4.13}$$

holding for any square matrix $M \in \mathbb{R}^{n\times n}$ with $n > 2$, gives

$$\mathrm{adj}(B) = \mathrm{adj}(\mathrm{adj}(\mathrm{Hess}\,(P))) = \det(\mathrm{Hess}\,(P))\mathrm{Hess}\,(P) = q_g\mathrm{Hess}\,(P), \tag{4.14}$$

and thus equation (4.9) follows. For the second part, we observe that the determinant,

$$\det(h_\alpha) = 8\det(B)^2 = 8\det\mathrm{Hess}\,(P)^4 = 8q_g^4, \tag{4.15}$$

is always positive, so the eigenvalues of (4.9) can only be *(i)* all positive or *(ii)* one positive and two negative. According to (4.9), *(i)* occurs when P is convex and case *(ii)* occurs when P is saddle shaped. Therefore, cases *(i)* and *(ii)* correspond to (2.67) being respectively elliptic or hyperbolic. □

Definition 4.1.2 is no longer directly applicable when generalized solutions are considered because the linearization procedure is not applicable on neighbourhoods of singular points. However, equation (4.9) suggests a characterization of ellipticity based on h_α, which readily applies to generalized solutions. Indeed, the equation type at a generalized solution is directly traceable to the signature of h_α in a definite way. In what follows, we will prove consistency of this characterization by relying on the local description of generalized solutions in terms of generating functions.

4.2 Pull-back on generalized solutions

We recall that any generating function G of a generalized solution L satisfies a Monge–Ampère equation which arises from the condition $\alpha|_L = 0$ in local coordinates. Moreover, as G is a classical solution to this equation, there are no obstructions to linearization. Thus, we can give the following

Definition 4.2.1. Let L be a generalized solution to (2.67) locally generated by G. We say that (2.67) is elliptic, parabolic or hyperbolic at some point $p \in L$ if G satisfies a Monge–Ampère equation of the same type at the point.

We remark that the symbol type of a differential equation is invariant under a change of variables [18], and this ensures consistency of Definition 4.2.1. We are thus in a position to prove the

Proposition 4.2.1. *Let L be a generalized solution to (2.67). Then, the pull-back metric $h_\alpha = g_\alpha|_L$ has signature $(3,0)$ on elliptic branches, $(1,2)$ on hyperbolic branches, and degenerates along parabolic branches of L.*

Proof. This proposition is proved by direct inspection of the linearized Monge–Ampère equation satisfied by the generating function G. We explicitly carry out the calculations for the case $G = Xx + Yy - S(X,Y,z)$ (the remaining cases are addressed similarly and lead to the same conclusions). Thus, let L be some generalized solution locally described by $S(X,Y,z)$ according to (3.21). Introducing a perturbation $S + \delta S$ of an exact solution S to (2.100) leads to a linear equation satisfied by the perturbation field,

$$q_g\left(\frac{\partial^2 S}{\partial X^2}\frac{\partial^2 \delta S}{\partial Y^2} + \frac{\partial^2 S}{\partial Y^2}\frac{\partial^2 \delta S}{\partial X^2} - 2\frac{\partial^2 S}{\partial X \partial Y}\frac{\partial^2 \delta S}{\partial X \partial Y}\right) + \frac{\partial^2 \delta S}{\partial z^2} = 0. \tag{4.16}$$

Its 3×3 coefficient matrix is

$$A = \begin{pmatrix} q_g \mathrm{adj}(H) & 0 \\ 0 & 1 \end{pmatrix}, \qquad H := \begin{pmatrix} \partial_X^2 S & \partial_X \partial_Y S \\ \partial_X \partial_Y S & \partial_Y^2 S \end{pmatrix}. \tag{4.17}$$

On the other hand, the Lychagin–Roubtsov metric $h_\alpha = g_\alpha|_L$ has the local coordinate expression

$$h_\alpha = 2q_g\left(\frac{\partial^2 S}{\partial x^2}\,\mathrm{d}x^2 + 2\frac{\partial^2 S}{\partial x \partial y}\,\mathrm{d}x\,\mathrm{d}y + \frac{\partial^2 S}{\partial y^2}\,\mathrm{d}y^2 - \frac{\partial^2 S}{\partial Z^2}\,\mathrm{d}Z^2\right), \tag{4.18}$$

and may be written in matrix form as

$$h_\alpha = 2\begin{pmatrix} q_g H & 0 \\ 0 & q_g^2 \det(H) \end{pmatrix}, \tag{4.19}$$

where we have used (2.100). We see from (4.17) that equation (2.100) is elliptic as long as H is positive definite, which, in light of (4.19), corresponds to h_α having signature $(3,0)$. Parabolic and hyperbolic cases correspond to $\det(H) = 0$ and $\det(H) < 0$ respectively. Therefore, it follows from equation (4.19) that h_α is degenerate on parabolic branches and of type $(1,2)$ on hyperbolic ones. □

The significance of Proposition 4.2.1 is that h_α encodes all the essential information about the equation type, and may be used to give an invariant definition of the symbol type based on its signature. This may be summarized as follows:

Definition 4.2.2. Let L be a generalized solution to (2.67) with Lychagin–Roubtsov metric h_α. We say that (2.67) is elliptic or hyperbolic at a point $p \in L$ if $h_\alpha|_p$ is respectively of type $(3,0)$ or $(1,2)$. We say that (2.67) is parabolic at $p \in L$ if $h_\alpha|_p$ is degenerate.

4.3 Connection with singularities

In this section we show that elliptic-hyperbolic transitions of the kinematic equation (2.67) are tied to singularities. This relationship is reflected in the pull-back metric h_α thanks to the Proposition 4.2.1.

Proposition 4.3.1. *Let L be a generalized solution to (2.67). Then the set of parabolic points on L coincides with the singular locus ΣL.*

Proof. Once again, we rely on a local description in coordinates and generating functions to prove our result. Let a solution L be locally generated by a function $G = Xx + Yy - S(X, Y, z)$, that is,

$$L = \left\{ (x, y, z, X, Y, Z) \in T^*\mathbb{R}^3 : x = \frac{\partial S}{\partial X},\ y = \frac{\partial S}{\partial Y},\ Z = -\frac{\partial S}{\partial z} \right\}. \quad (4.20)$$

In local coordinates (x, y, Z) on L, the projection mapping reads

$$\pi_{_L}(x, y, Z) = \left(\frac{\partial S}{\partial X}, \frac{\partial S}{\partial Y}, z \right), \quad (4.21)$$

and so it is singular on points satisfying

$$\det(\,\mathrm{d}\pi_{_L}) = \frac{\partial^2 S}{\partial X^2}\frac{\partial^2 S}{\partial Y^2} - \left(\frac{\partial^2 S}{\partial X \partial Y} \right)^2 = 0. \quad (4.22)$$

On the other hand, we know from the proof of Proposition 4.2.1 that parabolic points on L satisfy the same equation. To complete the proof, one should examine in turn each of the remaining classes of generating functions. However, calculations are almost identical to those we have already exhibited, and we omit them for conciseness. □

Propositions 4.2.1 and 4.3.1 are combined into

Corollary 4.3.1. *Given a generalized solution L to (2.67), the induced Lychagin–Roubtsov metric on L degenerates on the singular locus ΣL.*

Another way to state this result is that every regular branch of a multivalued solution $L \subset T^*\mathbb{R}^3$ is either elliptic or hyperbolic, with transitions happening at singular branches.

4.4 Characteristics of Monge–Ampère equations

The Lychagin–Roubtsov metric provides a canonical way to define the characteristics of a symplectic Monge–Ampère equation in the hyperbolic regime [30]. In this section, we review the results presented in [30] on this subject, and present an unpublished worked-out example to explain the theory. The building blocks of characteristic surfaces are the tangent vectors of null length, which, borrowing terminology from relativity theory, are called *light-like*. The set of light-like vectors based at a point in the phase space is called the *light cone* or the *characteristic variety*. Drawing ideas from the work of Kossowski [54] in two spatial dimensions, we give the following

Definition 4.4.1. Let g_α be given by (4.2) and let $p \in T^*\mathbb{R}^3$. The cotangent characteristic variety (or simply characteristic variety) $CV_p \subset T_p(T^*\mathbb{R}^3)$ is the cone

$$CV_p := \{\xi \in T_p(T^*\mathbb{R}^3) : g_\alpha(\xi, \xi) = 0\}. \tag{4.23}$$

Let $L \subset T^*\mathbb{R}^3$ be a Lagrangian submanifold and let $p \in L$. We denote the pull-back of the characteristic variety to L by

$$\mathrm{cv}_p := \{\xi \in T_pL : h_\alpha(\xi, \xi) = 0\}, \tag{4.24}$$

where $h_\alpha = g_\alpha|_L$ is the pull-back Lychagin–Roubtsov metric on L.

It easily follows from Definition 4.2.2 that the characteristic variety cv_p is a full-fledged cone if p is an hyperbolic point, a degenerate cone if p is a parabolic point, and the zero vector, $\{0\} \subset T_pL$, if p is an elliptic point. The characteristic variety is the basic ingredient to build the characteristic surfaces within a generalized solution L. We understand a characteristic surface $\mathcal{C} \subset L$ as the enveloping surface of the characteristic varieties cv_p as p varies across $\mathcal{C}$, as the following definition clarifies.

Definition 4.4.2. A surface $\mathcal{C} \subset L$ is called *characteristic* if at any point $p \in \mathcal{C}$, the tangent space $T_p\mathcal{C}$ includes one (and only one!) light-like direction.

We remark that Definition 4.4.2 closely parallels the notion of characteristics in general relativity, where they are identified with light-like surfaces [35]. Definition 4.4.2 may be considered as a generalization to nonlinear PDEs of the classical notion of characteristics for linear PDEs. To motivate this statement, fix coordinates $\{q^1, q^2, q^3\}$ on L and consider the surface

$$\mathcal{C} = \{(q^1, q^2, q^3) \in L : F(q^1, q^2, q^3) = 0\}. \tag{4.25}$$

Further, consider the following vector based at points on $\mathcal{C}$,

$$dF^\sharp = h^{ij}\frac{\partial F}{\partial q^i}\frac{\partial}{\partial q^j}, \tag{4.26}$$

where summation on repeated indices is implied and h^{ij} denotes the components of the inverse metric h_α^{-1}. It is straightforward to check equivalence of the following statements: *(i)* $dF^\sharp$ is a tangent vector to $\mathcal{C}$, *(ii)* $dF^\sharp$ is a light-like vector, *(iii)* F satisfies

$$h_\alpha^{-1}(dF, dF) = 0. \tag{4.27}$$

Equation (4.27) is the analogue of the eikonal equation in the linear setting, where the coefficient matrix is replaced by the inverse of h_α. We shall further elaborate on this analogy next. Note that equation (4.27) is only well defined away from parabolic points, where h_α is invertible, and has only nontrivial solutions on hyperbolic branches of L. Any hyperbolic branch is regular by virtue of Proposition 4.3.1, so it may be described as the graph of a function, e.g. $P^*(x, y, z)$, to the extent a classical solution is (we may take $\{x, y, z\}$ as local coordinates on hyperbolic branches). Therefore, the linearization of (2.67) about a hyperbolic branch of L is well defined, and, building on equation (4.9), we may write

$$h_\alpha^{-1} = \frac{A}{2\det(A)}, \tag{4.28}$$

where $A = \mathrm{adj}(\mathrm{Hess}\,(P^*))$ is the coefficient matrix of the linearized equation (2.67) about P^*. Since $\det(A) \neq 0$ on hyperbolic points, we may get rid of the denominator in equation (4.27), and write

$$\nabla F \cdot A \nabla F = \sum_{i,j=1}^{3} a_{ij}(x, y, z)\frac{\partial F}{\partial x_i}\frac{\partial F}{\partial x_j} = 0, \tag{4.29}$$

where $(x_1, x_2, x_3) = (x, y, z)$. This is precisely the classical *eikonal equation.*

Equation (4.27) is a nonlinear PDE of the first order, and may be solved by the methods of wave optics (see for example Appendix 4 of [1]). This involves the computation of "light rays", from which the characteristic surface is constructed by foliation. We briefly recall the main steps of the solution procedure for completeness of exposition (see for example [1, 18] for reference). Consider the cotangent bundle T^*L with coordinates $\{q^1, q^2, q^3, p_1, p_2, p_3\}$ and symplectic structure

$$\omega = dp_i \wedge \mathrm{d}q^i. \tag{4.30}$$

In this setting, equation (4.27) is interpreted as the zero level set of the Hamiltonian function $\mathcal{H} : T^*L \to \mathbb{R}$,

$$\mathcal{H}(p,q) = h(q)^{ij} p_i p_j, \tag{4.31}$$

under the identification $p_i = \partial F/\partial q^i$. Characteristic curves of (4.27) are defined by [1] as the integral curves of the Hamiltonian vector field $\xi_{\mathcal{H}}$,

$$-d\mathcal{H} = \iota_{\xi_{\mathcal{H}}}\Omega, \tag{4.32}$$

and satisfy the Hamilton's canonical equations of motion,

$$\dot{q}^i = \frac{\partial \mathcal{H}}{\partial p_i} = 2h(q)^{ij} p_j, \qquad \dot{p}_i = -\frac{\partial \mathcal{H}}{\partial q^i} = -\frac{\partial h^{jk}}{\partial q^i} p_j p_k. \tag{4.33}$$

Initial conditions cannot be chosen freely, but are subject to the compatibility condition

$$\mathcal{H}(p(0), q(0)) = 0. \tag{4.34}$$

Integral curves of (4.33) are called *bicharacteristics* [62]. Once projected to L along the cotangent bundle, $\bar{\pi} : T^*L \to L$, bicharacteristics foliate the characteristic surfaces $\mathcal{C} \subset L$.

Remark 4.4.1. *Light rays are equivalently described by the Lagrangian*

$$\mathcal{L} = h_{ij}(q)\dot{q}^i \dot{q}^j, \tag{4.35}$$

related to the Hamiltonian (4.31) by the classical Legendre transform. The equivalent condition to (4.34) in the present case reads

$$\mathcal{L}(q(0), \dot{q}(0)) = 0. \tag{4.36}$$

The Euler-Lagrange equations associated with (4.35) plus condition (4.36) yield the light-like geodesics of h_α. Therefore, characteristic surfaces $\mathcal{C}$ are foliated by light-like geodesics of h_α. This offers an alternative route for computing the characteristic surfaces.

An example of application of these ideas, consisting of a generalized solution to (2.67) with a fold singularity, has been presented in [30]. We next discuss a slightly more complex example, which contains a cusp singularity.

Example 4.4.1. Consider the generating function

$$T(x,y,Z) = -\frac{x^3}{6} + \frac{y^2}{2} + xyZ + \frac{1}{2}xZ^2 + \frac{Z^4}{12}. \tag{4.37}$$

It solves (2.103), and describes a Lagrangian submanifold $L \subset T^*\mathbb{R}^3$ as

$$L = \Bigg\{ (x, y, z, X, Y, Z) : X = -\frac{x^2}{2} + yZ + \frac{Z^2}{2}, Y = y + xZ, \tag{4.38}$$

$$z = -xy - xZ - \frac{Z^3}{3} \Bigg\} \tag{4.39}$$

The restriction of the bundle projection $\pi : T^*\mathbb{R}^3 \to \mathbb{R}^3$ to L reads, in local coordinates,

$$\pi_{\scriptscriptstyle L}(x, y, Z) = \left(x, y, -\frac{\partial T}{\partial Z} \right) = \left(x, y, -xy - xZ - \frac{Z^3}{3} \right), \tag{4.40}$$

and is singular at

$$\Sigma L = \left\{ (x, y, Z) \in T^*\mathbb{R}^3 : 0 = -\frac{\partial^2 T}{\partial Z^2} = -(x + Z^2) \right\}. \tag{4.41}$$

The parametric surface

$$\pi(\Sigma L) : \quad \begin{cases} x = -Z^2, \\ z = Z^2 y + \frac{2}{3} Z^3. \end{cases} \tag{4.42}$$

represents the caustics of the projection of L in $\mathbb{R}^3$. Now consider the pull-back of the Lychagin–Roubtsov metric (4.3) to this solution,

$$\begin{aligned} h_\alpha &= 2(T_{xx}\,\mathrm{d}x^2 + 2T_{xy}\,\mathrm{d}x\,\mathrm{d}y + T_{yy}\,\mathrm{d}y^2 - T_{ZZ}\,\mathrm{d}Z^2) \\ &= 2(-x\,\mathrm{d}x^2 + 2Z\,\mathrm{d}x\,\mathrm{d}y + \mathrm{d}y^2 - (x + Z^2)\,\mathrm{d}Z^2). \end{aligned} \tag{4.43}$$

Its eigenvalues,

$$\lambda_{1,2} = \frac{1}{2}(1 - x \pm \sqrt{(1 + x)^2 + 4Z^2}), \tag{4.44}$$

$$\lambda_3 = -(x + Z^2), \tag{4.45}$$

are all positive for $x < -Z^2$ and of different sign in $x > -Z^2$. Therefore, the problem is elliptic in the first case and hyperbolic in the second (see Figure 4.1). Note that the characteristic variety cv_p on points $p \in \Sigma L$ degenerates to a plane,

$$Z\,\mathrm{d}x + \mathrm{d}y = 0, \tag{4.46}$$

which is always transversal to the parabolic boundary ΣL. Also observe that the intersection

$$\mathrm{cv}_p \cap T_p \Sigma L \tag{4.47}$$

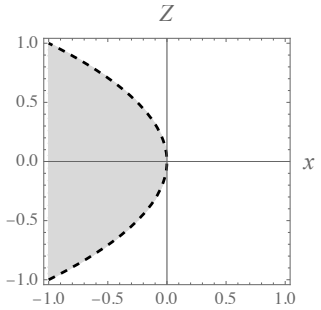

Figure 4.1: Elliptic domain (gray) and hyperbolic domain (white) of Example 4.4.1. The dashed line represents a section $y = constant$ through the singular locus ΣL.

determines a 1-dimensional distribution on ΣL whose integral lines are precisely the intersection of the characteristic surfaces with ΣL. Explicitly, taking $\{y, Z\}$ as coordinates on ΣL, the characteristic distribution on ΣL can be written

$$-2Z^2\,\mathrm{d}Z + \mathrm{d}y = 0, \tag{4.48}$$

and it is easily integrated to

$$y - \frac{2}{3}Z^3 = C. \tag{4.49}$$

In the hyperbolic region, characteristic surfaces are foliated by the light-like geodesics of h_α which satisfy

$$\begin{cases} \ddot{x} = \frac{-\dot{x}^2+2Z\dot{x}\dot{Z}-\dot{Z}(2\dot{y}+\dot{Z}))}{2(x+Z^2)}, \\ \ddot{y} = \frac{-2x\dot{x}\dot{Z}+Z(\dot{x}^2-\dot{Z}(2\dot{y}+\dot{Z}))}{2(x+Z^2)}, \\ \ddot{Z} = -\frac{Z\dot{Z}^2+\dot{x}(\dot{y}+\dot{Z})}{x+Z^2}. \end{cases} \tag{4.50}$$

We are not able to explicitly solve these equations, so we look for light rays following the Hamiltonian approach described above. The inverse LR metric reads

$$h_\alpha^{-1} = \frac{1}{2(x+Z^2)} \begin{pmatrix} -1 & Z & 0 \\ Z & x & 0 \\ 0 & 0 & -1 \end{pmatrix}. \tag{4.51}$$

In equation (4.31), we have defined the Hamiltonian as $\mathcal{H} = h_\alpha^{-1}(p, p)$, where now $p = (X, Y, -z)$. However, since $\mathcal{H} = 0$ along the desired solution curves, we can equivalently use

$$\mathcal{H} = X^2 - xY^2 + z^2 - 2XYZ. \tag{4.52}$$

Then, the Hamilton's equations of motion may be written

$$\frac{dx}{ds} = 2X - 2YZ, \qquad \frac{dy}{ds} = -2xY - 2XZ, \qquad \frac{dZ}{ds} = -2z, \tag{4.53}$$

$$\frac{dX}{ds} = Y^2, \qquad \frac{dY}{ds} = 0, \qquad \frac{dz}{ds} = -2XY. \tag{4.54}$$

Initial conditions are assigned on ΣL, that is,

$$x_0 = -Z_0^2, \tag{4.55}$$

and are subject to $H(p_0, p_0) = 0$, which implies both of

$$z_0 = 0, \quad \text{and} \quad X_0 = Y_0 Z_0. \tag{4.56}$$

Moreover, the condition that the initial point belongs to L implies

$$Y_0 = \frac{\partial T}{\partial y}(-Z_0^2, y_0, Z_0) = y_0 - Z_0^3. \tag{4.57}$$

Thus, the light rays originating from ΣL are labelled by two parameters (y_0, Z_0), which also form a set of coordinates on ΣL. To identify a particular characteristic surface, we fix the parameter C in (4.49), say $C = 0$, which gives

$$y_0 = \frac{2}{3} Z_0^3, \tag{4.58}$$

and leave us with just one free parameter, namely, Z_0. A characteristic surface built by this procedure is naturally parametrized by Z_0 and the arclength s along the rays of which it is foliated. It turns out that such a parametrization is not suitable for plotting purposes, so we replace s by

$$\delta = \frac{3}{Z_0^3 s}. \tag{4.59}$$

Then, the characteristic surface $C = 0$ is given parametrically by

$$\begin{cases} x(Z_0, \delta) = \frac{-1 + 4Z_0\delta + 3\delta^3 - 3Z_0^2\delta^4}{3\delta^4}, \\ y(Z_0, \delta) = \frac{2 + 10\delta^2 + 20Z_0^2\delta^2 + 10Z_0^3\delta^5 - 5Z_0\delta(2 + 3\delta^2)}{15\delta^5}, \\ Z(Z_0, \delta) = Z_0 - \frac{2}{3\delta^3} + \frac{2Z_0}{\delta^2}. \end{cases} \tag{4.60}$$

and depicted in Figure 4.2. Interestingly, the characteristic surface $C = 0$ has a cusped ridge at the intersection with the parabolic locus ΣL. It is possible to show, resorting to an adapted coordinate system on L, that these are semicubical cusps.

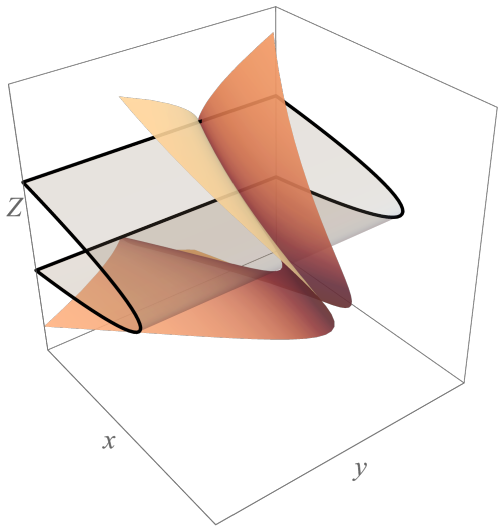

Figure 4.2: The characteristic surface $C = 0$ (orange) intersecting the singular locus ΣL (gray) along the parabolic characteristic curve $y = \frac{2}{3}Z^3$,

4.5 Summary of Chapter 4

After a brief introduction on the Lychagin–Roubtsov tensor, we turned our attention to its pull-back on the generalized solutions of the kinematic equation (2.67). The first key message of this chapter is that the geometry of generalized solutions is strongly dependent on the type of the Monge–Ampère equation (2.67) at such solutions. In the hyperbolic regime, a generalized solution locally resembles a Minkowski space, while, in the elliptic regime, it locally resembles a Euclidean space. This result is proven first on classical solutions of (2.67) in Section 4.1, and secondly on generalized solutions in Section 4.2. The second key message of this chapter is that hyperbolic-elliptic transitions of the equation (2.67) are possible, although they are always associated with a singularity. This result is established in Section 4.3 using the pseudo-Riemannian geometry language introduced previously. The concluding paragraph is devoted to a peculiar application of the pull-back metric, which enables a definition of the characteristic surfaces for the Monge–Ampère equation (2.67) in the hyperbolic context.

Chapter 5

The Eady problem

In this chapter, we revisit the classic Eady problem in light of the geometry of the Monge–Ampère equations presented in the previous chapters. The Eady problem concerns the simplest initial setting for the semigeostrophic equations that leads to the formation of atmospheric fronts. The physical mechanism underlying frontogenesis is the so-called "baroclinic instability", and it typically manifests itself when a north-south temperature gradient is combined with a zonal wind varying with height.

The semigeostrophic equations are known to be able to represent frontogenesis [46, 47]. The simplest setting in which baroclinic instability manifests is the Eady model [34], in which the troposphere is represented as a strip $0 < z < H$ with rigid and impermeable lids at the Earth's surface ($z = 0$) and the tropopause ($z = H$). Within this domain, the basic (stationary) flow consists of a linear zonal velocity profile which is sustained by a linear temperature gradient in the meridional direction. In formulas,

$$u_g = \frac{U}{H} z, \qquad v_g = 0, \qquad \theta = \theta_0 + \frac{N^2 \theta_0}{g} z - \frac{f \theta_0}{g} \frac{U}{H} y, \tag{5.1}$$

where U represents the top-lid value for the zonal wind and N is the constant buoyancy frequency.

The material contained in this chapter is entirely unpublished, and is organized as follows. We begin with the introduction of dimensionless variables [85], and the formalization and solution of the Eady problem provided by Hoskins [47] using the Legendre transform language. Next, we analyze Hoskins' solution in light of the geometric theory of Monge–Ampère equations discussed in Chapters 3 and 4. We show that the geometry of an Eady wave is essentially two-dimensional also from a metric point of view, and this is reflected in the curvature of such solutions. We close the chapter by applying what was discussed in Sections 3.3 and 3.4 about the reconstruction of

the physical information contained in a generalized solution in the particular case of Eady waves.

5.1 Dimensionless numbers

Using the dimensionless variables introduced in (2.3), we can write Eady's basic state in the form

$$u_g = Fr\, z, \qquad v_g = 0, \qquad \theta = 1 + z - Fr\, y, \tag{5.2}$$

where

$$Fr := \frac{U}{NH} \tag{5.3}$$

is the Froude number [45], and we have set

$$N = \frac{g}{fL}, \tag{5.4}$$

consistently with the usual definition of the buoyancy frequency (see for example [47]). Note that, in dimensionless variables, the atmosphere domain becomes

$$0 < z < \frac{gH}{f^2L^2} = Bu, \tag{5.5}$$

where

$$Bu := \frac{NH}{fL} = \frac{gH}{f^2L^2} \tag{5.6}$$

is the Burger number [45]. Thus, the top-lid value of the zonal velocity equals

$$u_g\big|_{z=Bu} = Fr\, Bu \equiv Ro, \tag{5.7}$$

where the parameter

$$Ro := \frac{U}{fL} \tag{5.8}$$

represents the Rossby number [45]. The geopotential function corresponding to the unperturbed state is

$$P_0 = \frac{x^2}{2} + \frac{y^2}{2} + \frac{z^2}{2} - Fr\, yz + z. \tag{5.9}$$

The basic state potential vorticity is found from (2.67), and turns out to be constant,

$$q_g = 1 - Fr^2. \tag{5.10}$$

If we assume that $q_g > 0$, equation (5.10) implies that $Fr < 1$, i.e., the wind is slower than gravity waves.

5.2 The mathematical problem and solution

The basic state specified by (5.9) solves a constant coefficients Monge–Ampère equation (2.67) with q_g given by (5.10). The linear stability analysis of this solution can be tackled by introducing perturbations of the geopotential field

$$P = P_0 + \varepsilon P_1, \qquad \varepsilon \ll 1, \tag{5.11}$$

that leave q_g constant (and equal to (5.10)). The perturbations are subject to the impermeable boundary condition,

$$w = 0 \qquad \text{on} \qquad z = 0, Bu. \tag{5.12}$$

Looking for a function P_1 which satisfies the Monge–Ampère equation (2.67) and the boundary conditions (5.12) to the first order in ε is called the Eady problem. As it stands, the Eady problem is fraught with technical difficulties due to the implicit dependence of the boundary conditions on P. Indeed, (5.12) has to be used in conjunction with (2.71) in order to obtain a (time-dependent) boundary condition in which P appear explicitly. This issue was solved in [47] using the geostrophic momentum transformation, which also achieves a simplification of the Monge–Ampère equation itself. We review the solution procedure below using the formalism of the (partial) Legendre transform introduced in Section 2.4.

5.2.1 Partial Legendre transform

The Eady basic state may equivalently be represented by the partial Legendre transform of (5.9),

$$S_0 = \frac{X^2}{2} + \frac{Y^2}{2} - q_g \frac{z^2}{2} + Fr\, Y z - z. \tag{5.13}$$

This function may be regarded as a stationary solution to the vorticity-streamfunction problem described in Section 2.4.3. In these variables, the Eady problem amounts to looking for an approximate solution,

$$S = S_0 + \varepsilon S_1, \qquad \varepsilon \ll 1, \tag{5.14}$$

that satisfies (2.100) and (2.118) to the first order in ε, with q_g given by (5.10). Following Hoskins [47], we introduce a shifted set of variables,

$$\tilde{X} = X - \frac{Ro}{2} t, \qquad \tilde{z} = z - \frac{Bu}{2}, \tag{5.15}$$

which compensate for the lack of symmetry in the basic flow and the domain. Observe that this change of variable does not affect the Chynoweth–Sewell equation (2.100). Now, look for a solution of the form

$$S = S_0 + \varepsilon S_1(\tilde{X}, Y, \tilde{z}, t), \qquad \varepsilon \ll 1. \tag{5.16}$$

This ansatz satisfies the Chynoweth–Sewell equation (2.100) to the first order in ε if

$$q_g\left(\frac{\partial^2 S_1}{\partial \tilde{X}^2} + \frac{\partial^2 S_1}{\partial Y^2}\right) + \frac{\partial^2 S_1}{\partial \tilde{z}^2} = 0. \tag{5.17}$$

Next, we examine the boundary conditions (2.118), which we rewrite here in a more compact form,

$$\left(\frac{\partial}{\partial t} + u_g\frac{\partial}{\partial X} + v_g\frac{\partial}{\partial Y}\right)\frac{\partial S}{\partial z} = 0. \tag{5.18}$$

Observe that the geostrophic wind may be expressed as an ε-expansion,

$$u_g = u_{g0} + \varepsilon u_{g1}, \qquad v_g = v_{g0} + \varepsilon v_{g1}, \tag{5.19}$$

where

$$u_{g0} := \frac{\partial S_0}{\partial Y} - Y = Fr\, z, \qquad u_{g1} := \frac{\partial S_1}{\partial Y}, \tag{5.20}$$

$$v_{g0} := X - \frac{\partial S_0}{\partial X} = 0, \qquad v_{g1} := -\frac{\partial S_1}{\partial X} = -\frac{\partial S_1}{\partial \tilde{X}}. \tag{5.21}$$

Therefore, (5.16) solves the boundary condition (5.18) to the order $O(\varepsilon)$ if

$$\frac{\partial^2 S_1}{\partial t \partial z} + u_{g0}\frac{\partial^2 S_1}{\partial X \partial z} + u_{g1}\frac{\partial^2 S_0}{\partial X \partial z} + v_{g0}\frac{\partial^2 S_1}{\partial Y \partial z} + v_{g1}\frac{\partial^2 S_0}{\partial Y \partial z} = 0, \tag{5.22}$$

which, using (5.15), becomes

$$\frac{\partial^2 S_1}{\partial t \partial \tilde{z}} + (u_{g0} - \frac{Ro}{2})\frac{\partial^2 S_1}{\partial \tilde{X} \partial \tilde{z}} + u_{g1}\frac{\partial^2 S_0}{\partial X \partial z} + v_{g0}\frac{\partial^2 S_1}{\partial Y \partial \tilde{z}} + v_{g1}\frac{\partial^2 S_0}{\partial Y \partial z} = 0, \tag{5.23}$$

and, using (5.13) and (5.20)–(5.21), boils down to

$$\frac{\partial^2 S_1}{\partial t \partial \tilde{z}} + (Fr\, z - \frac{Ro}{2})\frac{\partial^2 S_1}{\partial \tilde{X} \partial \tilde{z}} - Fr\,\frac{\partial S_1}{\partial X} = 0. \tag{5.24}$$

This condition holds at $z = 0$ and $z = Bu$. Recalling that $FrBu = Ro$, it becomes

$$\frac{\partial^2 S_1}{\partial \tilde{z} \partial t} + Fr\,\frac{\partial S_1}{\partial \tilde{X}} + \frac{Ro}{2}\frac{\partial^2 S_1}{\partial \tilde{X} \partial \tilde{z}} = 0 \quad \text{at} \quad \tilde{z} = \frac{Bu}{2}, \tag{5.25}$$

and

$$\frac{\partial^2 S_1}{\partial \tilde{z}\partial t} + Fr\,\frac{\partial S_1}{\partial \tilde{X}} - \frac{Ro}{2}\frac{\partial^2 S_1}{\partial \tilde{X}\partial \tilde{z}} = 0 \quad \text{at} \quad \tilde{z} = -\frac{Bu}{2}. \tag{5.26}$$

Next, assume that S_1 is a monochromatic wave in $\tilde{X}$ and Y, with $\tilde{z}$-dependent amplitude, namely,

$$S_1 = \psi(\tilde{z})e^{i(k\tilde{X}+lY-\omega t)}. \tag{5.27}$$

This perturbation field solves (5.17) if

$$\psi'' = m^2 q_g \psi, \qquad m := \sqrt{k^2+l^2}, \tag{5.28}$$

that is,

$$\psi(\tilde{z}) = C_1 e^{m\sqrt{q_g}\tilde{z}} + C_2 e^{-m\sqrt{q_g}\tilde{z}}. \tag{5.29}$$

The constants of integration in (5.29) are fixed by the boundary conditions. Equation (5.24) evaluated at $z = Bu$ gives

$$e^{\frac{1}{2}Bu\,m\sqrt{q_g}}(2Fr\,k + m\sqrt{q_g}(-kRo+2\omega))C_1 +$$
$$e^{-\frac{1}{2}Bu\,m\sqrt{q_g}}(2Fr\,k + m\sqrt{q_g}(kRo-2\omega))C_2 = 0,$$

and the same equation evaluated at $z = 0$ gives

$$e^{-\frac{1}{2}Bu\,m\sqrt{q_g}}(2Fr\,k + m\sqrt{q_g}(kRo+2\omega))C_1 +$$
$$e^{\frac{1}{2}Bu\,m\sqrt{q_g}}(2Fr\,k - m\sqrt{q_g}(kRo+2\omega))C_2 = 0.$$

This system admits nontrivial solutions (C_1, C_2) if the following *dispersion relation* holds,

$$-\frac{m^2 q_g}{Fr^2 k^2}\omega^2 = \left(1-\frac{Bu\,m\sqrt{q_g}}{2}\coth\frac{Bu\,m\sqrt{q_g}}{2}\right)\left(\frac{Bu\,m\sqrt{q_g}}{2}\tanh\frac{Bu\,m\sqrt{q_g}}{2}-1\right). \tag{5.30}$$

If (5.30) is satisfied, infinite solutions (C_1, C_2) for the pair of contants of integration in (5.29) are possible. A particular choice is

$$C_1 = e^{\frac{1}{2}Bu\,m\sqrt{q_g}}(2Fr\,k - m\sqrt{q_g}(kRo+2\omega)), \tag{5.31}$$

$$C_2 = -e^{-\frac{1}{2}Bum\sqrt{q_g}}(2Fr\,k + m\sqrt{q_g}(kRo+2\omega)). \tag{5.32}$$

Remark 5.2.1. *Despite being obtained as an approximate solution to the Eady problem, (5.16) together with (5.27) and (5.29), is in fact an exact solution. Higher order terms in ε happen to cancel out in both equation (2.100) and the boundary conditions (2.118).*

The dispersion relation (5.30) produces both stable and unstable waves, with instability occurring for sufficiently long waves. In the next section we analyse further Hoskins solution to the Eady problem, and provide an in-depth view on the frontogenesis mechanism associated with an unstable Eady wave.

5.2.2 Unidirectional waves

We regard the dispersion relation (5.30) as a surface $K_{Fr,Bu}(k,l,\omega) = 0$ in the (k,l,ω)-space (depending on two parameters (Fr, Bu)). Unstable wave numbers are those pairs (k,l) for which is impossible to find a frequency ω satisfying the dispersion relation. Introducing polar coordinates in the wave number plane,

$$m := \sqrt{k^2+l^2}, \qquad \nu := \arctan(l/k), \tag{5.33}$$

the dispersion relation may alternatively be written

$$K_{Fr,Bu}(m,\nu,\omega) = \cos(\nu)^2\varphi(m;F,B) + \omega^2 = 0, \tag{5.34}$$

where

$$\varphi(m;Fr,Bu) := \frac{Fr^2}{q_g}\left(1 - \frac{Bu\, m\sqrt{q_g}}{2}\coth\frac{Bu\, m\sqrt{q_g}}{2}\right)\left(\frac{Bu\, m\sqrt{q_g}}{2}\tanh\frac{Bu\, m\sqrt{q_g}}{2} - 1\right).$$

The set of marginally stable wave numbers is defined as the caustics of the projection of the surface $K_{Fr,Bu}(k,l,\omega) = 0$ onto the (k,l)-plane, and can be found using the implicit function theorem on (5.34). This yields the condition

$$\frac{\partial K_{Fr,Bu}}{\partial \omega} = 0, \tag{5.35}$$

which implies that either $\nu = 0$, or

$$\varphi(m;Fr,Bu) = 0. \tag{5.36}$$

Therefore, the stability of generically directed waves ($\nu \neq 0$) only depends on the magnitude of their wave number, i.e., their wavelength. A particular choice for these coefficients is

$$Fr = \frac{1}{\sqrt{2}}, \quad Bu = \sqrt{2} \qquad \Rightarrow \qquad Ro = 1, \quad q_g = \frac{1}{2}, \tag{5.37}$$

whereby,

$$\varphi(m;1/\sqrt{2},\sqrt{2}) = \left(1 - \frac{m}{2}\coth\frac{m}{2}\right)\left(\frac{m}{2}\tanh\frac{m}{2} - 1\right). \tag{5.38}$$

The corresponding dispersion relation (5.34) is depicted in Figure 5.1 for different values of ν. In order to discuss the qualitative properties of an

unstable Eady wave, we fix $m = 2$, which corresponds to the purely imaginary frequency

$$\omega = \frac{2i\cos(\nu)}{\sqrt{e^4 - 1}}. \tag{5.39}$$

The simplest solution having $m = 2$ is obtained by setting $k = 2, l = 0$ (which implies $\nu = 0$) and represents an X-travelling wave,

$$\begin{aligned} S = \frac{X^2}{2} + \frac{Y^2}{2} - \frac{z^2}{4} + \frac{Yz}{\sqrt{2}} - z - 2\sqrt{2}e^{\omega_i t}\Big[2e^{-\sqrt{2}z}\cos(t - 2X) + \\ + \omega_i(e^{\sqrt{2}z} + e^{-\sqrt{2}z})\sin(t - 2X)\Big]\varepsilon, \end{aligned} \tag{5.40}$$

where

$$\omega_i = \frac{2}{\sqrt{e^4 - 1}}. \tag{5.41}$$

5.3 Geometric picture

Equation (5.40) may be seen as a 1-parameter family of generating functions describing a family of Lagrangian submanifolds L_t indicized by time. Specifically, (5.40) provides an example of a cylindrical solution in the sense of (2.122) for each fixed t with

$$C = \frac{1}{\sqrt{2}}, \tag{5.42}$$

and

$$\begin{aligned} S'(X, z, t) = \frac{X^2}{2} - \frac{z^2}{4} - z - 2\sqrt{2}e^{\omega_i t}\Big[2e^{-\sqrt{2}z}\cos(t - 2X) + \\ + \omega_i(e^{\sqrt{2}z} + e^{-\sqrt{2}z})\sin(t - 2X)\Big]\varepsilon. \end{aligned} \tag{5.43}$$

Not every member of this family has a nice projection to the physical space, i.e., singularities may appear in L_t as t varies. The singular locus of L_t is

$$\Sigma L_t = \left\{(X, Y, z) \in L_t : \, f(X, z, t) = 0 \, , \, 0 < z < \sqrt{2}\right\}, \tag{5.44}$$

where

$$f(X, z, t) \equiv \frac{\partial^2 S}{\partial X^2}, \tag{5.45}$$

and is independent on Y. The time evolution of a slice $Y = \textit{constant}$ through ΣL_t within one solution period is depicted in Figure 5.2. Two topological

changes of ΣL_t occur as time evolves: (i) the singular set is empty for $t < t'$; (ii) at $t = t'$, the singular set consists of two A_3 points at $z = 0$ and $z = \sqrt{2}$ respectively; (iii) for $t' < t < t''$, the singular locus is a disconnected set made of two surfaces (curves in the (X, z)-plane) which originate and terminate on either $z = 0$ or $z = \sqrt{2}$, each one comprising a cusp point A_3 and a continuous set of fold points A_2; (iv) these two curves collide at $t = t''$, when the two A_3 points coalesce and a higher order singularity is produced; (v) the A_3 points are absent for $t > t''$, and the singular set consists of two disconnected components each of which comprises fold points (A_2) only.

The two singular times t', t'' may be determined by tracking the motion of the A_3 points using (3.8). Note that the projection mapping now reads

$$\pi|_{L_t}(X, Y, z) = \left(\frac{\partial S'}{\partial X}, Y + z/\sqrt{2}, z\right), \tag{5.46}$$

and its differential is

$$d\pi|_{L_t} = \begin{pmatrix} \partial^2 S' & \partial_X \partial_Y S' & \partial_X \partial_z S' \\ 0 & 1 & 1/\sqrt{2} \\ 0 & 0 & 1 \end{pmatrix}. \tag{5.47}$$

Therefore, a vector field ξ that generates the kernel of $d\pi|_{L_t}$ is $\xi = \partial_X$, and equations (3.8) together with (5.45) yield

$$A_3 \text{ points: } \begin{cases} \partial_X^2 S' = 0, \\ \partial_X^3 S' = 0. \end{cases} \tag{5.48}$$

If we set $z = 0$ or $z = \sqrt{2}$, we obtain the time of the first topological change of ΣL_t, i.e., when singularities first appear,

$$t' \approx 5.3, \tag{5.49}$$

which occur at the positions

$$X \approx 4.1 + k\pi, \qquad k \in \mathbb{Z}. \tag{5.50}$$

Setting $z = \sqrt{2}/2$ yields the time of the second topological change,

$$t'' \approx 7.6, \tag{5.51}$$

and the positions at which the pairs of A_3 points are annihilated through the production of higher order singularities,

$$X \approx 4.9 + k\pi. \tag{5.52}$$

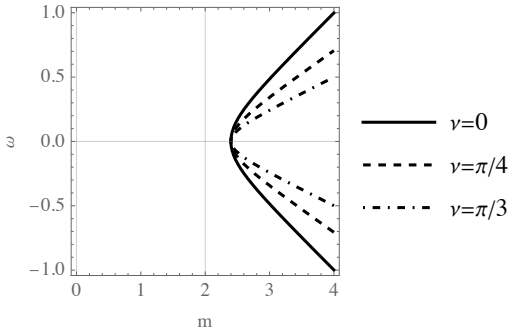

Figure 5.1: Dispersion relation (5.34) with $Bu = \sqrt{2}, Fr = 1/\sqrt{2}$ for different values of the angle ν that the wave direction forms with the X-axis.

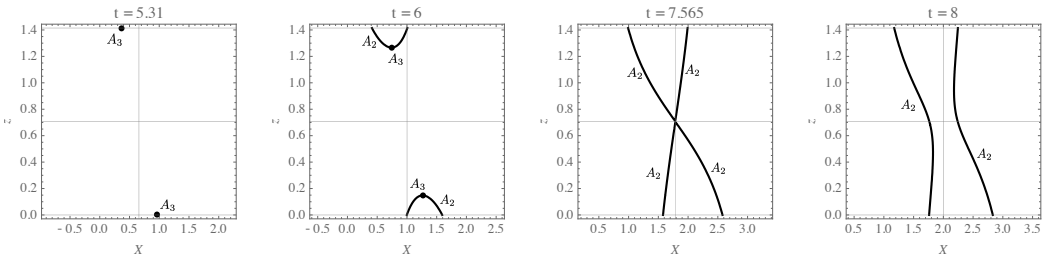

Figure 5.2: A slice through the singular locus ΣL_t for constant Y at different times.

5.4 Curvature of Eady solutions

This section collects unpublished material regarding the curvature of the pull-back metric h_α (cf. equation (4.1)) on Eady solutions. As we show below, the sign of the scalar curvature of an Eady solution L_t is directly connected to the signature of the pull-back metric, a feature that reveals the essential 2-dimensional nature of these solutions. We prove this statement with regards to X-travelling waves, and then extend our conclusions to general Eady waves by means of an adapted coordinate system.

Waves travelling in the X-direction are specified by a generating function of the form

$$S = \frac{Y^2}{2} + Fr\, Y z + S'(X, z, t), \tag{5.53}$$

where S_0 is the Eady basic state (5.13), and S_1 is the perturbation field (5.27). The pull-back metric (4.18) thus reads

$$h_\alpha = 2q_g\left(\frac{\partial^2 S'}{\partial X^2}dX^2 + dY^2 - \frac{\partial^2 S'}{\partial z^2}dz^2\right), \tag{5.54}$$

and, since S' satisfies (2.123), may be simplified to

$$h_\alpha = 2q_g\left(\frac{\partial^2 S}{\partial X^2}(dX^2 + q_g dz^2) + dY^2\right). \tag{5.55}$$

Because q_g is a constant, it follows from (5.55) that the geometry of a Lagrangian submanifold L_t representing an X-wave locally decomposes into the Cartesian product of the Y-axis and a slice $Y = const$. The scalar curvature of the constant-Y slices (which coincides with the scalar curvature of the whole L_t) is[1]

$$Sc = \frac{\left(\frac{\partial f}{\partial z}\right)^2 + q_g\left(\frac{\partial f}{\partial X}\right)^2 - f\left(\frac{\partial^2 f}{\partial z^2} + q_g\frac{\partial^2 f}{\partial X^2}\right)}{q_g f^3}, \tag{5.56}$$

where $f \equiv \partial_X^2 S$ is defined in (5.45), and, with the choice of coefficients (5.37), reads

$$f = 1 - 8\sqrt{2}e^{\omega_i t}\left[2e^{-\sqrt{2}z}\cos(t-2X) + \omega_i(e^{\sqrt{2}z} + e^{-\sqrt{2}z})\sin(t-2X)\right]\varepsilon. \tag{5.57}$$

Now observe that the second addendum in the numerator of (5.56) is identically zero. Indeed,

$$\frac{\partial^2 f}{\partial z^2} + q_g\frac{\partial^2 f}{\partial X^2} = \frac{\partial^3 S'}{\partial X \partial z^2} + q_g\frac{\partial^3 S'}{\partial X^3} = \frac{\partial}{\partial X}\left(\frac{\partial^2 S'}{\partial z^2} + q_g\frac{\partial^2 S'}{\partial X^2}\right) = 0, \tag{5.58}$$

[1] Curvature calculations were performed using Professor Leonard Parker's Mathematica notebook "Curvature and the Einstein Equation," available online here.

where we have used $q_g = constant$ and (2.123). We are thus allowed to write (5.56) in the form

$$Sc = \frac{\left(\frac{\partial f}{\partial z}\right)^2 + q_g \left(\frac{\partial f}{\partial X}\right)^2}{q_g f^3}. \tag{5.59}$$

Formula (5.59) brings up some basic facts about the curvature of X-travelling waves:

- Using (2.100) and the last of (2.90) in (5.45), we may write f as

$$f = \frac{\partial\theta/\partial z}{q_g} = \frac{N^2}{q_g}. \tag{5.60}$$

  The last equality follows from the definition of the Brunt–Vaisala frequency (see [47]) using the dimensional variables discussed in Section 5.1. The numerator in this expression represents a measure of the atmosphere stratification, and is directly related to the static stability of the atmosphere. For constant q_g and positive N^2, (5.59) represents a norm of the gradient $(\partial_X N, \partial_z N)$.

- As the numerator in (5.59) is always non-negative, the sign of Sc is inherited from f. This puts Sc in relation with the signature of h_α: the Riemannian branches of L are positively curved, whereas the psuedo-Riemannian branches of L are negatively curved (see Figure 5.3). This can also be stated in terms of ellipticity/hyperbolicity of the Monge–Ampère operator: the elliptic branches of L are positively curved whereas the hyperbolic branches of L are negatively curved [30].

- The numerator in (5.59) is a strictly positive quantity at generic points on $\Sigma L = \{f = 0\}$, which implies that Sc blows up at generic singular points (including A_3 points). This statement fails at $t = t''$, when the topology of the singular locus changes. At such time, higher order singularities are produced (see Figure 5.3) and the numerator in (5.59) vanishes. It can be verified that the numerator in (5.59) goes to zero faster than f^3 as one of these points is approached, which means that $Sc \to 0$ as well.

- The scalar curvature blows up at A_3 points (as f^{-3}). Thanks to this, Sc may be interpreted as a diagnostic tool which reveals the impending development of a front. Figure 5.4 shows a section through the graph of $Sc(X, z, t)$ for fixed z at different times before the catastrophe time. The maxima appear much earlier than the swallowtail singularities do,

and grow unbounded quickly. Tracing them can give an estimate of the position where the fronts will appear.

We conclude this section with a discussion on Eady waves propagating in a general direction. If $l \neq 0$, then S_1 depends also on Y, and neither (5.55) nor (5.59) are valid anymore. However, it is always possible to introduce a rotated coordinate system on L_t which allows us to write the pull-back metric and the scalar curvature in a form analogous to (5.55) and (5.59). Namely, we introduce a change of coordinates on $T^*\mathbb{R}^3$,

$$(x, y, z, X, Y, Z) \mapsto (x, y, z, X', Y', Z), \tag{5.61}$$

by

$$X' = \frac{kX + lY}{m}, \qquad Y' = \frac{kY - lX}{m}, \tag{5.62}$$

with inverse

$$X = \frac{kX' - lY'}{m}, \qquad Y = \frac{lX' + kY'}{m}. \tag{5.63}$$

Observe that

$$dX \wedge dY = \left(\frac{k}{m}dX' - \frac{l}{m}dY'\right) \wedge \left(\frac{l}{m}dX' + \frac{k}{m}dY'\right) = \tag{5.64}$$

$$= \frac{k^2}{m^2}dX' \wedge dY' - \frac{l^2}{m^2}dY' \wedge dX' = \frac{k^2 + l^2}{m^2}dX' \wedge dY' = dX' \wedge dY'. \tag{5.65}$$

Therefore, the Monge–Ampère form (3.13) becomes

$$\alpha = dX' \wedge dY' \wedge dZ - q_g dx \wedge dy \wedge dz. \tag{5.66}$$

The equations defining L_t (see (3.21) become

$$x = \frac{\partial S}{\partial X} = \frac{k}{m}\frac{\partial S}{\partial X'} - \frac{l}{m}\frac{\partial S}{\partial Y'}, \qquad y = \frac{\partial S}{\partial Y} = \frac{l}{m}\frac{\partial S}{\partial X'} + \frac{k}{m}\frac{\partial S}{\partial Y'}, \tag{5.67}$$

and

$$Z = -\frac{\partial S}{\partial z}. \tag{5.68}$$

Using these equations in $\alpha|_{L_t} = 0$ yields

$$q_g\left(\frac{\partial^2 S}{\partial X'^2}\frac{\partial^2 S}{\partial Y'^2} - \left(\frac{\partial^2 S}{\partial X' \partial Y'}\right)^2\right) + \frac{\partial^2 S}{\partial z^2} = 0. \tag{5.69}$$

This result says that the Chynoweth–Sewell equation (2.100) is invariant under rotations of the (X, Y)-plane. Next, consider the Lychagin–Roubtsov metric (4.3). The ambient metric becomes

$$\frac{g_\alpha}{2q_g} = dx\left(\frac{k}{m}dX' - \frac{l}{m}dY'\right) + dy\left(\frac{l}{m}dX' + \frac{k}{m}dY'\right) + dzdZ. \tag{5.70}$$

Using (5.67), a lengthy but straightforward calculation shows that the pull-back metric $h_\alpha = g_\alpha|_{L_t}$ becomes

$$h_\alpha = 2q_g\left(\frac{\partial^2 S}{\partial X'^2}dX'^2 + 2\frac{\partial^2 S}{\partial X'\partial Y'}dX'dY' + \frac{\partial^2 S}{\partial Y'^2}dY'^2 - \frac{\partial^2 S}{\partial z^2}dz^2\right). \tag{5.71}$$

Next, note that the general Eady solution may be written in the new coordinates as

$$S = S_0 + \varepsilon\Re(S_1), \tag{5.72}$$

where,

$$S_0 = \frac{X'^2}{2} + \frac{Y'^2}{2} - q_g\frac{z^2}{2} - z + Fr\, z(Y'\cos(\nu) + X'\sin(\nu)), \tag{5.73}$$

$$S_1 = \psi(\tilde{z})e^{i(m\tilde{X}' - \omega t)}, \tag{5.74}$$

and

$$\tilde{X}' := X' - \frac{k}{m}\frac{Ro}{2}t. \tag{5.75}$$

Therefore, the structure of a general Eady wave is the same of an X-travelling wave except for the additional term

$$Fr\, X' z\sin(\nu) \tag{5.76}$$

in S_0. Accordingly, the pull-back metric on L_t reads

$$h_\alpha = 2q_g\left(\frac{\partial^2 S}{\partial X'^2}(dX'^2 + q_g dz^2) + dY'^2\right), \tag{5.77}$$

and the scalar curvature becomes

$$Sc = \frac{\left(\frac{\partial f'}{\partial z}\right)^2 + q_g\left(\frac{\partial f'}{\partial X'}\right)^2}{q_g f'^3}, \qquad f' := \frac{\partial^2 S}{\partial X'^2}. \tag{5.78}$$

Equation (5.77) says that the geometry of L_t is naturally decomposed into the Cartesian product of constant-Y' slices and the Y'-axis. Since the curvature (5.78) has the same form as (5.59), all the considerations about the X-travelling waves apply to general Eady waves as well.

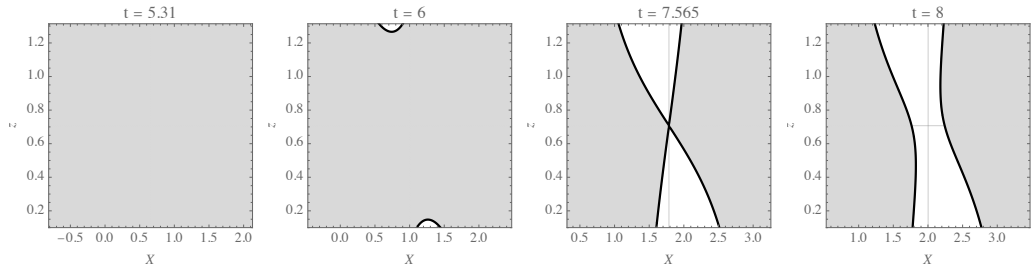

Figure 5.3: The regions of positive scalar curvature (gray) within a constant-Y slice of L_t at different times. The black boundaries represent (a slice through) the singular locus ΣL_t.

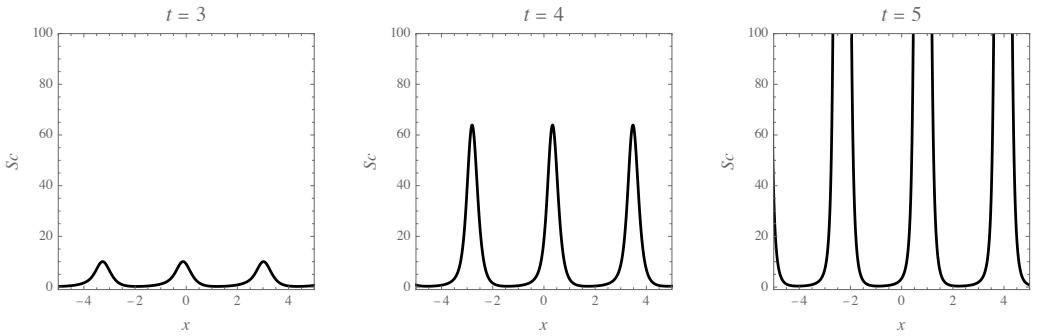

Figure 5.4: Slice at $z = 0$ through the graph of Sc for three times preceding $t' \approx 5.3$. Curvature maxima are already visible at $t = 3$ and grow unbounded quickly as $t \to t'$.

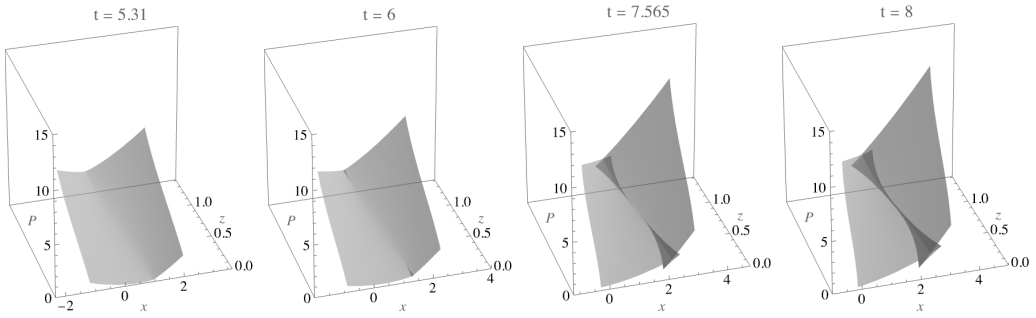

Figure 5.5: The slice $y = 0$ trough the graph of the multivalued P obtained by Legendre transforming (5.40). The snapshots refer to times $t = t', 6.5, t'', 8.5$.

5.5 Reconstruction of the physical fields

We devote this last section on the Eady model to describe the physical picture associated with an unstable baroclinic wave. We start by making more precise the features of the domain under consideration. As (5.40) is a periodic wave translating with constant speed, it is convenient to fix the attention on just one particular period. To this aim, we consider a moving observation window, linearly translating in time, of constant width π,

$$X_c(t) - \pi/2 < X < X_c(t) + \pi/2, \tag{5.79}$$

where

$$X_c(t) := X_0 + \frac{t - t_0}{2}. \tag{5.80}$$

The parameters (X_0, t_0), which we pick as

$$X_0 \approx 1.0, \qquad t_0 = 6, \tag{5.81}$$

are chosen so as to center the observation window upon a developing singularity.

The geopotential P is obtained through the inverse Legendre transform of (5.40), and its graph is depicted in Figure 5.5. The loss of convexity which occurs in $S(\,\cdot\,,\,\cdot\,,z,t)$ at $t = t'$ results in the appearance of two swallowtail points in the graph of P at $z = 0, Bu$. As the time increases, the two swallowtails grow against each other, and ultimately coalesce at $t = t''$. The two swallowtail points annihilate at this time, and, for $t > t''$, two cusped edges continuously running from $z = 0$ to $z = Bu$ are left. Self intersection in the multivalued graph of P is present for any time $t > t'$, and represent a Chynoweth–Sewell front.

The velocity field corresponding to (5.40) is obtained from (3.28), (3.29), and (2.116), and, like P, it is multivalued for $t > t'$. In order to produce a meaningful picture of the velocity field, we need to amend multivaluedness and introduce fronts in the picture. To do so, we use the Chynoweth and Sewell algorithm described Section 2.5. Namely, we look for the convex envelope $\check{S}(\,\cdot\,,\,\cdot\,,z,t)$ of the function (5.40) within the domain (5.79) for every fixed $0 < z < \sqrt{2}$ and $t > t'$. Due to the algebraic complexity of the solution (5.40) we are unable to solve the convex envelope problem analytically, so we resort to numerics. The algorithm we use is roughly summarised by:

1. Fix a time $t_k > t'$;

2. Take a partition $\{z_i\}$ of the interval $(0, \sqrt{2})$;

3. For each i, set $z = z_i$ and solve (2.125) with any root-finding algorithm using the solution to $f(X, z_i, t_k) = 0$ as the initial guess. This provides a pair of points $(X_1(z_i, t_k), X_2(z_i, t_k))$;

4. If the points $(X_1(z_i, t_k), X_2(z_i, t_k))$ are distinct, they are stored in memory. Otherwise they are discarded.

5. Interpolate the points $\{X_1(z_i, t_k)\}_i$ to build the curve $\Gamma_-(t_k)$ and interpolate the points $\{X_2(z_i, t_k)\}_i$ to build the curve $\Gamma_+(t_k)$.

Iterating the above algorithm for a few t_k provides an approximation of the physical region boundary $\Gamma_+(t_k) \cup \Gamma_-(t_k)$ for different times (see again figure Figure 5.6). The image of the curve $\Gamma_+(t_k) \cup \Gamma_-(t_k)$ under the inverse Legendre map (2.91) represents a Chynoweth–Sewell front in the physical plane (x, z) at $t = t_k$. To plot of the velocity field associated to (5.40) we proceed as follows:

1. Fix a time $t_k > t'$;

2. Discretize the *physical region* (the region bounded by $\Gamma_+(t_k) \cup \Gamma_-(t_k)$ in Figure 5.6) using any triangulation algorithm;

3. Map each vertex (X_j, z_j) of this triangulation to the physical plane (x, z) using the inverse Legendre map (2.91);

4. Apply to each point a vector (u_j, w_j) whose components are determined by (3.28) and (2.116) evaluated on (X_j, z_j).

Remark 5.5.1. *Note that neither* $\Gamma_-(t_k) \cup \Gamma_+(t_k)$ *nor the velocity field depend on* Y.

Both the algorithms described above are implemented in Wolfram Mathematica, and a description of the code used can be found in Appendix B. Figure 5.6 shows the region of physical interest at a particular time and its relationship with the singular set. Geometrically, the physical region of Figure 5.6 corresponds to the modified Lagrangian submanifold $\check{L}_t$ (see Section 3.4). It is worth noting that all the A_2 points of ΣL_t fall outside the physical region (i.e., $\check{L}_t$) while the A_3 points are found on its boundary (i.e., on $\partial\check{L}_t$). This has implications on the velocity field, as we discuss next.

Figure 5.7 provides a view of the physical picture associated with $\check{L}_t$. The physical velocity field (u, w) on a slice $y = \textit{constant}$ is shown along with the corresponding geopotential ϕ for several times. At $t \approx 5.29 < t'$, the solution is still regular – the geopotential contours and the velocity field

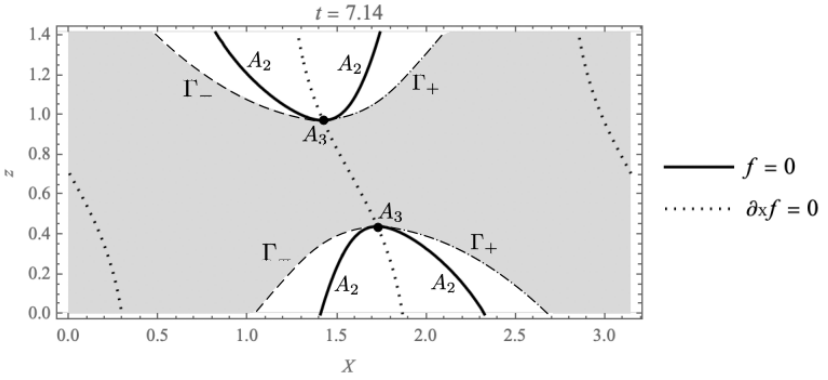

Figure 5.6: Region of physical interest in the (x, z)-plane for $t \approx 7.14$. The singular locus ΣL and the boundaries Γ_- and Γ_+ are shown as a bold, dashed, and dash-dotted curve respectively. All the fold points A_2 are found outside the physical region, whereas the cusp points A_3 are found on its boundary.

are smooth – but the singularity is about to occur. For $t \geq t'$, the solution contains frontal surfaces, where both the velocity field and the slope of the geopotential contours experience a jump discontinuity. As a consequence of the fact that (the closure of) $\check{L}_t$ shares the A_3 points with ΣL, the velocity field blows up at the projection of these points, which represent the fronts tip. The fronts keep growing over time until $t = t''$, when they meet and become a single front running continuously from $z = 0$ to $z = \sqrt{2}$. The velocity field is everywhere discontinuous but bounded for $t > t''$.

5.6 Summary of Chapter 5

In this chapter, we have presented the classical Eady problem in the contemporary language of Monge–Ampère geometry. We have reviewed Hoskins' solution to the Eady problem in Section 5.2 using the formalism of the Legendre transform. Next, we considered a subclass of Hoskins' solutions representing baroclinic waves traveling in the X-direction. In Section 5.3 we studied these solutions in light of the theory of Chynoweth–Sewell fronts presented in Section 2.5 and in Section 3.4. In Section 5.4, we studied these solutions from the point of view of the pseudo-Riemannian geometry introduced in Chapter 4. The geometry of such solutions is effectively two-dimensional also from the metric point of view, and, for this reason, the sign of the scalar curvature of the $Y = \textit{constant}$ sections is directly dependent on the signature of the pull-back metric. We then extended this result to a baroclinic wave traveling in an arbitrary direction using a coordinate system adapted

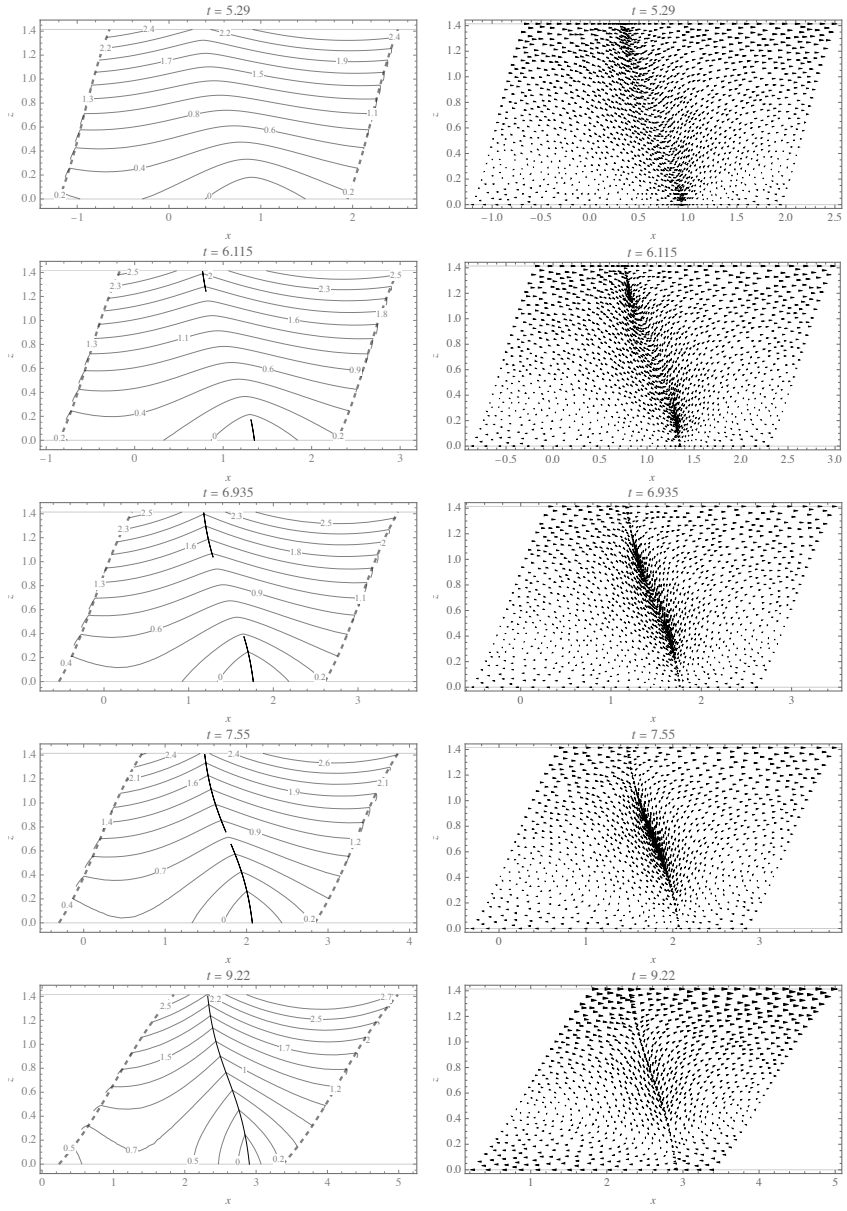

Figure 5.7: Left: contours of the geopotential ϕ on the plane $y = constant$ for different times. The observation window is deformed by the Legendre transform and its boundaries are indicated by dashed lines. The (section of the) frontal surfaces are represented by thin solid curves transverse to the geopotential contours. Right: the corresponding velocity field (u, w). The front corresponds to the region where the density of plotted points is higher.

to the vector wavenumber. The last section of this chapter is dedicated to the recovery of the physical information contained in a Hoskins solution. We have shown that, in physical space, the Hoskins solution precisely produces Chynoweth–Sewell fronts. Finally, we have detailed an algorithm that can be easily implemented on the computer for calculating the position of the Chynoweth–Sewell fronts and the velocity field within a period of the solution.

Chapter 6

Conclusions and future directions

In this thesis we studied two classical models of fluid dynamics, paying particular attention to the relationship between singularities and the parabolic regime.

In Chapter 1, we considered shallow water equations, and were interested in the time evolution of a class of initial conditions containing a singularity. Specifically, we investigated the behavior of first-order or higher-order singularities, and showed that this strongly depends on whether the singular point is hyperbolic (located within the fluid-filled region) or parabolic (located on a dry boundary). The main method used in these studies is the so-called wavefront expansion which allows to locally analyze the SWE solution near the singular point.

Chapters from the second onwards concern the semi-geostrophic equations. We have dedicated Chapter 2 to reviewing the derivation of the equations and classical methods for their manipulation, such as the vorticity-streamfunction formulation and the Legendre transform.

In Chapter 3, we introduced the rudiments of Monge–Ampère geometry, and applied its main results to singular solutions of semigeostrophic equations. We characterized the construction of Chynoweth–Sewell fronts in geometric terms and this allowed us to draw a parallel with the theory of unsteady shocks in one-dimensional gas flows.

In Chapter 4, we introduced and studied the Lychagin–Roubtsov metric in the context of semigeostrophic equations. We have shown that the metric geometry of generalized solutions is strongly dependent on the character of the Monge–Ampère equation for the solution considered: hyperbolic character corresponds to Lorentzian geometry while elliptic character corresponds to Riemannian geometry. We finally showed that the pull-back metric degen-

erates on the singular set, and that this, consequently, necessarily corresponds to a hyperbolic-elliptic transition of the system.

The final chapter deals with the Eady problem, a benchmark example to demonstrate the results of the previous chapters. The main result of this chapter is that the essentially two-dimensional character of the baroclinic waves is reflected in the geometry of the solutions, whose curvature is directly dependent on the signature of the pull-back metric.

Our investigations have given rise to questions which, due to the limited time, are not yet answered.

In the context of SWEs, the study of class C^1 singular points in two spatial dimensions is particularly intriguing. In this setting, in fact, preliminary numerical studies have suggested that a notion of shoulder does not exist, and that the dynamics of C^1 singularities is subject to laws entirely different from those described in Chapter 1.

Aside, we observe that the SWE system in one spatial dimension can be understood as a Jacobi system [55]. This makes available all the tools of Monge–Ampère geometry and catastrophe theory that we reviewed in Chapter 3 for the SWE (see also [63]). More importantly, it allows us to define a Lychagin–Roubtsov metric associated with SWEs, and study its behavior on generalized solutions and singularities.

On the side of semigeostrophic equations, further work is needed to understand the parallelism between Chynoweth–Sewell fronts and gas dynamical shocks. Indeed, some of the properties pointed out in the Section 5.5 are in apparent contrast with the classical literature on weather fronts. For example, Cullen [19] establishes that atmospheric fronts are advected by the fluid flow, and that a front continuously running from sea level to the tropopause cannot exist, but the solution to the Eady problem of Section 5.5 violates both of these statements.

There are a few side questions concerning the geometry of semigeostrophic equations. The physical and geometric meaning of the curvature of generalized solutions is not yet clear, and we have partially addressed the question in the context of Eady waves. As we showed in the Section 5.4, the curvature of baroclinic wave-type solutions does not add any essential information to that already encoded by the Lychagin–Roubtsov metric. This is due to the essentially two-dimensional nature of such solutions, and richer behavior may be expected in fully three-dimensional solutions. A further fascinating question concerns the possibility of describing the dynamics of semigeostrophic equations in terms of a geometric flow on Lagrangian submanifolds. This would be a result of great theoretical value because it would provide a unified view on the kinematics and dynamics of singularities. However, the attempts made so far have been inconclusive, and, to date, it does not seem that an entirely

geometric formulation of the dynamics of the system is possible.

Appendix A

Curvature of the phase space

This is a collection of partial results regarding the curvature of the phase space in the semigeostrophic setting. From a mathematical perspective, the most general situation in which (4.3) gives a well defined metric on $T^*\mathbb{R}^3$ is when q_g depends on all the coordinates on $T^*\mathbb{R}^3$,

$$q_g = q_g(x, y, z, X, Y, Z). \tag{A.1}$$

The following statements are easy to check

1. The scalar curvature of the phase space is

$$Sc = -5\frac{\partial_x\partial_X q_g + \partial_y\partial_Y q_g + \partial_z\partial_Z q_g}{q_g^2}. \tag{A.2}$$

2. Introducing the change of variables

$$\xi_1 = x + X, \qquad \xi_2 = x - X = -v_g, \tag{A.3}$$
$$\eta_1 = y + Y, \qquad \eta_2 = y - Y = u_g, \tag{A.4}$$
$$\zeta_1 = z + Z, \qquad \zeta_2 = z - Z, \tag{A.5}$$

it is possible to write the scalar curvature (A.2) in the form

$$Sc = -5\frac{\Delta_1 q_g - \Delta_2 q_g}{q_g^2}, \tag{A.6}$$

where

$$\Delta_1 := \partial^2_{\xi_1} + \partial^2_{\eta_1} + \partial^2_{\zeta_1}, \qquad \Delta_2 := \partial^2_{\xi_2} + \partial^2_{\eta_2} + \partial^2_{\zeta_2}. \tag{A.7}$$

In particular, q_g locally solves the *ultrahyperbolic equation*,

$$\Delta_1 q_g = \Delta_2 q_g. \tag{A.8}$$

on points of zero scalar curvature.

3. If q_g only depends on (x, y, z), the scalar curvature of the phase space vanishes. Moreover, the Ricci curvature tensor takes the form

$$Ric_{ij} = \begin{cases} \frac{3\partial_i q_g \partial_j q_g - 2q_g \partial_i \partial_j q_g}{q_g^2}, & \text{for } i \leq 3, j \leq 3 \\ 0, & \text{otherwise.} \end{cases} \tag{A.9}$$

4. Under the same hypothesis, the Ricci tensor takes the following form at critical points of q_g,

$$Ric_{ij} = \begin{cases} -2\frac{\partial_i \partial_j q_g}{q_g}, & \text{for } i \leq 3, j \leq 3 \\ 0, & \text{otherwise.} \end{cases} \tag{A.10}$$

This shows that the signature Ric is related to maxima and minima of the potential vorticity in a definite way. A similar result is obtained in [72], where the sign of the scalar curvature of the phase space is put in relation with the local accumulation of vorticity in 2-dimensional Euler flows.

Appendix B

Wolfram Mathematica codes

In this section, we collect the Mathematica codes that implement the algorithms described in the Section 5.5. We start with the definition of the generalized solution (5.40):

```
In[•]:= S := X^2/2 + Y^2/2 - z + Y z/Sqrt[2] - z^2/4 - 2 Sqrt[2] η E^(ωi t) (2 E^(-Sqrt[2] z) Cos[2 X - t] - ωi (E^(Sqrt[2] z) + E^(-Sqrt[2] z)) Sin[2 X - t])

In[•]:= ωi := 2/Sqrt[-1 + E^4]

In[•]:= η := 1 / 100
```

Our algorithm for the computation of the fronts and the velocity field is dependent on whether $t < t'$, $t' < t < t''$, or $t > t''$. We assume $t' < t < t''$, and discretize this time interval into

```
In[•]:= times = Table[5.5 + 0.205 j, {j, 0, 10}]
Out[•]= {5.5, 5.705, 5.91, 6.115, 6.32, 6.525, 6.73, 6.935, 7.14, 7.345, 7.55}

In[•]:= Length[times]
Out[•]= 11
```

Next, we define the moving observation window (5.79) with $X_c(t)$ given by

```
In[•]:= Xc[t_] := 1.0025666287101322` + 1/2 (-6 + t)

In[•]:= Iconize[Map[Xc, times], "ListXc"]
Out[•]= ListXc
```

In the time interval considered, the solution features two A_3 (cusp) points in the observation window. To locate them, we define

```
In[•]:= Iconize[D[S, X, X], "f"]
Out[•]= f

In[•]:= Iconize[D[S, X, X, X], "fx"]
Out[•]= fx
```

These expressions are then used to define the (X, z)-coordinates of the two A_3 points as

```
In[•]:= Iconize[Table[Extract[FindRoot[{f == 0, fx == 0}, {X, Xc[t]}, {z, √2}] /. Rule → List, {1, 2}], {t, times}], "Xtop(t)"]
Out[•]= Xtop(t)

In[•]:= Iconize[Table[Extract[FindRoot[{f == 0, fx == 0}, {X, Xc[t]}, {z, √2}] /. Rule → List, {2, 2}], {t, times}], "Ztop(t)"]
Out[•]= Ztop(t)

In[•]:= Iconize[Table[Extract[FindRoot[{f == 0, fx == 0}, {X, Xc[t]}, {z, 0}] /. Rule → List, {1, 2}], {t, times}], "Xbot(t)"]
Out[•]= Xbot(t)

In[•]:= Iconize[Table[Extract[FindRoot[{f == 0, fx == 0}, {X, Xc[t]}, {z, 0}] /. Rule → List, {2, 2}], {t, times}], "Zbot(t)"]
Out[•]= Zbot(t)
```

Next, we define the system of equations (2.125) to be solved for the unknowns points $X_1(z,t)$ and $X_2(z,t)$ delimiting the physical region,

```
In[•]:= Iconize[S /. X → X1, "S1"]
Out[•]= S1

In[•]:= Iconize[S /. X → X2, "S2"]
Out[•]= S2

In[•]:= Iconize[D[S, X] /. X → X1, "dS1"]
Out[•]= dS1

        Iconize[D[S, X] /. X → X2, "dS2"]
Out[•]= dS2

In[•]:= Iconize[{S2 - S1 == dS1 (X2 - X1), S2 - S1 == dS2 (X2 - X1)}, "equations"]
Out[•]= equations
```

These equations are solved for several values of $0 < z < z_{bot}(t)$ and $z_{top}(t) < z < \sqrt{2}$ and the resulting points are interpolated to get the boundaries of the upper and lower fronts within the observation window at a given time:

```
upperfront[k_] := Interpolation[Flatten[{
    Reverse[
     Table[
      {Extract[FindRoot[equations /. t → times[[k]], {{X1, Extract[ListXc, k] - 1.2},
           {X2, Extract[ListXc, k] + 1.2}}] /. Rule → List, {1, 2}], z},
      {z, Table[i, {i, Extract[Ztop(t), k] + 0.001, √2, (√2 - Extract[Ztop(t), k]) / (5 k)}]}], 1],
    {{Extract[Xtop(t), k], Extract[Ztop(t), k]}},
    Table[
     {Extract[FindRoot[equations /. t → times[[k]], {{X1, Extract[ListXc, k] - 1.2},
          {X2, Extract[ListXc, k] + 1.2}}] /. Rule → List, {2, 2}], z},
     {z, Table[i, {i, Extract[Ztop(t), k] + 0.001, √2, (√2 - Extract[Ztop(t), k]) / (5 k)}]}]
   }, 1]]

lowerfront[k_] :=
 Interpolation[
  Flatten[
   {Table[
     {Extract[FindRoot[equations /. t → times[[k]], {{X1, Extract[ListXc, k] - 1.2},
          {X2, Extract[ListXc, k] + 1.2}}] /. Rule → List, {2, 2}], z},
     {z, Table[i, {i, 0.001, Extract[Zbot(t), k], Extract[Zbot(t), k] / (5 k)}]}],
    {{Extract[Xbot(t), k], Extract[Zbot(t), k]}},
    Reverse[
     Table[
      {Extract[FindRoot[equations /. t → times[[k]], {{X1, Extract[ListXc, k] - 1.2},
           {X2, Extract[ListXc, k] + 1.2}}] /. Rule → List, {1, 2}], z},
      {z, Table[i, {i, 0.001, Extract[Zbot(t), k], Extract[Zbot(t), k] / (5 k)}]}], 1]}, 1]]
```

The upper and lower boundaries of the physical region within the observation window are found by

```
upperboundary[k_, X_] :=
 Piecewise[
  {{upperfront[k][X], Extract[upperfront[k]["Domain"], {1, 1}] < X < Extract[upperfront[k]["Domain"], {1, 2}]}},
  √2]

lowerboundary[k_, X_] :=
 Piecewise[
  {{lowerfront[k][X], Extract[lowerfront[k]["Domain"], {1, 1}] < X < Extract[lowerfront[k]["Domain"], {1, 2}]}},
  0]
```

Thus, the (triangulated) physical region is provided by

```
meshregion[k_] :=
 DiscretizeRegion[
  ImplicitRegion[{Extract[ListXc, k] - π / 2 < X < Extract[ListXc, k] + π / 2,
    lowerboundary[k, X] < z < upperboundary[k, X]}, {X, z}], MaxCellMeasure → 0.002, PlotTheme → "Scientific",
  MeshCellStyle → {{2, All} → LightGray, {1, All} → Gray, {0, All} → Black}, FrameLabel → {X, z},
  GridLines → {{}, {0, √2}}, LabelStyle → Directive[ FontFamily → "Times New Roman"],
  PlotLabel → Row[{t, " = ", times[[k]]}]]
```

Once we have the triangulation for the physical region, we can extract the coordinates of the vertices and map them into the physical plane using the inverse Legendre map (2.91). Then, to each mapped point is attached a vector with components (3.28) and(2.116), that is,

```
In[•]:= Iconize[D[S, Y] - Y, "ug"]
Out[•]= ug

In[•]:= Iconize[Simplify[X - D[S, X]], "vg"]
Out[•]= vg

In[•]:= Iconize[D[S, t, X] + ug D[S, X, X] + vg D[S, X, Y] + w D[S, X, z], "u"]
Out[•]= u

In[•]:= Iconize[Simplify[-(D[S, t, z] + ug D[S, X, z] + vg D[S, Y, z]) / D[S, z, z]], "w"]
Out[•]= w
```

The plot of the velocity field (u, w) is done by the following piece of code

```
In[•]:= velocityplot[k_] := ListVectorPlot[
  Map[
   Function[A, {{x} /. X → A[[1]] /. z → A[[2]] /. t → times[[k]], A[[2]]},
    {u} /. X → A[[1]] /. z → A[[2]] /. t → times[[k]], w /. X → A[[1]] /. z → A[[2]] /. t → times[[k]]}],
   MeshCoordinates[meshregion[k]]
  ]
  , VectorPoints → All, ImageSize → Medium, AspectRatio → 1 / 2, PlotTheme → "Scientific", VectorStyle → Black,
  VectorColorFunction → None, VectorScaling → "Linear", VectorMarkers → Placed["Pointer", "Middle"],
  FrameLabel → {x, z}, PlotLabel → Row[{t, " = ", times[[k]]}], GridLines → {{}, {0, √2}}, VectorSizes → Tiny]
```

The plot of the velocity field in the intervals $t < t'$ and $t > t''$ is handled similarly, except that it is easier. Indeed, for $t < t'$, the fronts have not formed yet, and the physical region is the whole observation window. For $t > t''$, the physical region is disconnected, and there are two curves $X_1(z,t)$ and $X_2(z,t)$ continuously running from $z = 0$ to $z = \sqrt{2}$. Thus, the piece of code that computes the front boundaries within the physical region is re-

placed by

```
leftpoints[k_] :=
 Table[
  {z,
   Extract[
    FindRoot[equations /. t → times[[k]], {{X1, Extract[ListXc, k] - 1.2}, {X2, Extract[ListXc, k] + 1.2}}] /.
     Rule → List, {1, 2}]}, {z, -.2, √2 + .2, 0.02}]

rightpoints[k_] :=
 Table[
  {z,
   Extract[
    FindRoot[equations /. t → times[[k]], {{X1, Extract[ListXc, k] - 1.2}, {X2, Extract[ListXc, k] + 1.2}}] /.
     Rule → List, {2, 2}]}, {z, -.2, √2 + .2, 0.02}]

frontleft[k_] := Interpolation[leftpoints[k]]

frontright[k_] := Interpolation[rightpoints[k]]

meshregion[k_] :=
 DiscretizeRegion[
  ImplicitRegion[
   {Extract[ListXc, k] - π / 2 < X < frontleft[k][z] || frontright[k][z] < X < Extract[ListXc, k] + π / 2,
    0 < z < √2}, {X, z}], MaxCellMeasure → 0.0015, PlotTheme → "Scientific",
  MeshCellStyle → {{2, All} → LightGray, {1, All} → Gray, {0, All} → Black}, FrameLabel → {X, z},
  GridLines → {{}, {0, √2}}, LabelStyle → Directive[ FontFamily → "Times New Roman"],
  PlotLabel → Row[{t, " = ", times[[k]]}]]
```

Bibliography

[1] V. I. Arnold (1978) *Mathematical Methods of Classical Mechanics*. New York: Springer

[2] V. I. Arnold, S. M. Gusein-Zade and A. N. Varchenko (2012) *Singularities of Differentiable Maps, Volume 1, Classification of Critical Points, Caustics and Wave Fronts*. Basel: Birkhäuser

[3] B. Banos (2002) "Nondegenerate Monge-Ampère Structures in Dimension 6", *Letters in Mathematical Physics*, **62**, 1–15

[4] J. D. Benamou & Y. Brenier (1998) "Weak Existence for the Semigeostrophic Equations Formulated as a Coupled Monge-Ampère/Transport Problem", *SIAM J. Appl. Math.*, **58**, 1450–1461

[5] B. Banos (2006) "Integrable geometries and Monge-Ampere equations", *https://arxiv.org/abs/math/0612514*

[6] H. R. Birkett & A. J. Thorpe (1997) "Superposing semi-geostrophic potential-vorticity anomalies", *Q. J. R. Meteorol. Soc.*, **123**(543), 2157–2163

[7] B. Banos, V. N. Roubtsov & I. Roulstone (2016) "Monge–Ampère structures and the geometry of incompressible flows", *J. Phys. A: Math. Theor.*, **49**, 244003 (17pp)

[8] Banos B., Rubtsov V., Roulstone I. (2019) On the Geometry Arising in Some Meteorological Models in Two and Three Dimensions. In: Kycia R., Ułan M., Schneider E. (eds) Nonlinear PDEs, Their Geometry, and Applications. Tutorials, Schools, and Workshops in the Mathematical Sciences. Birkhäuser, Cham. https://doi.org/10.1007/978-3-030-17031-8_5

[9] L. Bers, *Mathematical Aspects of Subsonic and Transonic Gas Dynamics*, Wiley & Sons Chapman & Hall, 1958

[10] R. Camassa, R. D'Onofrio, G. Falqui, G. Ortenzi & M. Pedroni (2022) "Evolution of interface singularities in shallow water equations with variable bottom topography", *Stud. Appl. Math.*, **148**(4), 1439–1476

[11] R. Camassa, G. Falqui, G. Ortenzi and M. Pedroni (2019) "On the Geometry of Extended Self-Similar Solutions of the Airy Shallow Water Equations" *SIGMA* **15**

[12] R. Camassa, G. Falqui, G. Ortenzi, M. Pedroni and G. Pitton (2019) "Singularity formation as a wetting mechanism in a dispersionless water wave model" *Nonlinearity* **32** 4079–4116

[13] R. Camassa, G. Falqui, G. Ortenzi, M. Pedroni and G. Pitton (2020) "On the "Vacuum" Dam-Break Problem: Exact Solutions and Their Long Time Asymptotics" *SIAM J. Appl. Math* **80** 44–70

[14] R. Camassa, G. Falqui, G. Ortenzi, M. Pedroni and C. Thomson (2019) "Hydrodynamic Models and Confinement Effects by Horizontal Boundaries" *J. Nonl. Sci.* **29** 1445–1498

[15] G. F. Carrier and H. P. Greenspan (1958) "Water waves of finite amplitude on a sloping beach" *J. Fluid Mech.* **4** 97–109

[16] S. Chynoweth & M. J. Sewell (1989) Dual variables in semigeostrophic theory, *Proc. R. Soc. Lond. A*, **424**, 155–186

[17] R. Courant, K. O. Friedrichs, *Supersonic Flow and Shock Waves*, Springer-Verlag New York, 1976

[18] R. Courant & D. Hilbert (1962) *Methods of mathematical physics. Volume II, Partial differential equations*, Wiley Interscience, New York

[19] M. Cullen (1983) "Solutions to a model of a front forced by deformation", *Q. J. R. Meteorol. Soc.*, **109**(461), 565–573

[20] M. Cullen (2006) *A Mathematical Theory of Large-Scale Atmosphere/Ocean Flow*, Imperial College Press, London

[21] M. Cullen (2021) *The Mathematics of Large-Scale Atmosphere and Ocean*. Singapore: World Scientific

[22] M. J. P. Cullen & R. J. Douglas (1998) "Applications of the Monge-Ampère equation and Monge transport problem to meteorology and oceanography", in "Monge-Ampère Equation: Applications to Geometry and Optimization" (L.A. Caffarelli, M. Milman, eds.), Contemp. Math. 226, American Mathematical Society, Providence, 33–53

[23] M. Cullen & R. Purser (1984) "An extended Lagrangian theory of semi-geostrophic frontogenesis", *J. Atmos. Sci.*, **41**, 1477–97

[24] M. Cullen, R. Purser & J. Norbury (1991) "Generalised Lagrangian solutions for atmospheric and oceanic flows", *SIAM J. Appl. Math.*, **51**, 20–31

[25] M. Cullen, J. Norbury, R. Purser & G. Shutts (1987) "Modelling the Quasi-Equilibrium Dynamics of the Atmosphere", *Q. J. R. Met. Soc.*, **113**, 735–757

[26] M. J. P. Cullen & I. Roulstone (1993) "A Geometric Model of the Non-linear Equilibration of Two-Dimensional Eady Waves", *J. Atmos. Sci*, **50**(2), 328–332

[27] S. Delahaies & I. Roulstone (2010) "Hyper-Kähler geometry and semi-geostrophic theory", *Proc. R. Soc. A.*, **466**, 195–211

[28] Ph. Delanoë (2008) "Lie solutions of Riemannian transport equations on compact manifolds", *Differential Geom. Appl.*, **26**(3), 327–338

[29] R. D'Onofrio (2023) "A note on optimal transport and Monge-Ampère geometry", *J. Geom. Phys*, **186**: 104771

[30] R. D'Onofrio, G. Ortenzi, I. Roulstone & V. Rubtsov (2023) "Solutions and Singularities of the Semigeostrophic Equations via the Geometry of Lagrangian Submanifolds", *Proc. Roy. Soc. A*, **479**: 20220682

[31] D. Dritschel, A. Viudez (2002) "An explicit potential-vorticity-conserving approach to modelling nonlinear internal gravity waves" *J. Fluid Mech.* **458** 75–101

[32] D. Dritschel, A. Viudez (2003) "A balanced approach to modelling rotating stably stratified geophysical flows" *J. Fluid Mech.* **488** 123–150

[33] S.V. Duzhin (2004) "Infinitesimal Classification of Systems of Two First Order Partial Differential Equations in Two Variables", *J. Math. Sci*, **119**, 30–34

[34] E. T. Eady (1947) "Long waves and cyclone waves", *Tellus*, **1**(3), 33–52

[35] J. Ehlers & E. T. Newmann (2000) "The theory of caustics and wave front singularities with physical applications", *J. Math. Phys.*, **41**, 3344

[36] L. C. Evans (1997) "Partial differential equations and Monge-Kantorovich mass transfer", in: Current Developements in Mathematics, Int. Press, Boston, MA, 65–126

[37] L. C. Evans (1998) *Partial Differential Equations* American Mathematical Society, Providence, RI

[38] R. Gilmore (1993) *Catastrophe theory for scientists and engineers*, Dover Publications Inc., New York, 1993

[39] M. Golubitsky, V. Guillemin *Stable Mappings and Their Singularities*, Springer-Verlag New York, 1973

[40] H.P. Greenspan (1958) "On the breaking of water waves of finite amplitude on a sloping beach" *J. Fluid Mech.* **4** 330–334

[41] M. E. Gurtin (1975) "On the Breaking of Water Waves on a Sloping Beach of Arbitrary Shape" *Quart. Appl. Math.* **33** 187–189

[42] A. Jeffrey and J. Mvungi (1980) "On the breaking of water waves in a channel of arbitrarily varying depth and width" *J. Appl. Math. Phys.* **31** 758–761

[43] R. Harvey & H. Lawson (1982) "Calibrated geometry", *Acta Mathematica*, **148**, 47–157

[44] M. W. Holt & G. J. Shutts (1990) "An analytical model of the growth of a frontal discontinuity", *Q. J. R. Meteorol. Soc.*, **116**, 269–286

[45] J. R. Holton & G. J. Hakim (2013) *An introduction to dynamic meteorology* (5th ed.). Amsterdam: Academic Press, Elsevier

[46] B. J. Hoskins & F. P. Bretherton (1972) "Atmospheric Frontogenesis Models: Mathematical Formulation and Solution", *J. Atmos. Sci.*, **29**, 11–37

[47] B. J. Hoskins (1975) "The Geostrophic Momentum Approximation and the Semi-Geostrophic Equations", *J. Atmos. Sci.*, **32**, 233–242

[48] B. J. Hoskins (1982) "The Mathematical Theory of Frontogenesis", *Ann. Rev. Fluid Mech.*, **14**, 131-151

[49] G. Ishikawa & Y. Machida (2006) "Singularities of improper affine spheres and surfaces of constant Gaussian curvature", *International J. Math.*, **17**(3), 269–293

[50] A. Kasahara (1974) "Various Vertical Coordinate Systems Used for Numerical Weather Prediction", *Mon. Wea. Rev.*, **102**, 509–522

[51] G. Ishikawa & Y. Machida (2006) "Extra singularities of geometric solutions to Monge-Ampère equation of three variables", *Kyoto Univ. Res. Inf. Repos.*, **1502**, 41–53

[52] Y-H Kim & R. J. McCann (2010) "Continuity, curvature, and the general covariance of optimal transportation", *J. Eur. Math. Soc.*, **12**(4), 1009–1040

[53] Y-H Kim, R. J. McCann & M. W. Warren (2010) "Pseudo-Riemannian geometry calibrates optimal transportation", *Mathematical Research Letters*, **17**, 1183–1197

[54] M. Kossowski (1991) "Local Existence of Multivalued Solutions to Analytic Symplectic Monge-Ampère Equations (The Nondegenerate and Type Changing Cases)", *Indiana University Mathematics Journal*, **40**(1), 123–148

[55] A. Kushner, V. Lychagin & V. Rubtsov (2006) *Contact Geometry and Nonlinear Differential Equations*. Cambridge, UK: Cambridge University Press

[56] T. P. Liu (1996) "Compressible flow with damping and vacuum" *Japan J. Indust. Apph Math.* **13** 25–32

[57] T. P. Liu and J. A. Smoller (1980) "On the vacuum state for the isentropic gas dynamics equations" *Adv. Appl. Math.* **1** 345–359

[58] T. P. Liu and T. Yang (1997) "Compressible Euler equations with vacuum" *J. Diff. Eq.* **140** 223–237

[59] T. P. Liu and T. Yang (2000) "Compressible flow with vacuum and physical singularity" *Meth. Appl. Anal.* **7** 495–510

[60] L. D. Landau & E. M. Lifshitz (1987) *Fluid Mechanics – Course of Theoretical Physics, Volume 6*, 2nd Edition. Oxford, UK: Pergamon Press

[61] G. Loeper (2009) "On the regularity of solutions of optimal transportation problems", *Acta Math*, **202**, 241–283

[62] V. Lychagin (1985) "Singularities of multivalued solutions of nonlinear differential equations, and nonlinear phenomena", *Acta Appl. Math.*, **3**, 135–173

[63] V. Lychagin & M. Roop (2020) "Singularities in Euler Flows: Multivalued Solutions, Shockwaves, and Phase Transitions", *Symmetry*, **13**(54), 1–11

[64] V. Lychagin & V. Rubtsov (1983) "Local classification of Monge–Ampère differential equations", *Dokl. Akad. Nauk SSSR*, **272**(1), 34–38

[65] V. Lychagin, V. Rubtsov & I. Chekalov (1993) "A classification of Monge–Ampère equations", *Ann. scient. Ec. Norm. Sup*, **26**, 281–308

[66] J. Loftin, S.-T. Yau & E. Zaslow (2005) "Affine manifolds, SYZ geometry and the "Y" vertex", *J. Differential Geom.*, **71**(1), 129–158

[67] X-N Ma, N. Trudinger & X-J Wang (2005) "Regularity of Potential Functions of the Optimal Transportation Problem", *Arch. Rational Mech. Anal.*, **177**, 151–183

[68] J. Marsden & T. Hughes (1983) *Mathematical foundations of elasticity*, New York: Dover Publications, Inc.

[69] R. McCann, B. Pass & M. Warren (2012) "Rectifiability of Optimal Transportation Plans", *Can. J. Math.*, **64**(4), 924–934

[70] M. E. McIntyre, I. Roulstone (2002). "Are there higher-accuracy analogues of semi-geostrophic theory?" In *LargeScale Atmosphere-Ocean Dynamics*, Vol. 2: *Geometric Methods and Models*, ed. I Roulstone, J Norbury, pp. 301–64. Cambridge, UK: Cambridge Univ. Press

[71] T. B. Moodie, Y. He, and D. W. Barclay (1991) "Wavefront expansions and nonlinear hyperbolic waves" *Wave Motion* **14** 347–367

[72] L. Napper, I. Roulstone, V. Rubtsov & M. Wolf (2023) "Monge–Ampère geometry and vortices", submitted to *Nonlinearity*, https://doi.org/10.48550/arXiv.2302.11604

[73] A. O. Remizov, "A brief introduction to singularity theory", https://www.sissa.it/fa/download/publications/remizov.pdf

[74] V. N. Rubtsov (2019) Geometry of Monge–Ampère Structures In: *Nonlinear PDEs, Their Geometry, and Applications*. Basel: Birkhäuser

[75] M. Oliver (2006) "Variational asymptotics for rotating shallow water near geostrophy: a transformational approach", *J. Fluid Mech.*, **551**, 197–234

[76] A. Rybkin, D. Nicolsky, E. Pelinovsky and M. Buckel (2020) "The Generalized Carrier–Greenspan Transform for the Shallow Water System with Arbitrary Initial and Boundary Conditions" *Water Waves* https://doi.org/10.1007/s42286-020-00042-w

[77] A. Rybkin, E. Pelinovsky, and I. Didenkulova (2014) "Nonlinear wave run-up in bays of arbitrary cross-section: Generalization of the Carrier–Greenspan approach" *J. Fluid Mech.* **748** 416–432

[78] I. Roulstone, B. Banos, J. D. Gibbon & V. N. Roubtsov (2009) "A Geometric Interpretation of Coherent Structures in Navier-Stokes Flows", *Proc. R. Soc. Lond. A*, **465**(2107), 2015–2021

[79] I. Roulstone & J. Norbury (1994) "A Hamiltonian structure with contact geometry for the semi-geostrophic equations", *J. Fluid Mech.*, **272**, 211–234

[80] V. Rubtsov (2019) "Geometry of Monge–Ampère structures", in *Nonlinear PDEs, their geometry, and applications*, Birkhauser/Springer, 95–156

[81] J.A. Sanders and F. Verhulst (1985) *Averaging Methods in Nonlinear Dynamical Systems*, Springer, New York.

[82] M. J. Sewell (1987) *Maximum and Minimum Principles*, Cambridge University Press

[83] M. J. Sewell (2002) "Some Applications of Transformation Theory in Mechanics", in *Large-Scale Atmosphere-Ocean Dynamics, Volume II, Geometric Methods and Models* edited by J. Norbury and I. Roulstone, Cambridge University Press

[84] G. Shutts (1991) "Some exact solutions to the semi-geostrophic equations for uniform potential vorticity flows", *Geophys. Astrophys. Fluid Dyn.*, **57**(1-4), 99–114

[85] G. J. Shutts & M. J. P. Cullen (1987) "Parcel Stability and its Relation to Semigeostrophic Theory", *J. Atmos. Sci*, **44**(9), 1318–1330

[86] B. Schutz (2013) *Geometrical methods of mathematical physics*, Cambridge University Press, Bath, UK

[87] J.J. Stoker (1948) "The formation of breakers and bores – the theory of nonlinear wave propagation in shallow water and open channels" *Comm. Pure Appl. Math.* **1** 1–87

[88] A. M. Vinogradov & B. A. Kupershmidt (1977) "The Structures of Hamiltonian Mechanics", *Russ. Math. Surv.*, **32**, 177

[89] M. Warren (2010) "Calibrations associated to Monge-Ampère equations", *Trans Am Math Soc*, **362**(8), 3947–3962

[90] M. Warren (2011) "A McLean Theorem for the moduli space of Lie solutions to mass transport equations", *Differ. Geom. Appl.*, **29**(6), 816–825

[91] A. White (2002) "A view of the equations of meteorological dynamics and various approximations", in *Large-Scale Atmosphere-Ocean Dynamics, Volume II, Geometric Methods and Models* edited by J. Norbury and I. Roulstone, Cambridge University Press

[92] G. B. Whitham (1999) *Linear and Nonlinear Waves*, John Wiley & Sons, Inc., New York